A Study of the Cometary Globules in the Gum Nebula

A *Thesis submitted*
for *the degree* of
Doctor of Philosophy
in *the Faculty* of *Science*

by

T.K. Sridharan

Department of Physics
Indian Institute of Science
Bangalore
October 1992

Declaration

I hereby declare that the work presented in this thesis is entirely original, and has been carried out by me at the Raman Research Institute under the auspices of the Department of Physics, Indian Institute of Science. I further declare that' this has not formed the basis for the award of any degree, diploma, membership, associateship or similar title of any University or Institution.

T.K.Sridharan
October 1, 1992.

Department of Physics
Indian Institute of Science
Bangalore 560 012
India.

To My Parents

One should not abandon one's duty suited to one's nature, *O Arjuna,* though it *may* be *imperfect;* for every enterprise is involved in *imperfection,* like fire *in smoke.*
    -Bhagavadgita XVIII:48 (borrowed *from Arora)*

Acknowledgements

It is my belief that any feeling of gratitude is diluted by publicly expressing it. Also, those who ought to be thanked do not expect to be thanked. Nevertheless, in order to avoid deviating too much from customary practice I would like to record my deep sense of indebtedness to several people, perhaps in a subdued manner.

I am very grateful to the organizers of the Joint Astronomy Programme, and S.Ramadurai in particular who was of great help during my troubled initial phase. After the course work at the Department of Physics I went to the Raman Research Institute for doing research, and I would like to thank the Director of RRI for making available to me all the facilities at the Institute.

Library facilities are obviously of utmost importance for any research worker. It was, indeed, a luxury to have the facilities and services offered by RRI Library. I am deeply indebted to Ratnakar and all the other members of the staff of the Library for their continued help over the years. Equally important was the help offered by Ramachandra Rao and Raju Varghese of the Photographic Lab.

The first part of my thesis was to construct a tunable Gunn Oscillator and it was R.S.Arora who introduced me to this field. I am very grateful to him for all his help and also to Valsan who decided the machining steps and fabricated the Oscillator. Narayanaswamy and Achankunju also helped in important ways in the machining. I also wish to thank Ananthasubramanian of the Millimeterwave Lab for help in testing and phase-locking the Oscillator.

My grateful thanks are also due to all the members of the Millimeterwave Lab and the Observatory, especially Sarma, Ganesan, Narayanan, Ramesh Kumar and Ramachandran. Rengarajan, Sukumar and Lakshmy were of immense help with the data acquisition and telescope software. During my last observing season when things started going wrong Rajasekar, Lakshmy and Seetha helped me with the observations by putting in extra hours - I would like to thank them profusely for this. Rajasekhar also helped me during data processing on AIPS.

Contents

A Summary of Main Results Presented in the Thesis

The first part of the thesis deals with the development of a *wide-band mechanically tuned local oscillator. using the Gunn diode* for use with the 10.4m millimeter-wave radio telescope at the Raman Research Institute. This provides sufficient power to efficiently operate two cryogenic Schottky mixers (dual polarisation) and tunes over the frequency range 75-115 GHz covering most of the 3-mm atmospheric transmission window (W-band). Rotational transitions of many astrophysically important molecules including CO fall in this range.

A study of the cometary globules in the Gum Nubula forms the second part. Among the smaller interstellar molecular clouds the Cometary Globules (CGs) stand out due to their peculiar morphology. They are characterised by compact, dusty heads with long faintly luminous tails extending on one side and narrow bright rims on the other side. There exists a significant population of such CGs in the Gum Nebula. The Gum Nebula is a large structure $\sim$ 12.5 parsec in radius delineated by Hα emitting filaments. The true nature of the Gum Nebula is ill understood; according to various conjectures it could be an old supernova remnant, or a bubble in the interstellar medium excavated by strong stellar winds from hot stars, or an evolved HII region. The CGs in the Gum Nebula are distributed over a region $\sim$ 80 parsec in radius with their tails pointing away from an apparent common center. In the visible region these globules have bright rims on the side facing the common central region. Some of the heads have embedded young stars. In the region bounded by the CGs there are a few massive hot stars including ζ Puppis believed to be the most luminous star in the southern sky. It has been suspected that the morphological appearance of the CGs may be due to the influence of these stars.

Although these globules have been known for more than a decade now there has been no satisfactory attempt to study their origin and kinematics. A detailed study was therefore undertaken using the 10.4 m millimeter-wave radio telescope at the Raman Research Institute. The study consisted of ^{12}CO observations of the heads and the tails of the CGs using the $J = 1 \rightarrow 0$ millimeter-wave rotational transition of the carbon monoxide molecule. In addition. the Globule No.22 was mapped in both ^{12}CO and ^{13}CO.

An analysis of tlie radial velocities obtained from the survey and the maps have led to the following findings:

1. The system of CGs is expanding with respect to a common morphological center at ~ 12 kms^{-1}. The expansion age is ~ 6 Myr.

2. Some of the tails observetl show systematic velocity gradients. If the tails were formed due to the elongation resulting from these velocity gradients then the estimated stretching age is ~ 3 Myr.

3. The mass of CG 22 is $\sim 27 M_\odot$. Interestingly, if tlie cloud was in virial equilibrium then its mass must be $\sim 250 M_\odot$.

There have been previous conjectures that the young stars embedded in the heads of some of the globules may have been formed as a result of external triggering. In order to clarify this question an analysis of the locations of the embedded young stellar objects (YSOs) in tlie dark clouds in the Gum-Vela region was undertaken. Since these embedded YSOs are obscured in tlie visible region by dust in the molecular clouds, the far-infrared point sources from tlie Infra-Red Astronomical Satellite catalogue were used to identify them. This study has clearly shown that the YSOs have a stastically significant tendency to fall on the sides of dark clouds facing the morphological center rather than the far sides.

From the above analysis we come to the following conclusions:

1. The rough agreement between tlie *expansion age* and the *tail-stretching* age suggests a common origin for the expansion and the formation of tlie tails. The presence of young stars of comparable ages in the heads of some of the globules suggests that tlie processes responsible for the expansion may have also triggered star formation in them.

2. The radiation pressure from the hot stars in tlie central region or the stellar winds from them cannot account for the momentum of tlie expanding globules. It is more likely that the *rocket effect* arising out of the heating and the consequent anisotropic ablation of tlie globules can supply the necessary momentum.

All the above conclusions can be reconciled easily if one could argue tliat they are causally connected and have a common origin. The main apparent obstacle to such a unified picture for the system of CGs in tlie Gum Nebula is tliat although there appears to be a morphological center there arc no identifiable objects, say, massive

stars, *presently* located at or near tlie morphological center. However, the observed large proper motion of tlie massive star ζ Puppis holds an important clue, leading to tlie following scenario: It is an extraordinary fact that ζ Puppis has a large proper motion $\sim$ 75 kms^{-1}, and its trajectory when extrapolated backwards passes close to the morphological center of the system of CGs. It lias been known for a long time that large space velocities of massive stars can only be understood in terms of the disruption of a massive binary system when one of tlie stars explodes as a supernova. If the supernova explosion is spherically symmetric then the binary will disrupt due to a sudden mass loss only if the mass ejected exceeds half tlie total mass of the binary system. Since the estimated mass of ζ Puppis is $\sim 40 M_\odot$, it follows that its former companion must have been even more massive than this. If one accepts this picture then it follows that till roughly half a million years ago there must have been a massive binary system (ζ Puppis and its companion) near the center of the system of CGs. The combined effect of the ultra-violet radiation and the stellar wind from this binary as well as from other stars in tlie neighbourhood, must have resulted in much of the molecular material in the vicinity being blown away except the numerous regions of enhanced density (*condensations*) in tlie original molecular cloud. Continued effect of the radiation and stellar winds resulted in these condensations being set in motion, as well as developing cometary tails. Roughly half a million years ago the companion ζ Puppis exploded as a supernova propelling the latter towards its present location.

Chapter 1

Introduction

1.1   Millimeter-wave Astronomy

Millimeter radio astronomy as an important branch of astronomy was born with the discovery in 1971 of carbon monoxide in the interstellar rnedium at 115 GHz by Wilson et al.(1971). In tlic two decades since this discovery, over 60 molecules have been detected in the ISM. Some of the organic molecules identified are quite complex containing as many as 13 atoms. Line radiation from molecules in the ISM has given us a wealth of new information. Molecular line studies arc about the only way to probe tlie cold, dense regions where new stars are believed to he born. These studies have led to the discovery of tlie Giant Molecular Clouds, the most massive structures in the galaxy, tlie unexpected outflow phase of young stars, the circumstellar arid interstellar masers, and a variety of chemical species.

Molecular clouds are mainly made up of H_2. Being a homomorphic molecule H_2 has coincident charge and mass centers. Consequently it has no permanent dipole moment and so does not radiate in its lower rotational transitions. Molecular hydrogen has been studied, however, through its vibrational-rotational quadrupole transitions. These lines fall in the **IR** region requiring higher energies to be excited restricting tlie direct study of H_2 to shock excited regions with temperatures $\sim 1000K$. H_2 has also been observed through its UV absorption lines but obviously only along selected lines of sight. In essence, direct observation of H_2 in tlic cold interstellar medium is not possible. Fortunately tlie next most abundant molecule **CO** has a permanent diplole moment leading to conveniently observable radio lines. The lowest rotational transition (J=1 $\rightarrow$ 0) of CO at 115.271 GHz corresponds to an $h\nu/k = 5.5K$. This transition is easily excited by collisions with molecular hydrogen even in clouds with very low kinetic temperature. The minimum density required is ~ 100 cm^{-3}. Therefore CO is widely used as a tracer of H_2 in cold interstellar clouds. The less abundant species. ^{13}CO, is used to overcome difficulties posed by the high optical depth of ^{12}CO in probing deeper into molecular clouds. Molecules with different dipole moments and formation chemistry are used to study regions of different physical conditions and activities.

Advances in millimeter-wave radio astronomy were limited by developments in antenna arid receiver technology. During tlie eighties, many large telescopes some with surface accuracy high enough to go upto 1000 GHz have been built arid receiver technology has matured sufficiently to permit routine observations.

1.2 Molecular Clouds

Over the past decade several ^{12}CO and ^{13}CO surveys have been undertaken on the galactic scale which have led to the realisation that most of the molecular gas is concentrated in Giant Molecular Cloud complexes. GMCs are at the high end of the molecular cloud aggregates. In order of magnitude their masses are $\sim 10^6 M_\odot$ and sizes are ~ 100pc. They are the birth sites of high mass stars but they also form low mass stars. The dark cloud complexes like Taurus and Ophiucus are smaller with masses in the range 10^{3-4} $M_\odot$ and mainly form low mass stars. Towards the lower end of the molecular cloud distribution we have the dust globules, which are further discussed below.

It was first suggested by Bok and Reilly(1947) that dark dust globules are probable sites of star formation. For a long time no direct evidence was forthcoming to support this claim. The first evidence was provided by Schwartz(1977) when he discovered star formation in a globule in the Gum Nebula (GDC 1). This globule has turned out to be very interesting: It has an embedded young star, the Herbig-Haro object HH46-47; and is a strong case for star formation caused by external mechanisms (Schwartz 1977). Globules have been grouped into four classes based on their optical morphology (Leung 1985). They are: (a) the elephant trunk globules, (b) globular filaments, (c) isolated dark globules, and (d) cometary globules. Elephant trunk globules are long tongues of obscuring gas and dust seen in projection against bright HII regions. Their sizes are ¯ 0.01 - 0.5 pc, and their masses are in the range $\sim$ 5-10 $M_\odot$ and densities $\sim 10^{3-4}$ cm^{-3}. The best examples of elephant trunks are found in the Rosette Nebula. Globular filaments are dark nebulae with elongated filamentary structure. Isolated dark globules are also known as Bok globules. They have sharp boundaries and are not near HII regions or bright nebulosities. Well studied examples are B68 and B335. Cometary globules (CGs) have a cometary morphology: a dusty head with a luminous tail on one side and bright rims on the other side. They are discussed in more detail in the rest of this chapter.

1.3 Cometary Globules

Bright rimmed globules, many of which have cometary structure, have been subject of study since the thirties. Pottasch(1965) studied a number of bright rims and concluded that they are ionised hydrogen regions caused by nearby O-type stars. Interest in cometary globules was revived with the discovery of HH46-47 and a sizable

population of CGs in tlie Gum-Vela region. The CGs in the Gum-Vela region were first noted by Hawarden and Brand(1976) and Sandqvist(1976). Later, Zealey *et al.* (1983, hereafter referred to as Z83) and Reipurth(1983) independently found, a total of 38 CGs in a surveys of the SERC IIIa-J and ESO B plates of which 32 were in the Gum-Vela region. Figure 1.1 shows a photograph of CG 15, a typical CG. The Gum globules have the following characteristics (see figure 1.1):

- A compact dusty head

- A long faintly luminous tail extending from one side of tlie head; the other side has a sharp edge with narrow bright rims.

- The tails of these CGs point away from a general center.

- Sometimes the heads have embedded young stars in them.

It is now well established that many bright rimmed globules found in association with HII regions are sites of on-going low mass star formation (Dibai 1963, Sugitani *et al.* 1989, Sugitani, Fukui and Ogura 1991. Cernicharo *et al.* 1992, Duvert *et al.* 1992). The earliest example of such star formation is the discovery of HH 46-47 in the cloud GDC 1 (ESO 210-6A) in the Gum Nebula mentioned earlier. GDC 1 has characteristics similar to tlie cometary globules. It is now known that CGs are not restricted to the Gum Nebula. The original list contains CGs in Orion and recently CGs have also been found in the Rosette Nebula (Block,1990). Carbon monoxide maps of molecular clouds in Orion show cometary structure with tails pointing away from tlie Ori OB1 Association (Bally *et al.* 1'391). It is believed that the cometary globules are formed by the effect of UV radiation from young stars, stellar winds, and supernova shocks on nearby molecular clouds.

The globules in the Gum Nebula arc in a complicated setting (see figure 1.2). This nebula is a large shell like structure (radius $-18°$) seen in Hα (Gum, 1952;1955). The estimated distance of ~ 400 pc implies a radius of 125 pc (Brandt *et al.* 1971). In the general direction of the centre of the nebula are the Vela SNR (age $\sim 10^4$ yrs), the Pup A SNR (age ~ 3700 yrs), ζ Pup (O4f), the most luminous star in the southern sky, the Wolf-Rayet binary γ^2 Vel (WC8+O9), and a possible B Association. These objects together represent a significant source of ionising radiation and stellar wind. Various models have been proposed for the Gum Nebula in which some of these objects play an important role (see, for example, Bruhweiler, 1983). Whether the Gum Nebula is expanding or not has been a point of controversy in the past, but latest studies indicate expansion at 10 kms^{-1} (Srinivasan *et al..* 1987). In the central region of the Gum Nebula the CGs are distributed non-uniformly over a
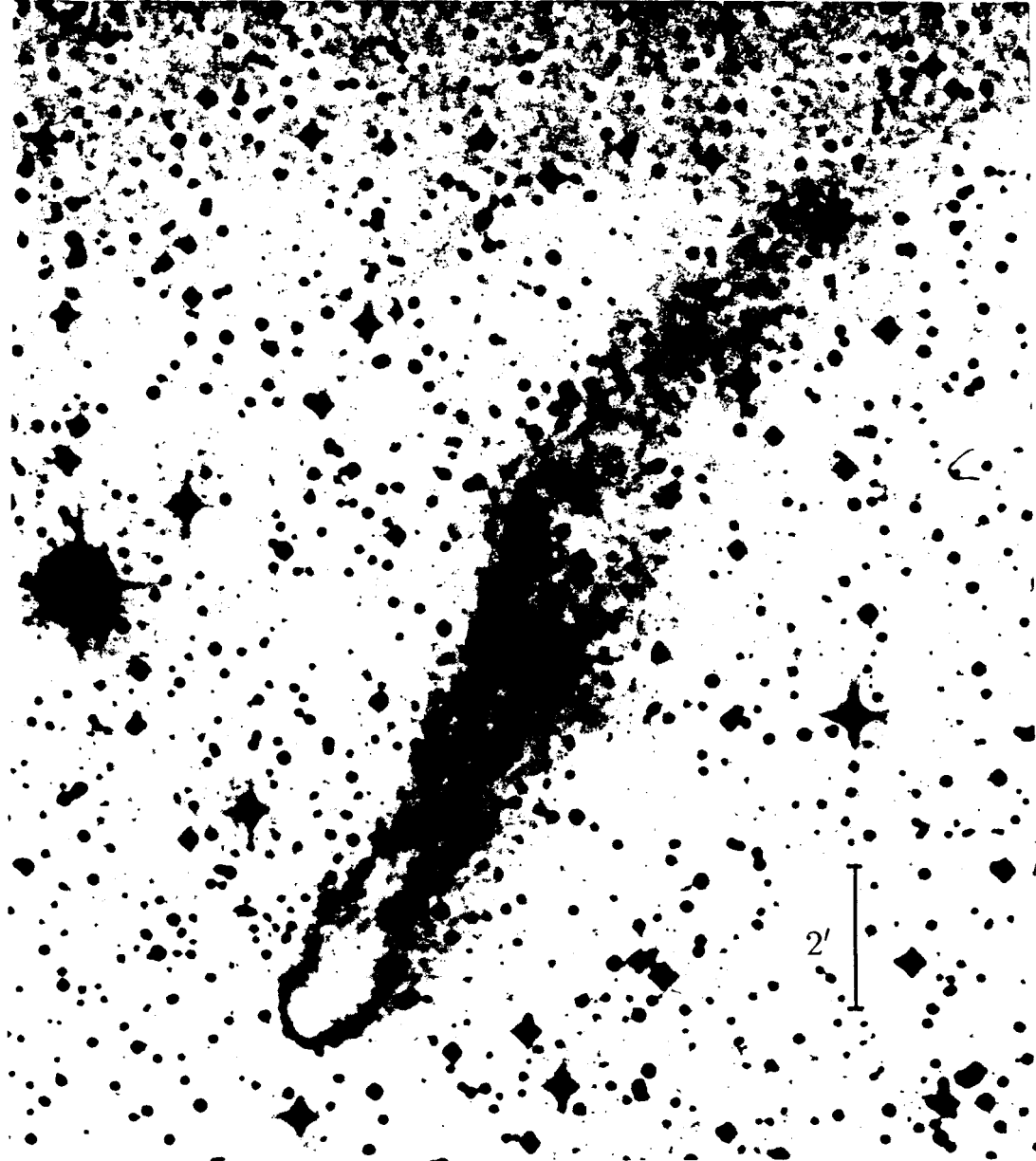
Figure 1.1: An optical image of CG 15, a typical cometary globule reproduced from the SERC survey plate (what is shown is a negative image). The obscuring head is seen as a white patch whereas the tail and the bright rim are black.
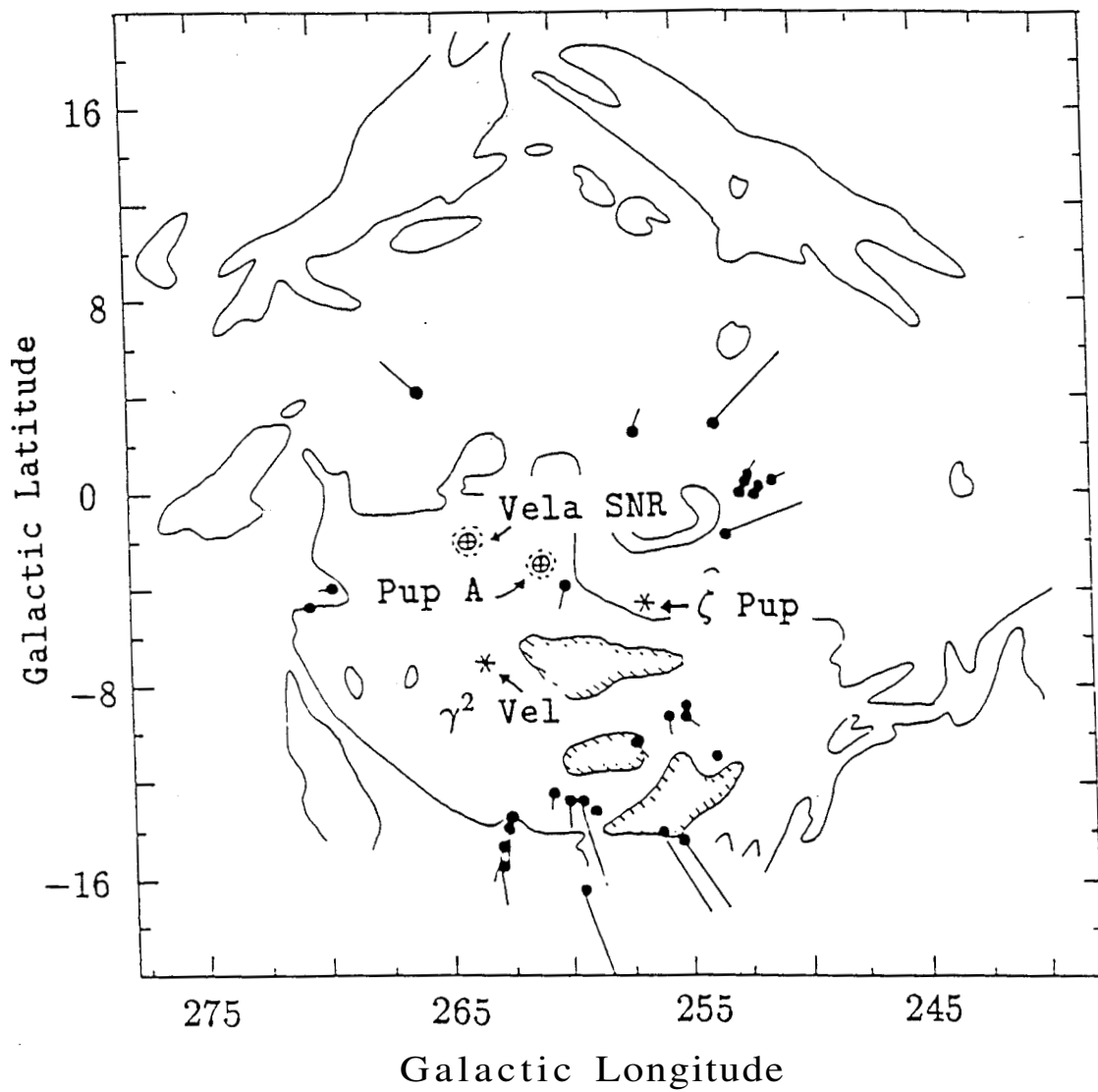
Figure 1.2: The Gum-Vela region. The solid lines mark the regions of H a emission. The cometary globules are shown as filled circles, with tails scaled up 10 times for clarity. The locations of objects in this figure are approximate (adapted from Pettersson 1991).

rough *annulus whose center* is close to the place from which the tails point away. This *morphological center* is offset from the approximate center of the Gum Nebula by about 4°. The best fit circle to the distribution of CGs has a radius of ≈ 9.5°. There is firm evidence for star formation in some of the CGs as well as some of the other dark clouds in tlie Gum-Vela region (Schwartz 1977; Bok 1978; Reipurth 1983; Pettersson, 1987,1991; Graham 1986; Graham and Heyer 1989)

Soon after the discovery of HH46-47, it was suggested that low mass star formation in the Gum Nebula may have been triggered by external events (Schwartz 1977), quite possibly tlie events responsible for the origin of the Gum Nebula itself (Brand *et* al.. 1983). Stellar winds, SN shocks. arid shocks associated with the expansion of HII regions can compress small globules into gravitational instability leading to star formation. Numerical studies of such processes give credence to this idea (Woodward 1976;1979). Reipurth(1983) has argued in favor of UV radiation from young stars being the cause for the origin of CGs as well as star formation in them. There have also been studies of radiation driven implosion as a mechanism for star formation (Sandford,Whitaker and Klein 1982, Bertoldi and McKee 1990). Specifically, Bertoldi and McKee have shown that clouds exposed to UV radiation will acquire a cometary structure.

1.4   Previous Studies

Tlie first systematic study of the cometray globules in tlie Gum Nebula was done by Zealey *et. al.*(1983). They made 4 cm formaldehyde absorption observations of 9 CGs with the Parkes 210 foot telescope. O1113' CGs big enough to have a good chance of detection with the 4.4' beam were observed. Goss *et al.*(1980) had observed some of tlie CGs in an independent survey. Radial velocities for a total of 10 CGs were thus obtained. Z83 concluded from this data that the radial velocities were consistent with rotation of tlie system about an axis perpendicular to the galactic plane. They suggested that the orientation of this axis implied that the kinematics of the CGs is dominated by galactic rotation. In addition they found that in an $l - v$ plot the CGs lined up on a straight line parallel to the HI data for tlie region, but offset in l. They took this to mean that the observed velocities of the CG complex are wholly due to large scale effects of tlie local spiral structure. Assurning that such a *line* represented galactic rotation effects they studied the deviations from the straight line fit to look for expansion or rotation. Their conclusion was that the CGs may be on a shell expanding with velocities upto 5 kms^{-1}. [We find this surprising since the residuals (i.e. the deviations from their straight line fit) were

only $\pm$ 2 kms^{-1}]. In addition, from a study of the tails seen in optical photographs they identified two *centers* from where maximum number of tails pointed away.

1.5   Present Study

In this thesis we present a study of the system of cometary globules in the Gum Nebula using mainly the 10.4m millimeter-wave radio telescope at the Raman Research Institute, Bangalore.The thesis is organised in three parts:

(1) The first part deals with the development of a wide-band mechanically tuned local oscillator using the Gunn diode for use with the 10.4m millimeter-wave radio telescope at the Raman Research Institute. This is described in chapter 2.

(2) The second part is devoted to a study of the cometary globules in the Gum-Vela region. As mentioned earlier, there has been no satisfactory study of the system of CGs in the Gum Nebula. A detailed study of the system was therefore undertaken using the mm-wave rotational transitions (J=1 $\rightarrow$ 0) of the molecules ^{12}CO and ^{13}CO. The observations consist of a ^{12}CO survey of the heads and the *tails* of the CGs, and mapping one of them viz., CG22 in ^{12}CO and ^{13}CO. The aim of the survey was to study the kinematics of the CGs and gas motions along the tails. The main objective was to make a more complete study of the *kinematics* of the system than was possible before. As mentioned above, in previous attempts the velocity information was available only for 10 out of the more than 30 CGs. Since our beam size was 1' we could detect even the smaller clouds that were not detected in the previous surveys. The mapping of one of the globules was done primarily for estimating its mass. The telescope and observations are described in chapter 3. The analysis of the survey data is the subject of chapter 4 and chapter 5 deals with the maps of CG 22.

(3) The third part of the thesis, presented in chapter 6, deals with an analysis of the locations of embedded young stellar objects (YSOs) inside the dark clouds in the Gum Nebula region. The aim of this study was to look for evidence for externally triggered star formation in these clouds. We have used the far-infrared point sources from the IRAS PSC (with suitable flux criteria) to identify embedded YSOs. By simple statistical methods we show that the YSOs have higher tendency to fall on the side of the clouds facing the morphological center than the far side.

In chapter 7 we discuss the results and present an overall view of the system of CGs in the Gum Nebula.

REFERENCES

Bally, J., Langer, W.D., Wilson, R.W., Stark, A.A., Pound, M.W. 1991, preprint

Bertoldi, F., McKee, C.F. 1990, *Ap. J.*, 354, 529.

Block, D.L. 1990, *Nature*, 347, 452.

Bok, B. 1978, *Pub.A.S.P.*, 90. 489.

Bok, B., Rielly, E.F., 1947, *Ap. J.*. 105. 255.

Brand, P.W.J.L., Hawarden, T.G.. Longmore, A.J., Williams, P.M., Caldwell, J.A.R. 1983, *Monthly Notices* Roy. *Astron. Soc.*, 203, 215.

Brandt, J.C., Stecher, T.P.,Crawford, D.L.,Maran, S.P. 1971, *Ap.J.(Letters)*, 163, L99.

Bruhweiler, F.C. 1983, *Comments* on *Astrophys.*, 10, 1.

Caswell, J.L., Lerche, I. 1'37'3, *Monthly Notices Roy. Astron. Soc.*, 187, 201.

Chernicharo, J., Bachiller, R., Duvert, G., Gonzalez-Alfonso, E., Gomez-Gonzalez, J. 1991, Astron. *Astrophys.*, accepted.

Dibai, E.A. 1963, Soviet *Astr.* - AJ, 7, 606.

Duvert, G., Cernicharo, J., Bacliiller, R., Gomez-Gonzalez, J. 1990, Astron. *Astrophys.*, 233, 190.

Goss, W.M., Manchester, R.N., Brooks, J.W., Sinclair, M.W., Mansfield, G.A., Danziger, I.J. 1980, *Monthly Notices* Roy. *Astron. Soc.*, 191, 537.

Graham, J.A. 1986, *Ap.J.*, 302, 352.

Graham, J.A., Heyer, M.H. 1989, *Pub.A.S.P.*, 101, 573.

Gum, C.S. 1952, *Observatory*, 72, 151.

Gum, C.S. 1955, *Mem.* Roy. *Astr. Soc.*, 47, 1.55.

Hawarden, T.G., Brand, P.W.J.L. 1976, *Monthly Notices Roy. Astron. Soc.*, **175**, 19P.

Leung, C.M., 1985, in *Protostars and Planets II*, ed. D.C. Black & M.S. Matthews(The University of Arizona Press), p. 124.

Pettersson, B. 1984, *Astron. Astrophys.*, 139. 135

Pettersson, B. 1987, *Astron. Astrophys.*, 171. 101.

Pettersson, B. 1991, in *Low Mass Star Formation* in Southern *Molecular* Clouds, ed. Reipurth, B., ESO Scientific Report No. 11, p. 69.

Pottasch, S.R., 196.5, *Vistas in astronomy.* 6. 147.

Reipurth, B. 1983, *Astron. Astrophys.*, 117, 183. Sandford, M.T., Whitaker, R.W., Klein, R.I. 1982. *Ap. J.*, 260. 183.

Sandqvist, Aa. 1976, *Monthly Notices* Roy. *Astron. Soc.*, 177, 69P.

Schwartz, K.D. 1977 Ay. J. *(Letters)*, 212, L25.

Srinivasan, M., Pottach, S.R., Sahu, K.C., Pecker, J.-C. 1987, ESO Messenger, No.51, 11.

Sugitani, K., Fukui, Y., Mizuno, A. and Ohashi, N. 1989, *Ap. J.(Letters)*, 342, L87.

Sugitani, K., Fukui, Y., Ogura, K. 1991. *Ap. J. Suppl.*, 77, 59

Wilson, R.W., Jefferts, K.B., Penzias, A.A., 1971, *Ap. J. (Letters)*, 161, L43.

Woodward, R.P. 1976, Ap. J., 207, 484.

Woodward, R.P. 1979, in Large Scale *Characteristics* of *the Galaxy, IAU Symp.* 84, ed. Burton, W.B., (Riedel, Dordrecht, Holland), p. 1.59.

Zealey, W.J., Ninkov, Z., Rice, E., Hartley, M., Tritton, S.B. 1983, *Ap.* Letters, 23, 119 (Z83).

Chapter 2

Wide-band Local Oscillator

2.1 Millimeter-Wave Receivers

Fortunately for astronomers, tlie millimeter wave part of the electromagnetic spectrum is not used for radio communication arid most transmitters have low power and narrow beams thus reducing drastically tlie problem of man made interference. But tlie millimeter wave astronomers have to contend with the problem of *atmospheric absorption* especially due to water vapour and oxygen. As seen in figure 2.1, the atmospheric attenuation over the millimeter wave range sliows some windows of low attenuation which tlie ground based telescopes utilise. The amount of absorption is strongly dependent on the geographical location, and season, through the atmospheric water vapour content. Over the past two decades, better and better receivers have been developed for operation over these low attenuation bands.

The block diagram of a typical millimeter wave receiver is shown in figure 2.2. These are of super-heterodyne design. The first element is a mixer, either of a cryogenic Schottky or superconductor-insulator-superconductor junction design, because low-noise amplifiers at these frequencies have not yet become available. The IF signal is amplified by a cooled low-noise GaAs or HEMT amplifier. Since the mixer is a lossy device, the IF amplifier should have very low noise temperature. The AM side band noise of the LO at the signal and image frequencies also contributes to the receiver noise. The IF signal is then fed to spectrometers after further amplification and down conversion. In this chapter we describe tlie development of an ultra wide-band Gunn oscillator tunable over tlie 3-mm atmospheric transmission window for use as local oscillator at the 10.4m millimeter wave radio telescope at the Raman Research Institute, Bangalore. Rotational transitions of many astrophysically important molecules including CO fall in tlis range.

2.2 Local Oscillator Requirements

The power output requirement of the LO depends on tlie type of mixer used. Cryogenically cooled mixers using metal-semiconductor junctions (Schottky barrier diodes) as the 11011-linearelement typically require 0.25 mW of CW power for efficient operation. The SIS mixers which are fast replacing the Schottky mixers require less than a microwatt. With tlie development of quasi-optical diplexers (Erickson 1977) which couple the LO power to tlie miser with an insertion loss <1dB, an LO power output of 0.5 mW is adequate. An output of 1 mW will be sufficient to operate a dual polarisation receiver. Low AM sideband noise at tlie signal and image frequencies will be an advantage, though tlie diplexers can be designed to have nulls
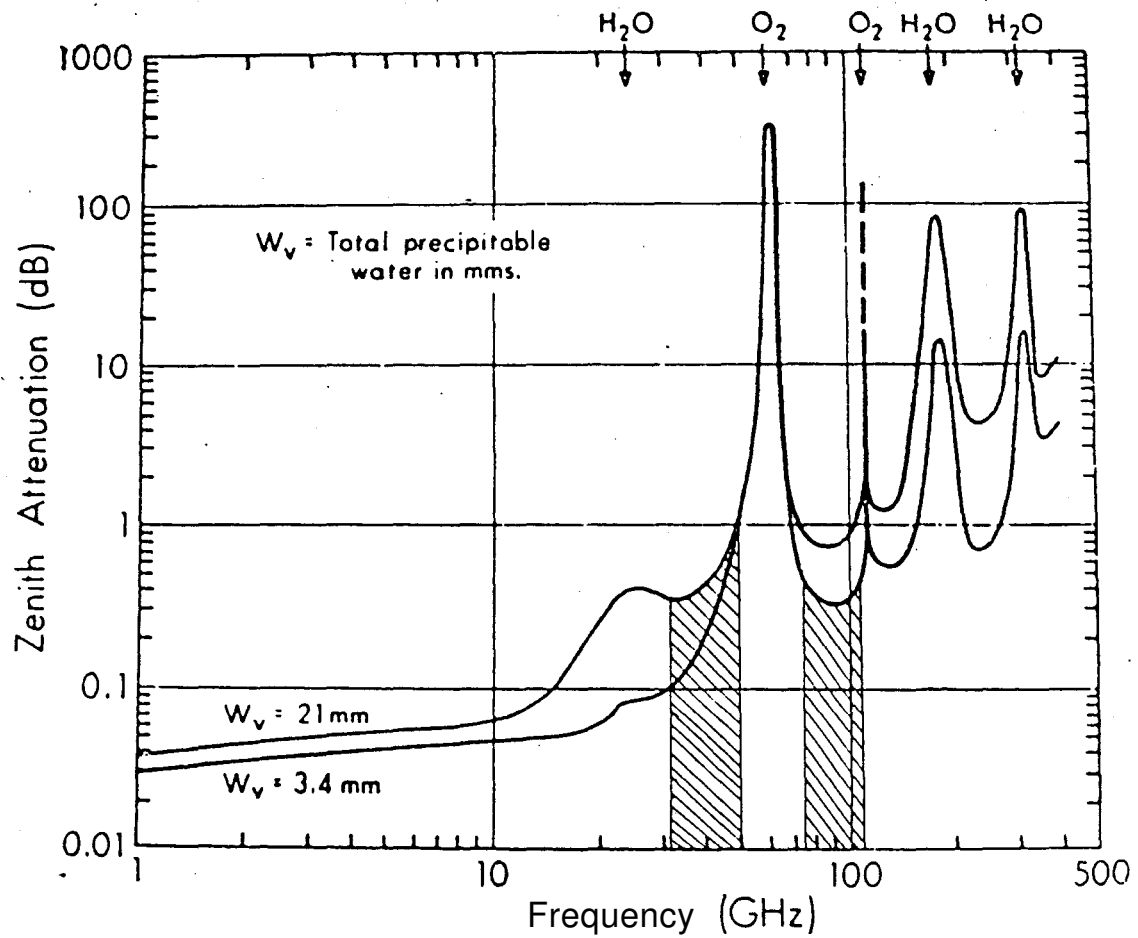
Figure 2.1: Atmospheric attenuation over the millimeter-wave region of the electromagnetic spectrum. The hatched regions are used by ground based telescopes (adapted from Penzias and Burrus 1973).
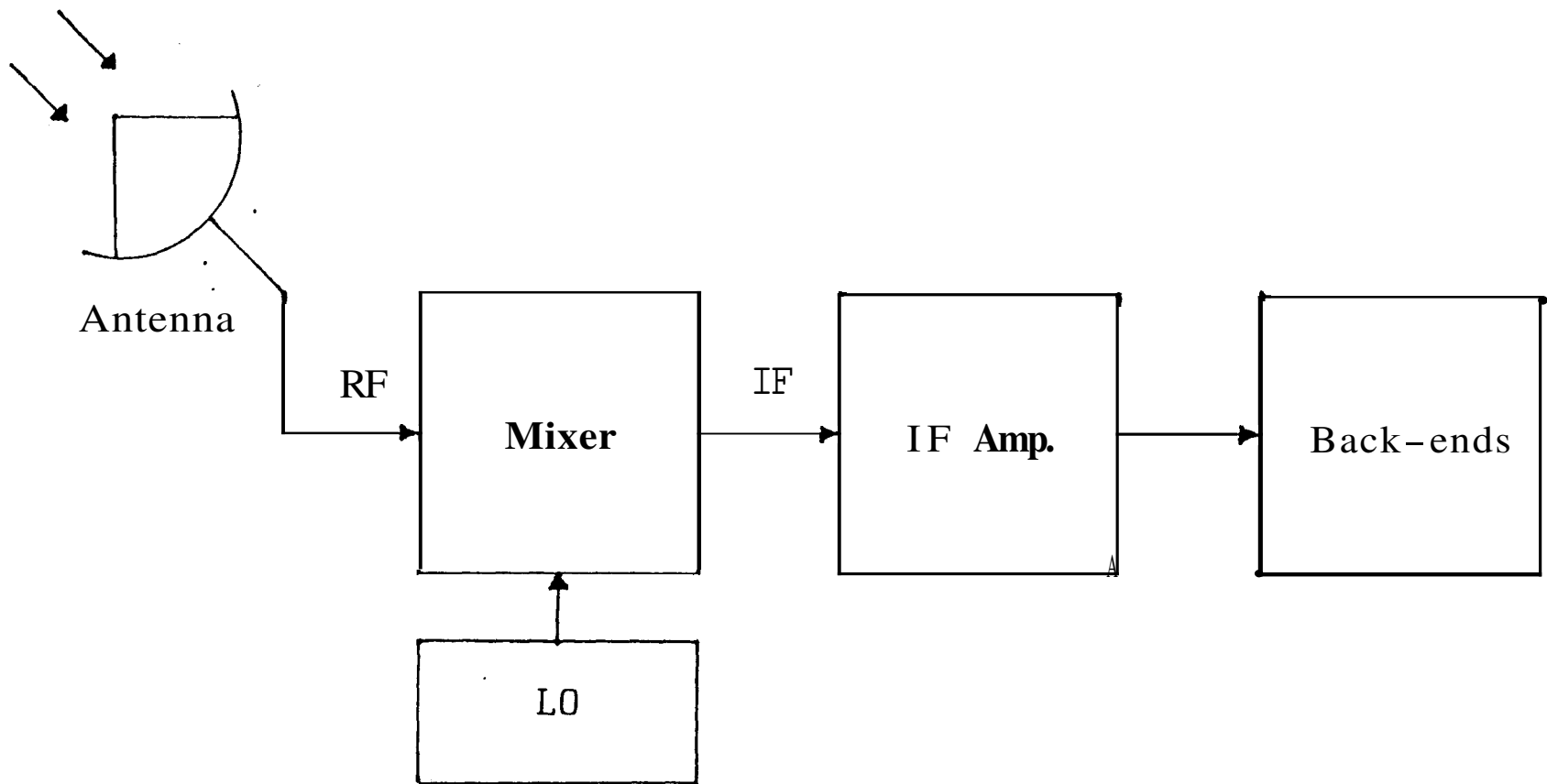
Figure 2.2: **A** block diagram of a typical millimeter-wave receiver.

at these frequencies. Frequency stability is a vital consideration. In other words, it should be possible to easily phase-lock the oscillator to a stable reference. Another important consideration is tunability. Since there are many rotational transitions of a vareity of molecules spread over the 3 mm window, a single oscillator tunable over the W-band will avoid changing local oscillators every time a new line is to be observed. Klystrons, IMPATTS and Gunns are some of the devices used as LOs. We briefly discuss the advantages and disadvantages of these methods of generating LO power.

2.2.1   Klystrons

Until recently millimeter wave reflex klystrons, phase locked to a highly stable reference source, were used as LOs. The limited life time *(500* hours) and the bulky high voltage power supplies and cooling systems required are their main drawbacks. High power output and wide tunability were their main attractions. Only klystrons can give enough power to pump multipliers used to generate sub-mm LO power.

2.2.2   IMPATTS

Local oscillators made using IMPATT diodes arc capable of power outputs and tunability comparable to klystrons. They are also cheaper than klystrons and being solid state devices require only low voltage power supplies and no cooling. The main disadvantage of IRIPATT oscillators, however, is their excessive noise. Low AM sideband noise can be acheived only over a limited frequency range making a wide band tunable oscillator difficult to realise.

2.2.3   Gunn device

Also called tlie *transferred electron device,* it exhibits low AM sideband noise comparable to klystrons. It is possible to have tunability over a wide frequency range without any change in the noise level. Like the IMPATT, being a solid state device it requires only low voltage power supplies arid no cooling. Electronic tunability of upto 500 MHz is possible by varying the bias voltage with easy phase locking. The main disadvantage of Gunn oscillators is their low power output, but it is enough to operate cryogenic mixers. In adition availability of InP Gunn devices higher power output has become possible.

Clearly the Gunn oscillators meet the requirements of an LO for a mm-wave radio telescope. In the rest of this chapter, we will discuss in more detail the Gunn device and the construction of oscillators using the Gunn device.

2.3   The transferred electron effect

The Gunn diode falls under the general class of devices called negative conductance devices. The device is simply a piece of bulk semiconductor such as GaAs or InP and has no junction. The negative conductance arises due tlie trasferred electron mechanism operative over a certain range of the voltage applied across this piece of semiconductor. It is called tlie Gunn diode after 5.13. Gunn who first dernonstrated in 1963 one form of oscillation in these devices. The theory of this effect had already been proposed by Ridley arid Watkins(1961), arid Hilsum(1962).

To understand the origin of negative conductance we refer to figure **2.3** which shows simplified energy band digrams for the widely used III-V semiconductors, GaAs and InP. The conduction band consists of a central valley (primary minimum) and satellite valleys (secondary minima) at energies about half an eV higher than tlie central valley. Since at room temperature this energy difference is much larger than $k_B T$, the conduction electrons are in the central valley and the satellite valleys are unoccupied. If the material is subjected to an electric field above some critical field of about 3000 Vcm^{-1}, the electrons in tlie central valley gain enough energy frorn the field and get scattered into the higher energy satellite valley. The important point now is that the effective mass of an electron in the upper valley is almost 20 times its value in the main valley. making tlie mobility in the upper valley 20 times less. Therefore the electroris move slower, thus reducing the current. In other words as the applied voltage on a sample of GaAs or InP is increased, the current increases till the field in the sample reaches a critical value, arid then begins to decrease with increase in the applied voltage and one has negative differential conductance. The carrier velocity versus electric field characteristics for GaAs and InP plotted in figure 2.4 show clearly the negative conductance region. By scaling tlie X-axis by the length of the sample used one gets the V-I cliaracteristic. This negative conductance gives rise to sustained oscillations when the device is placed in a suitable cavity.
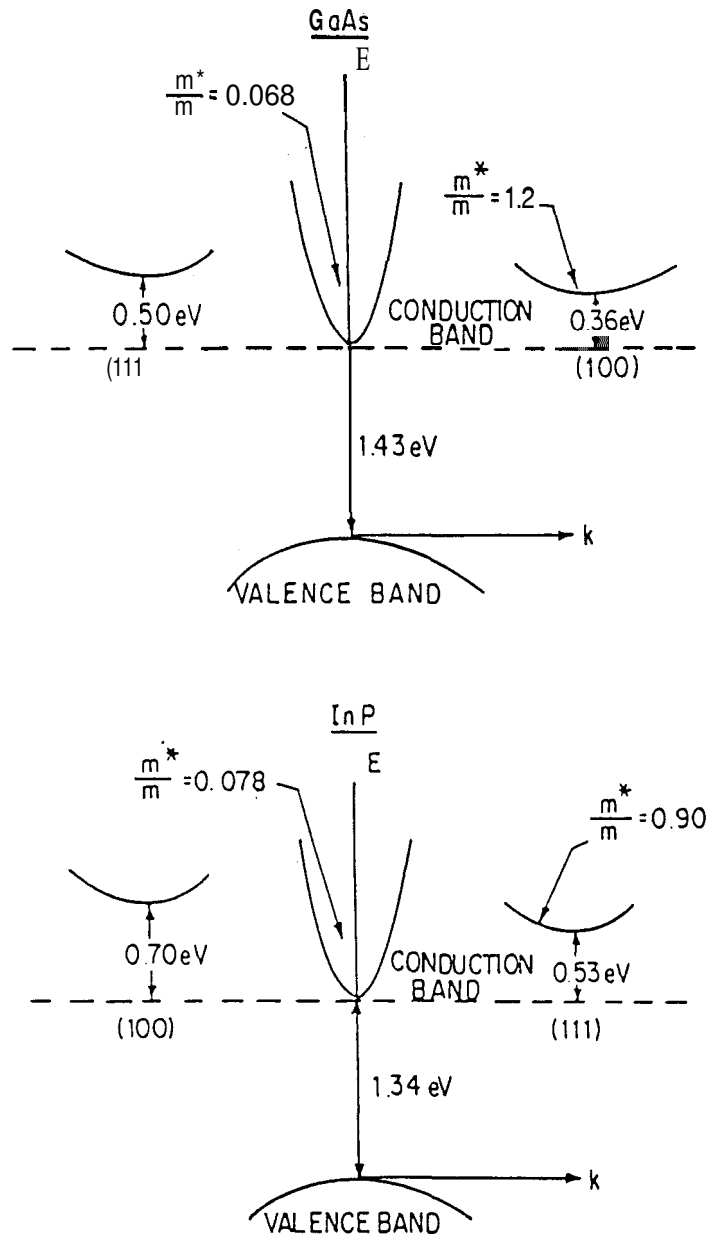
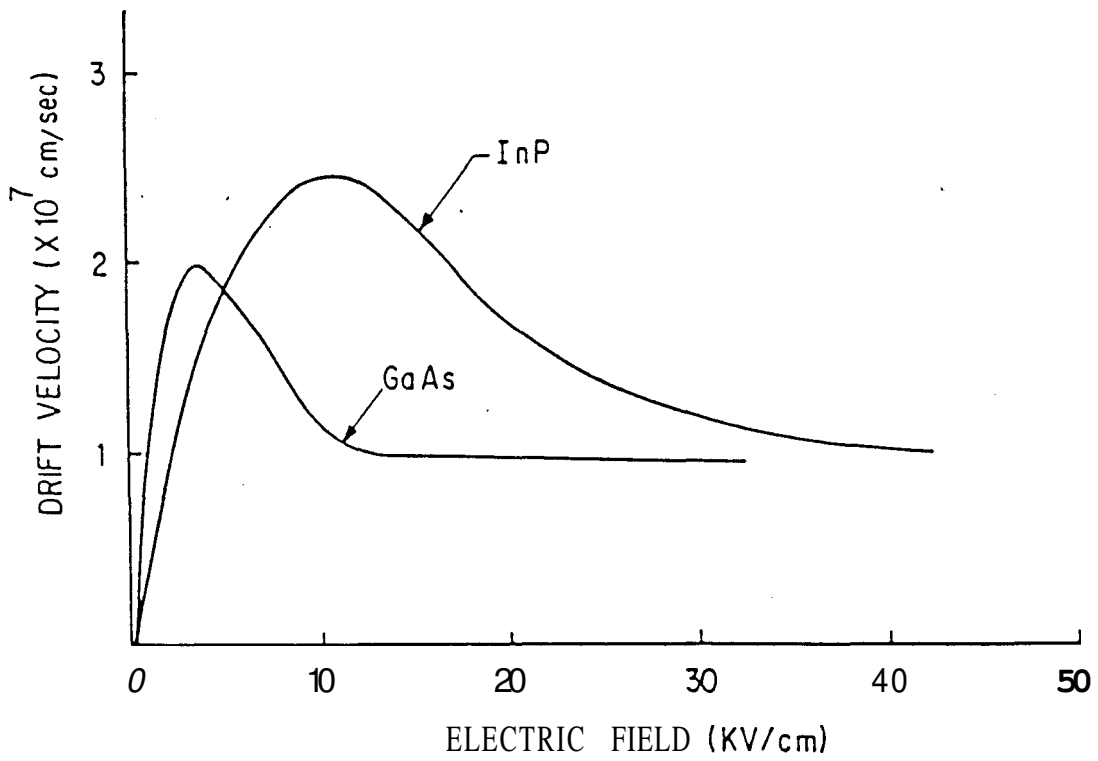Figure **2.3:** Energy band diagrams for GaAs and InP (after Eastman 1976).

Figure 2.4: Electric field versus drift velocity characteristics for GaAs and InP (after Kuno 1981).

2.4 Oscillator designs for W-band

Nearly all the designs reported in the literature consist of a Gunn diode embedded in a resonator whose fundamental frequency is in the range 30-60 GHz with the second harmonic being coupled out through a waveguide which is below cut-off for the fundamental. The differences are in the design of the fundamental frequency resonator. Tuning is done by mechanically changing the resonance frequency of this resonator. The resonator may be a waveguide cavity tuned by a backshort (Lazarus et *al.* 1981; Barth 1981; Bester, Jacobs and Vowinkel 1983) or a disk and post co-axial arrangement tuned either by inserting a tuning rod near the disk giving a small tuning range (Ruttan 1975; Haydl 1981) or by changing the resonator position resulting in a wider tuning range (Ondria 1979; Arora and Sarma 1984) or by mechanically changing the post length giving the largest tuning range reported so far (Haydl 1983; Carlstrom, Plambeck and Thornton 1984). A second backshort is incorporated in the second harmonic guide which helps improve the power output. Crossed waveguide oscillators with separate waveguides for the fundamental and second harmonic frequencies have been built but with limited tunability (Bester, Jacobs and Vowinkel 1983). The oscillator with a mechanically adjustable post length was chosen for fabrication in view of its excellent performance. Being a second harmonic extraction oscillator, its frequency is not very sensitive to loading because the fundamental is not coupled to the output. This gives enough isolation that there is no need to provide a separate isolator between the LO and the mixer.

2.5 Wide-band oscillator design

The design of the oscillator described below is the same as that of Carlstrom, Plambeck and Thornton(1985) but for modifications to do away with the miniature linear bearing as described below. Figure 2.5 shows the cross sectional view of the oscillator. It consists of a half-height W-band waveguide with a taper to full-height on one side. The Gunn diode is mounted in a hole drilled in the half-height portion. The lower impedence of the reduced height waveguide improves the matching to the low impedence Gunn diode. A co-axial cavity whose central conductor supplies the bias voltage to the diode, intersects the guide directly above the diode. The bias choke which forms the top wall of the cavity can be moved vertically. The central conductor has a thin disk at the end where it contacts the diode. The motion of the choke changes the length of the cavity giving frequency tuning.
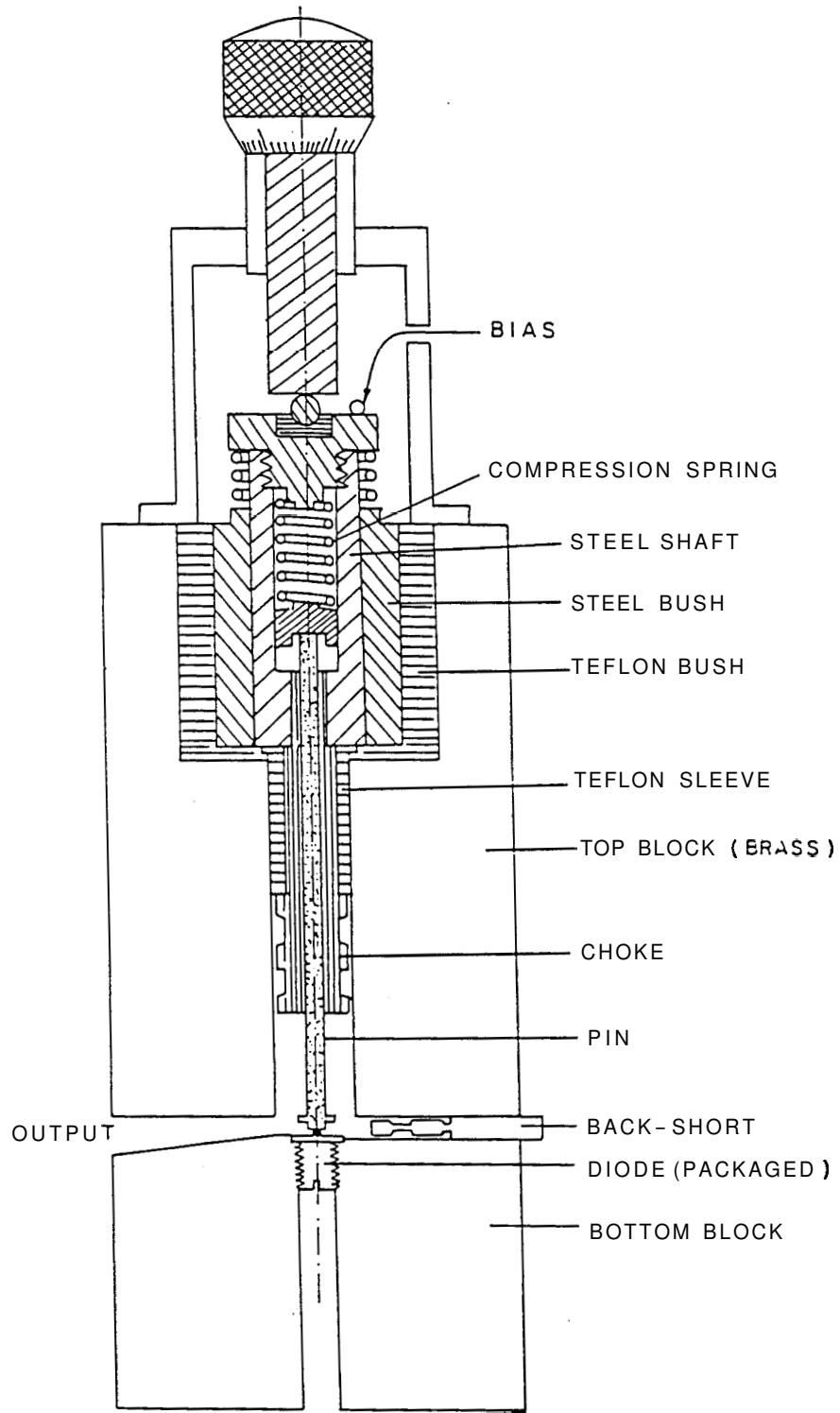
BIAS

COMPRESSION SPRING

STEEL SHAFT

STEEL BUSH

TEFLON BUSH

TEFLON SLEEVE

TOP BLOCK (BRASS)

CHOKE

PIN

OUTPUT

BACK–SHORT

DIODE (PACKAGED)

BOTTOM BLOCK

Figure 2.5: Cross-sectional view of the tunable Gunn oscillator (not to scale).

If tlie diode is placed in tlie negative conductance region by applying a suitable bias voltage, oscillations build up at the resonance frequency of the circuit formed by the co-axial cavity, the disk, the post and the diode. The parameters are such that this frequency is half the desired output frequency. The oscillations are confined to the cavity because the waveguide is below cut-off for this frequency. But the non-linearity of the diode V-I characteristic results in fields oscillating at the second (and higher) harmonic freequency which the guide propagates. The disk now acts as a radial line transformer helping to match the guide impedance to the diode. The reactive part of tlie diode impedance is tuned out by tlie non-contacting backshort provided.

2.6 Fabrication

The fabrication of the oscillator requires extreme care, especially because the choke sections with small airgap ~ 50 micron (crucial for the output power level) should be able to move without touching the outer wall. The oscillator is fabricated as a split block in brass. First two cylindrical brass blocks are fixed together with screws and dowels in tlie bottom block. The diode mounting hole is drilled first extending upto the top block. The bottom block is then removed arid the hole in the top block is reamed to 2.95mm to form the outer wall of the co-axial cavity. This ensures that the co-axial cavity is centered above tlie diode. The outer surface of the block and the hole are machined in one setting and hence are concentric. Then the top face of the top block is bored to receive the teflon bush, with the outer diameter of the block dialled to ensure concentricity. Then the teflon bush is press fitted to this hole and bored to receive the steel bush. The steel bush is made out of oil hardening non-shrinking steel (OIINS), hardened and made smooth by grinding and lapping the inner surface. Hardening is necessary to acheive low wear. This steel bush is press fitted into the teflon bush.

The next operation is to mill the waveguide in the bottom block with the taper on one side. The steel shaft which carries tlie choke is seperately machined out of OHNS, ground, lapped arid hardened. It has a central hole to accomodate the compression spring. Its outer diameter is such that it makes a smooth sliding fit to the steel bush. An over-sized teflon sleeve and brass rod arc assembled together and press fitted to the steel shaft. The brass rod is then machined to form the choke after dialling the steel shaft to ensure concentricity. This should be done accurately to avoid the choke shorting while tuning. Finally a central hole is drilled through the choke for the pin and lapped. The pin is separately machined out of brass to

make a snug fit to this hole. A wire is soldered to the steel bush and brought out for bias supply. We have shown if figures 2.6 a,b,c and d the fully assembled oscillator and split views.

2.7   Performance

The oscillator was tested in a set-up consisting of an attenuator, a wavemeter and a power-head. Pins with different disk diameters were tried and the one that gave the best performance was chosen and different diodes were tried. It was found that even diodes of the same type from the same batch gave markedly different power outputs and tuning ranges. It became clear that every time a new diode is to be used some experimentation is necessary with the pin before one gets optimum performance. The way the characterictics of the oscillator would change with pin dimensions is predictable to a large extent based on previous work and is also understood phenomenologically (see, for expample, Arora 1984).

A 35 GHz diode made by Microwave Associates (MA49713) performed best. Its tuning and power curves are shown in figure 2.7. The phase lock system described by Arora(1984) was used to lock the oscillator using the bias tuning property of the Gunn oscillators.

2.8   Conclusion

An ultra wide-band mechanically tunable Gunn oscillator of simplified construction based on a design by Carlstrom, Plambeck and Thornton(1985) has been fabricated for use as local oscillator with low-noise receivers for the 3 mmm atmospheric transmission window. It gives a CW power output of at least 1 mW which is more than adequate for pumping a low-noise Schottky mixer, covering the frequency range 75-115 GHz. It has been successfully phase-locked to a highly stable VHF reference source using the bias tuning property of the oscillator.

Figure 2.6 (a): A fully assembled Gunn oscillator.

Figure 5.2 (b) A pseudo color image of the kinetic temperature distribution over CG22-Blob-1. The scale is in units of Kelvin.
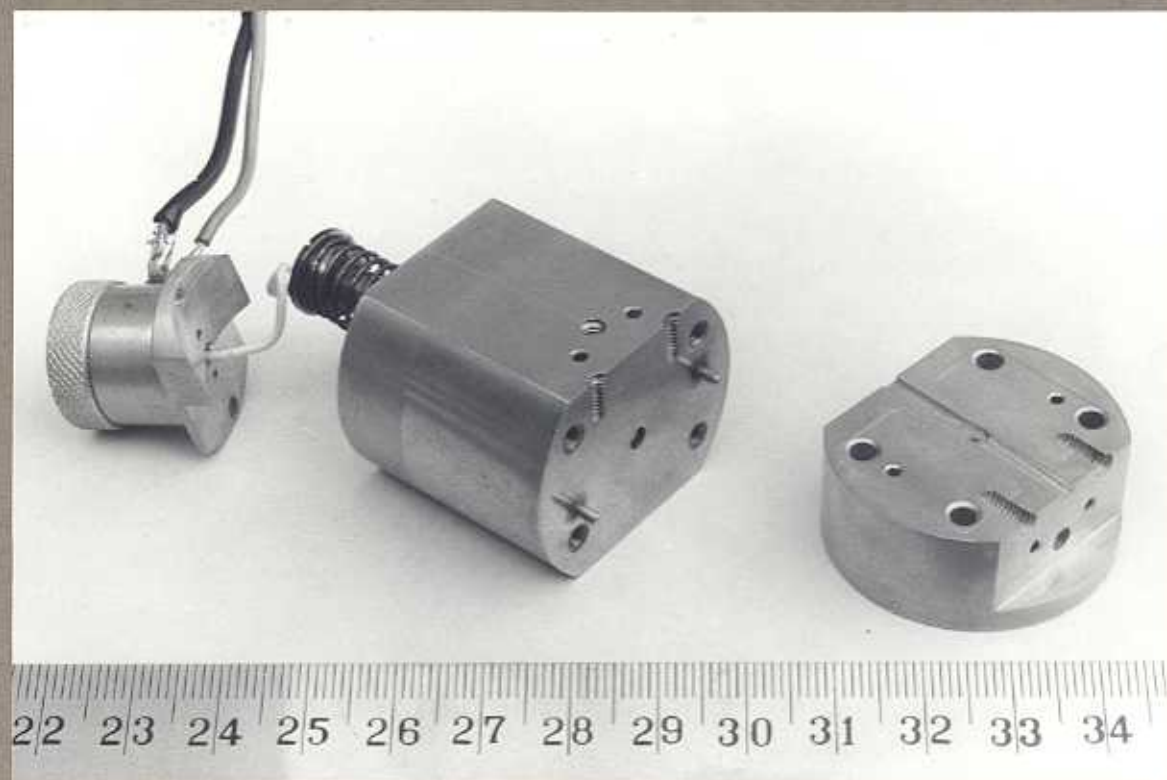
Figure 2.6 (c): Split view of the Gunn oscillator showing the Gunn diode mounted in the waveguide.
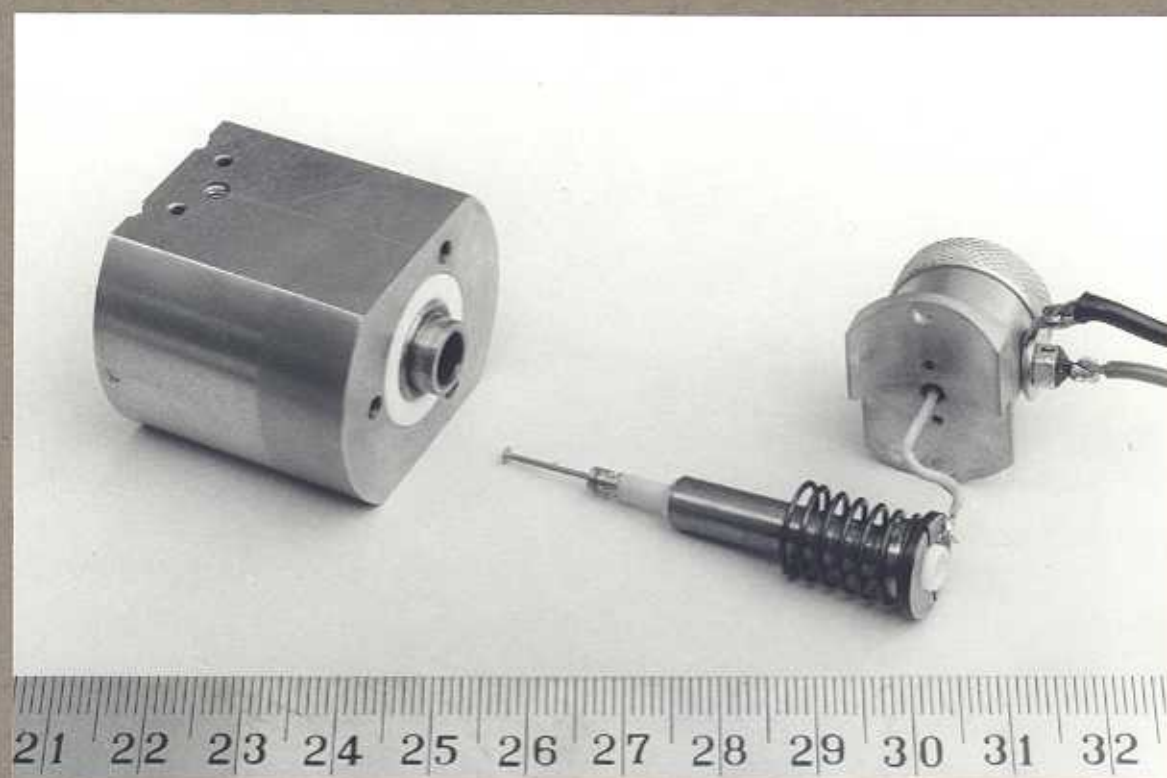
Figure 2.6 (d): Split view of the Gunn oscillator showing bias choke mounted on the movable steel shaft and the pin.
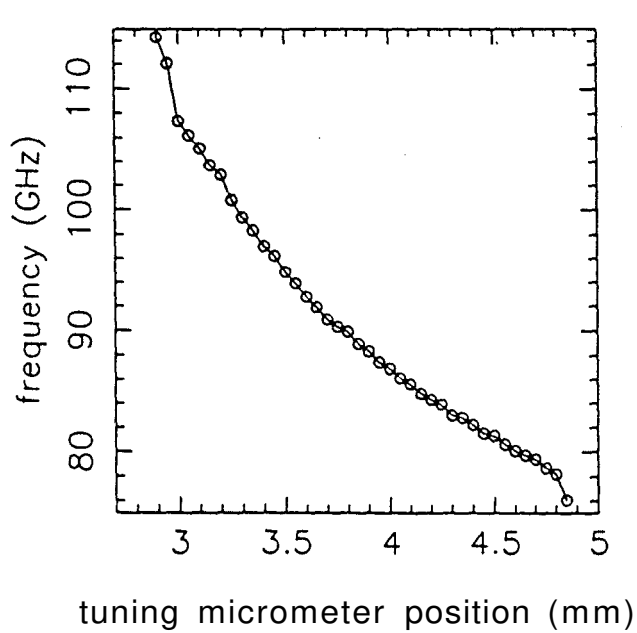
(a)
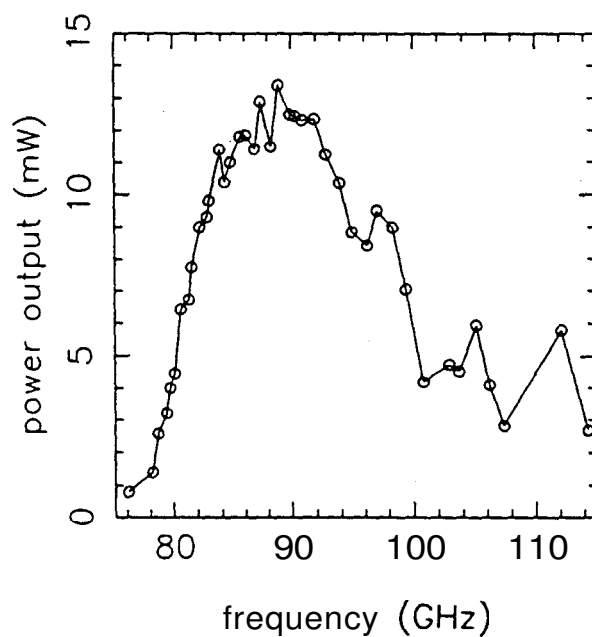
(b)

Figure 2.7: (a) Tuning curve of the tunable oscillator. The tuning micrometer position is with respect to an arbitrary reference. (b) Power output of the oscillator. The tuning backshort and the bias voltage were optimised to get maximum power output.

REFERENCES

Arora, R.S., 1984, Ph.D Thesis, Indian Institute of Science, Bangalore.

Arora, R.S., Sarma, N.V.G., 1984, *IETE Technical Review*, 1, 25.

Barth, H., 1981, Proc. IEEE *MTT-S International* Alicrowave *Symp.*, 334.

Bester, M., Jacobs, K., Vowinkel, B., 1983, in *Proc.* of the *13th* European Microwave Conference (Nurnberg). 308.

Carlstrom, J.E., Plambeck, R.L., Thornton, D.D., 1985, IEEE Trans. Microwave Theory Tech., MTT-33, 610.

Eastman, L.F., 1976 in *Microwave* Derices, ed. M.J. Howes & D.V. Morgan (John Wiley & Sons), p. 11.

Erickson, N.R., 1977, IEEE *Trans. Microwave Theory* Tech., MTT-25, 865.

Gunn, J.B., 1963, Solid State *Communications*, 1, 88.

Hilsum, C., 1962, Proc. IRE, 50, 185.

Haydl, W.M., 1981, *Electron.* Left., 17, 825.

Haydl, W.M., 1983, IEEE Trans. *Microwave* Theory Tech., MTT-31, 879.

Kuno, H.J., 1981, *Microwave Journal*, **24**, 21.

Lazarus, F.R., Pantoja, F.R., Novak. S., Somekh, M.G., 1981, IEEE *Trans.* Microwave *Theory Tech.*, **MTT-30**. 824.

Ondria, J., 1979, in *Proc. 7th Biennial Conf. Active Microwave Semiconductor* Devices *and Circuits*(Cornell Univ., Ithaca, NY).

Penzias, A.A., Burrus, C.A., 1973, *Annu. Rev. Astron. Astrophys.*, **11**, 51.

Ridley, B.K., Watkins, T.B., 1961, Proc. *of* the *Physical* Society, bf 78, 293.

Ruttan, T.G., 197.5, *Electron. Lett.*, 11. 293.

Rydherg, A., 1988, Ph.D. Thesis, Chalmers University of Thechnology, Goteborg.

Chapter 3

Observations

3.1 The Observing System

All the observations were made with the 10.4m millimeter wave radio telescope at the Raman Research Institute campus at Bangalore (longitude: 77° 35'; latitude: 13° 01'N; 930m above mean sea level.) The observing system used lias been described in some detail by Patel(1990). We give a brief description here. Figure 3.1(a) shows the telescope. A schematic diagram of the system is shown in figure 3.1(b). Tlie telescope has an altitude-azimuth mount with the receiver at the Nasmyth focus. The primary is a 10.4m paraboloid made from hexagonal honeycomb sandwiched aluminium panels, with a surface accuracy of $\sim 100\mu$ rms. Tlre secondary is a hyperboloid of diameter 60cms and eccentricity 1.06. The tertiary mirror can be switched to throw tlie beam a few arcminutes. The receiver is a 20K cooled Schottky mixer type with 1.5 GIIz IF. Tlie IF output is further down converted to 400 MHz before being fed to tlie backencls. The backends in use are a 256 channel filterbank with 250 kHz resolution and a 500 channel acousto-optic spectrometer (AOS) with 50 kHz resolution.

3.2 Observing Method

All the CG observations were carried out in the *frequency switched mode* for three reasons. (i) Some of the CGs are bigger than the beam throw available in the beam switching system. The largest CG (CG 22) lias a size of $\sim 5'$. The beam switching system can give a maximum beam throw of only 160"; (ii) Tlie system is not stable enough to allow position switching; (iii) Frequency switching makes best use of tlie available time and is the only method possible for extended sources; the other two methods waste at least half the time looking at source-free positions, even if possible. In frequency switching the line from the source is received in different parts of the receiver pass band during alternate switching periods. This means that no time is wasted. But because between successive switching periods the receiver characteristics arc. changed (by re-tuning) the subtraction between tlie ON and OFF spectra will not be esact leading to curved baselines. Since we are not looking for low level extentled spectral features, baseline curvature is not a serious handicap in this case. A frequency offset of 15.25 MIIz was used between the ON and OFF frequencies, this being the period of the baseline ripple. This choice recluced considerably the ripple in tlie final spectra requiring only polynomial fits to remove baselines. A typical baseline is shown in figure 3.2, along with a fourth order polynomial fit. The two spectral features seen arc from tlie ON and OFF frequency

Figure 3.1 (a): The 10.4-meter millimeter-wave radio telescope at the Raman Research Institute campus, Bangalore.
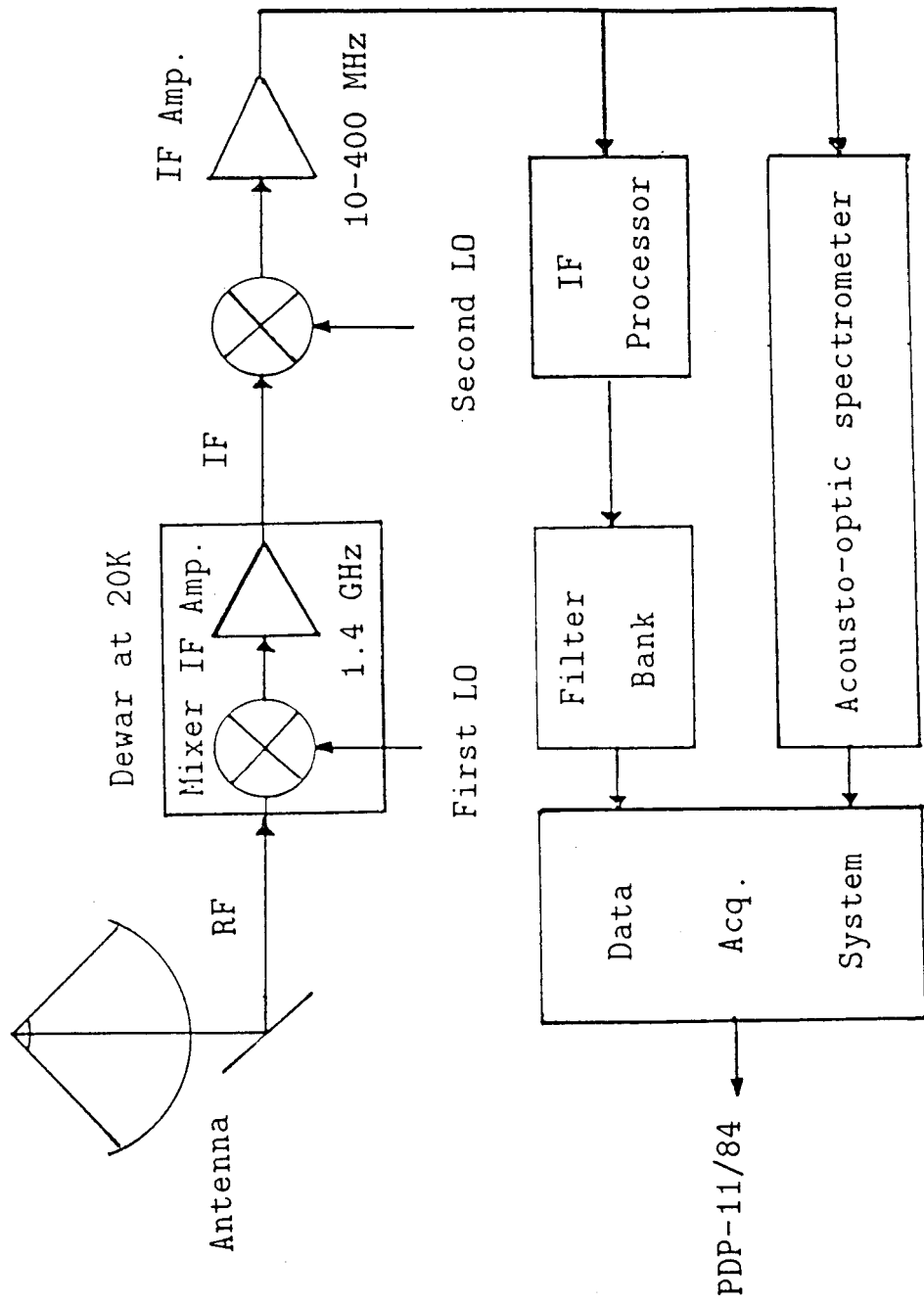
Figure 3.1 (b): A simplified block diagram of the receiver system at the 10.4m telescope.
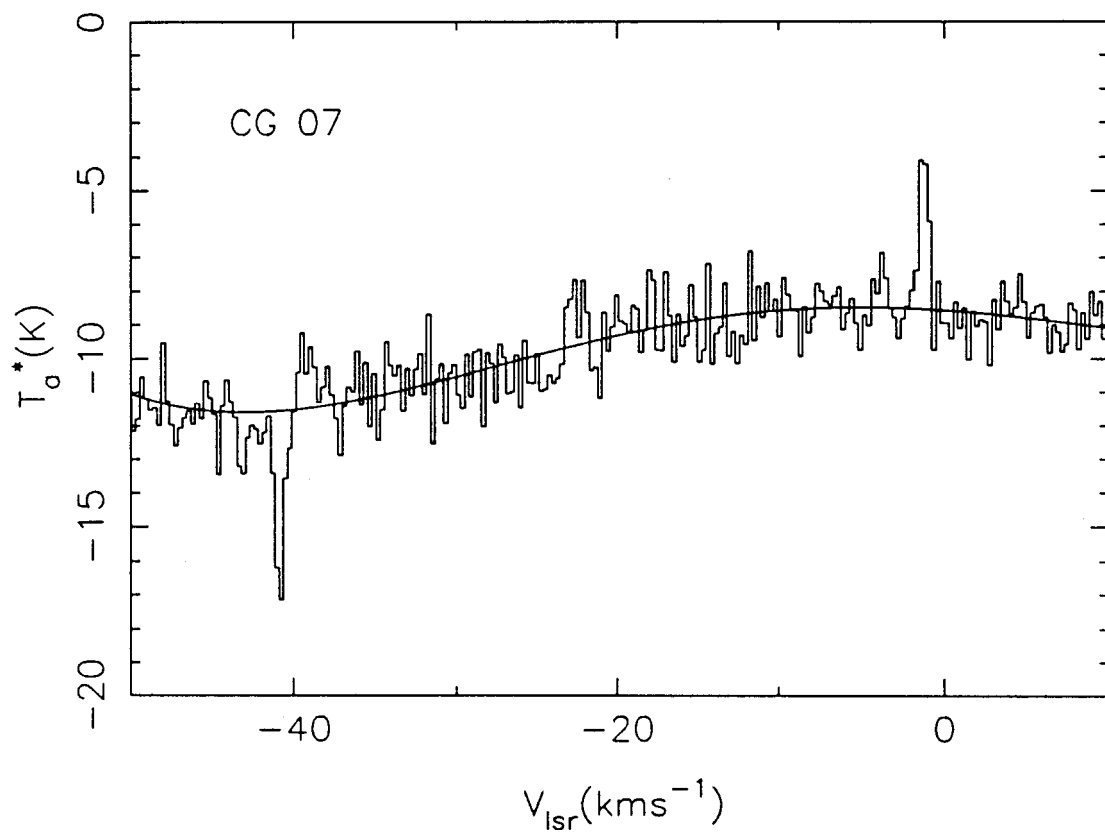
Figure 3.2: A typical baseline obtained with frequency switching. The positive and negative spectral lines of ^{12}CO are from the ON and OFF frequency observations. A fourth order polynomial fit is also shown.

observations. This spectrum is shifted, inverted and averaged with tlie unshifted to get full S/N in the final spectrum.

The switching rate was 2 Hz. Calibration was done using an ambient temperature chopper at intervals of several minutes. During the observations the atmospheric optical depth at zenith was typically 0.2. measured by telescope tipping. All tlie observations were carried out at elevations ranging froni 25 to 40 deg. Pointing was checked by observing Jupiter in the beam switched mode, by a procedure described by Patel(1990). Even though Jupiter covers only a specific track in tlie sky, the pointing model itself has been found to be applicable to all parts of tlie sky from observations of SiO masers. The pointing errors during the observations were less than $20''$ with the rms being $6''$. Figure 3.3 shows the distribution of tlie pointing errors. All the data interpreted in this thesis were obtained during 1990-91 using an AOS with 50 kIIz resolution as back-elid. The data froni this AOS was later bunched to get 100 kHz resolution spectra giving a velocity resolution of 0.26 kms^{-1}. The frequency stability arid resolution of the AOS was checked by injecting a CW before observation every clay. In addition, the head of CG22 was observed several times spread over two months to get an estimate on the overall error in velocity measurements. A histograni of the distribution of errors is shown of figure 3.4. *The rms of this distribution is 0.15 kms^{-1} and we regard this number as the error on all velocity measurements reported in this thesis.* Ttie telluric CO line was seen in many spectra. It was easy to identify these lines froni the fact that the telluric lines always appear at an LSR velocity equal to the negative of tlie LSR correction applied.

3.3 The 1989 run

The co-ordinates for the CGs in the Gum Nebula have been listed by various authors (Ilawardeen and Brand 1976; Sandqvist 1976: Zealey *et al.* 1983; Reipurth 1983). Hartley *et al.*(1986) and Feitzinger and Stuwe(1984) have noted many of tlie CGs in their catalogues of dark clouds and globules found from the SERC plates and the ESO B plates, respectively. Ilowever, a comparison of co-ordinates listed by the various authors showed inconsistencies. The ZS3 co-ordinates were sometimes found to have large errors (as much as $25'$ for CG2). Whenever there was disagreement we used those values which agreed with more than one list. In cases where only 283 or one more author listed co-ordinates, values from ZS3 were used. Using these criteria 27 CGs were observed during 1989. Frequency switching by 16 MHz was used. An ambient-temperature chopper-wheel was used for calibration. The back-end was an acousto-optic spectrometer with 216 kIIz resolution and 120 MIIz coverage. Pointing
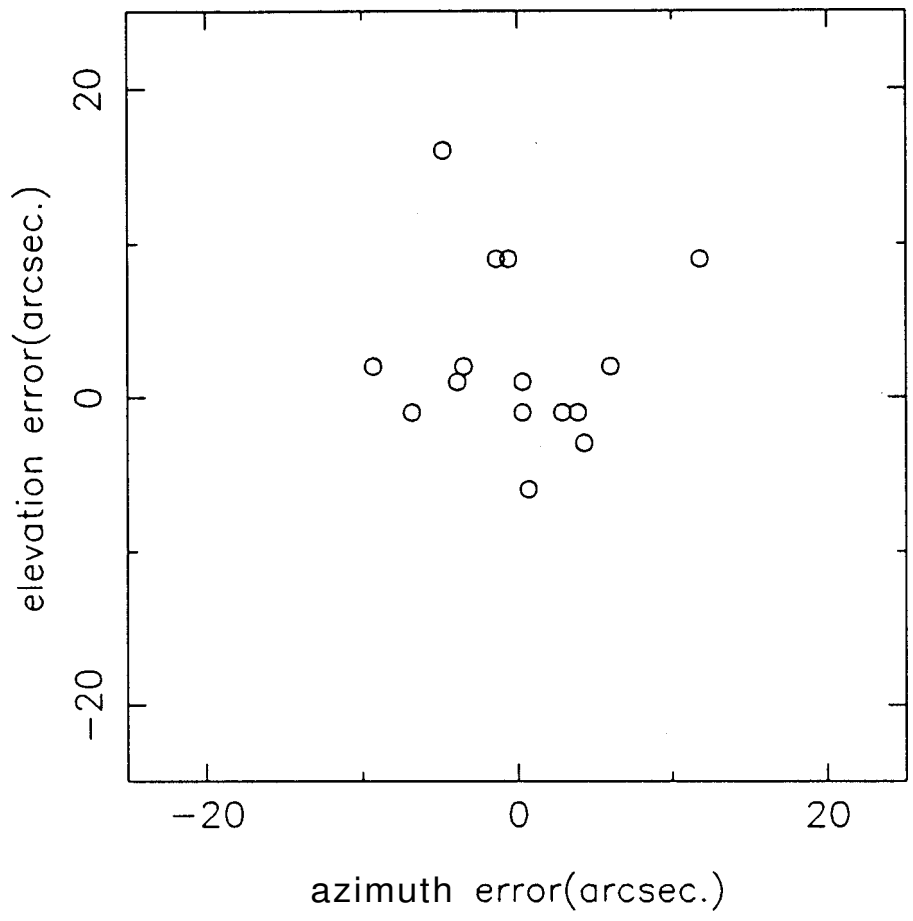
Figure **3.3:** Distribution of pointing errors measured on Jupiter.
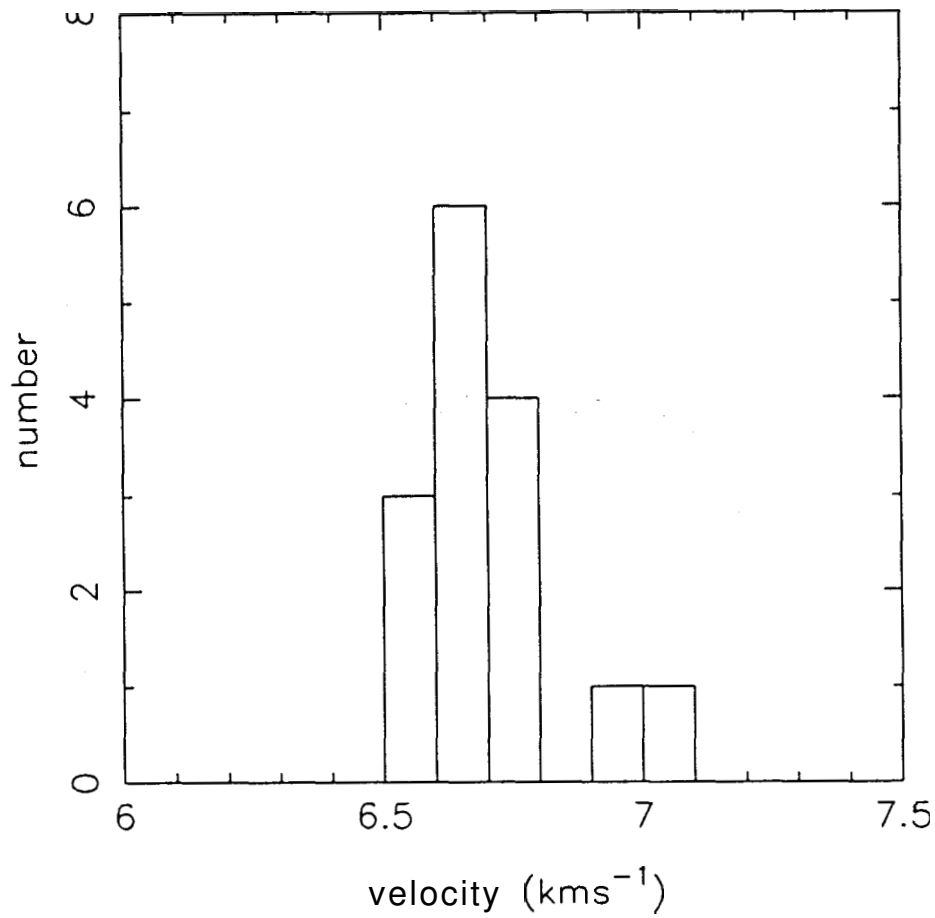
Figure 3.4: Histogram showing the distribution of the velocities measured for the head of CG22 over two months. The velocities were obtained by fitting gaussians to the lines. The rms of the distribution is 0.15 kms^{-1}.

acousto-optic spectrometer with 216 kHz resolution and 120 MHz coverage. Pointing was checked by continuum scans on Jupiter (See Patel, 1990 for details). Fourth order polynomials were fitted to remove baseline curvature. A sample spectrum is shown in figure 3.5. The noise levels and measured antenna temperatures are given in Table 3.1. Only 18 out of the 29 CGs could he detected. This was surprising because the 1′ beam of the telescope is ideally suited for detecting the CGs. It was therefore suspected that co-ordinate errors could he the cause for non-detections, especially in view of the disagreement between the different catalogs. So it was decided to remeasure tlie co-ordinates for all the CG heads and their tails from the ESO plates.

3.4   New co-ordinates

The co-ordinates of the CGs were measured from contact prints of ESO plates by relatively crude methods using magnifiers and graph sheets. The plate parameters were derived using a few known stars (listed in the SAO catalog 1966) which were used to estimate the co-ordinates for the heads and tail-ends of CGs. The errors on these measurements (estimated by leaving out one star at a time from the set used to estimate plate parameters and comparing the co-ordinate estimated for this star to its co-ordinate listed in the SAO catalog) are less than $10''$. CG17, CG18, CG23 and CG34, however, could riot be located in these plates. The new measured co-ordinates of the head and tail-ends along with the tail lengths are listed in Table 3.2. Tlie co-ordinates listed are largely from our measurements. For sorne CGs and the Gum Dark Clouds (GDCs, Reipurth 1983) the co-ordinates are from published literature as mentioned in the table. CG32 seems to have two components which are listed as CG32A and B. We have listed tlie individual blobs in CG22 as seperate CGs. The measured co-ordinates show significant differences from those reported earlier. The distribution of these errors is shown is figure 3.6.

3.5   1990-91 run

During 1990-1991 a second run of ^{12}CO observations was carried out using tlie new co-ordinates. In addition to tlie heads, a few points along tlie tails were observed. All the CGs, except CG23 and CG34, were now detected. Tlie observation procedure was the same as before, except that tlie back-end used was an AOS with 50 kHz resolution arid 30 MHz coverage. A sample spectrum is shown in figure 3.7. We have
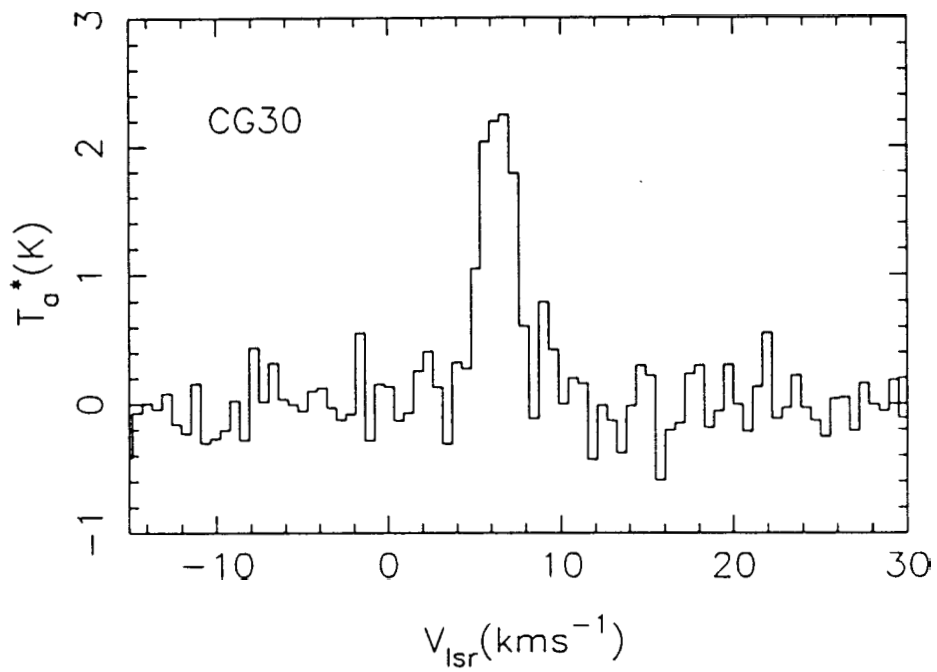
Figure 3.5: A sample ^{12}CO spectrum from observations made during 1989. A fourth order polynomial has been subtracted to remove the baseline curvature due to frequency switching. The back-end was an AOS with 216 kHz resolution.

Table 3.1. 1989 observations.

CG number	$T_a^*(89)$ K	v_{LSR} kms^{-1}	rms K
1	2.3	4.8	0.23
2	2.3	5.4	0.21
3	1.4	0.9	0.34
4	2.1	2.6	0.28
5			0.28
6	1.1	0.9	0.28
7			0.20
8	1.4	−4.9	0.35
10			0.36
13	2.5	4.8	0.21
14	2.3	0.1	0.50
16	1.4	−0.8	0.27
17	0.9	4.8	0.24
18			0.29
22	3.5	7.1	0.37
23			0.31
24	1.3	−11.5	0.23
25			0.34
26			0.16
27	1.5	5.8	0.28
28	0.9	6.5	0.21
29			0.31
30	2.2	5.9	0.22
31	4.9	6.4	0.36
32	0.8	4.8	0.25
33			0.36
36			0.45
37	1.2	7.6	0.25
38			0.21

Note: **a** blank indicates non-detection

Table 3.2. co-ordinates of the cometary globules in the Gum Nebula.

source	co-ordinates (1950.0)												tail length (arc min)	ref.
	head						tail-end							
	RA			DEC			RA			DEC				
	h	m	s	o	'	"	h	111	s	o	'	"		
CG01	7	17	49.7	−44	29	26.2	7	15	39.4	−44	29	2	23	M
CG02	7	14	31.3	−43	52	43.8	7	12	49.3	−43	51	24.6	18	M
CG03	7	37	45.9	−47	45	35.1	7	37	26	−47	47	51.4	4	M
CG04	7	32	45.6	−46	50	8.9	i	30	40.5	−46	56	43.2	22	M
CG05	7	39	15.8	−43	42	8.3	7	39	4.6	−43	41	55.1	2	M
CG06	7	29	2.1	−46	37	14.5	i	28	18.9	−46	41	35	9	M
CG07	9	12	26.1	−42	16	54.4	9	13	14.2	−42	18	14.6	9 ·	M
CG08	7	41	1.3	−41	8	32.8	7	40	46.5	−41	S	23.2	3	M
CG09	7	39	7.4	−41	20	4.1	7	38	52.6	−41	19	6.3	3	M
CG10	7	40	55.2	−41	58	11.9	7	40	34.6	1	59	48.4	4	M
CG13	7	12	49.1	−48	23	16.4	7	10	17.6	−48	30	0.2	26	M
CG14	7	37	16.2	−49	1	29.5	7	36	22.4	−49	52	51.8	12	M
CG15	7	31	0.5	−50	39	20.2	i	29	55.2	−50	45	29.1	12	M
CG16	7	26	19.4	−50	58	32.6	7	25	47	−51	1	48.7	6	M
CG17	S	51	0	−51	41		S	51	6.5	−51	42	44.4	2	Z
CG18	8	51	0	−50	29		8	51	2.6	−50	30	57.4	2	Z
CG22B1	S	26	48.0	−33	34	12.0	S	27	1 6	−33	14	12	21	S
CG22B2	S	27	16.7	−33	14	12.0	8	28	-1.1	−32	46	11	30	S
CG23	7	34	48	−50	6		7	34	14.6	−50	10	30	7	Z
CG24	8	17	33.0	−42	44	58.4	S	17	14.5	−42	48	45.S	5	M
CG25	7	35	56.0	−47	50	15.1	7	35	19.2	−47	54	47.5	S	M
CG26	8	14	3.3	−33	40	52.8	S	14	12.9	−33	37	36.1	4	M
CG27	8	10	28.4	−33	36	11.6	8	10	33	−33	33	53.6	2	M
CG28	S	10	26.2	−33	46	32.4	S	10	25.8	−33	45	12	1	M
CG29	8	10	27.9	−33	51	54.2	S	10	32.6	−33	49	36.1	3	M
CG30	S	7	40	−35	56	2	8	i	13.4	−35	30	34.1	26	R
CG31A	S	7	10	−3.5	52	24	8	6	36.9	−35	26	53.2	26	R
CG31B	8	6	55	−35	54	14								R
CG31C	S	6	40	−35	50	44								R
CG31D	S	6	24	−35	52	58								R
CG31E	S	6	21	−35	55	1 s								R
CG32A	8	12	28.6	−34	21	8.4	8	12	10.8	−34	8	27.9	13	M
CG32B	S	12	2 2 .	−34	18	58.6	8	12	10.8	−34	8	27.9	11	M

Table **3.2.** continued.

source	co-ordinates (1950.0)												tail length (arc min)	ref.
	head						tail-end							
	RA			DEC			RA			DEC				
	h	m	s	o	′	″	h	m	s	o	′	″		
CG33	8	13	33.7	−33	55	19.4	8	13	40.3	−33	52	39	**3**	M
CG34	7	27	54	−41	4		7	27	19	−40	57	24	9.4	Z
CG36	8	35	22.7	−36	27	23.9	8	*35*	46.5	−36	22	47.1	7	M
CG37	8	10	29.4	−32	56	21.7	8	10	30.8	−32	52	25.1	4	M
CG38	8	7	47	−36	1	42								R
GDC1	8	24	17	−50	52	5								R
GDC2	8	25	10	−50	51	42								R
GDC3	8	24	56	−50	41	13								R
GDC4	8	25	2	−50	29	53								R
GDC5	8	26	1	−51	0	2								R
GDC6	8	30	30	−50	22	46								R
GDC7	8	32	**39**	−50	S	21								R

References:

Z: Zealey *et. al.*, 1983

R: Reipurth, 1983

S: Sahu ef. *al.*, 1988

M: Our measurements from ESO plates.

Notes:

1. For CGs 31B,C,D,E and 38 tail co-ordinates are not available.
2. The Gum Dark Clouds (GDCs) have been included for completeness.
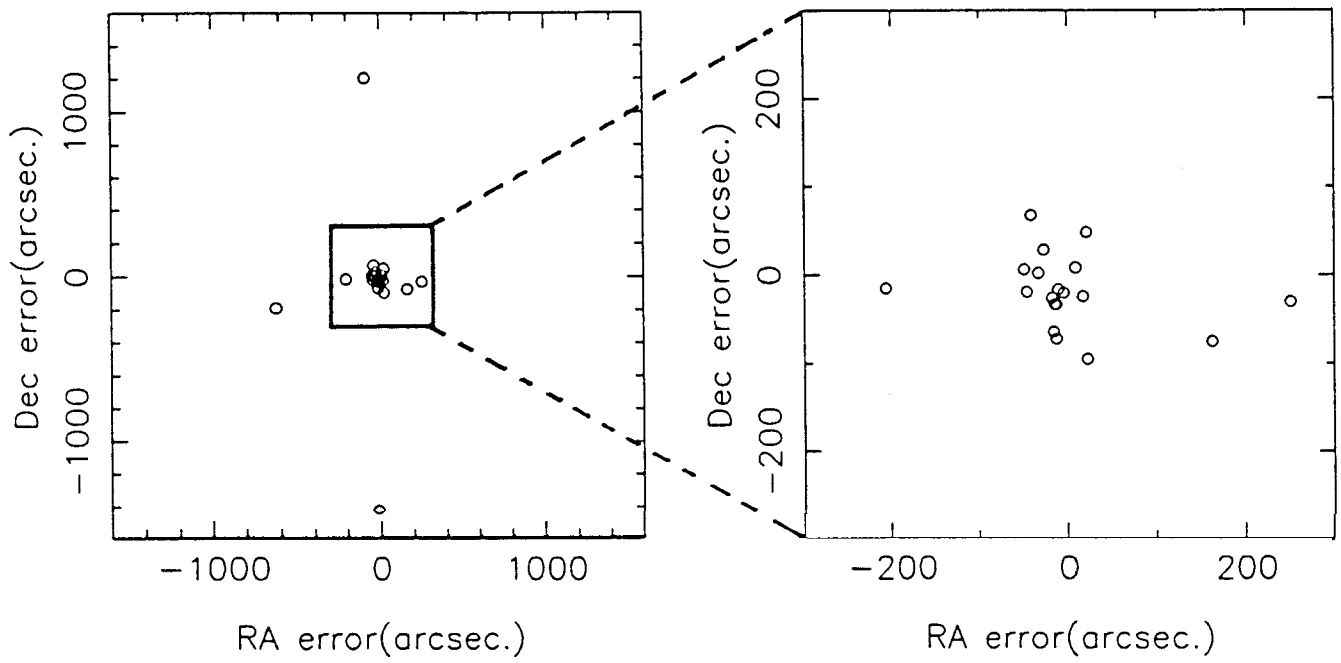
Figure 3.6: Distribution of the errors in the co-ordinates of the CGs. The *error* is defined as the difference between the co-ordinate obtained from literature and that measured from SERC plates.
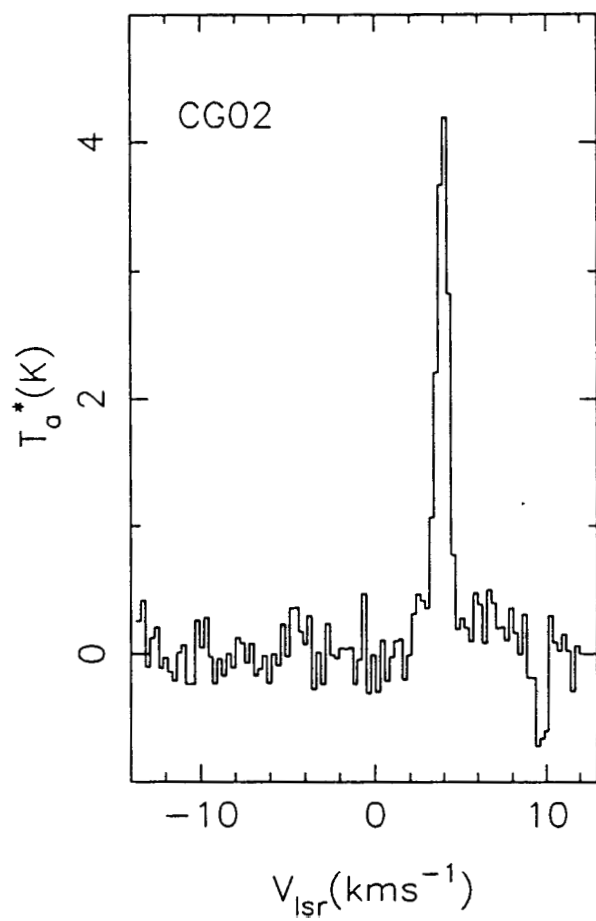
Figure 3.7: A sample ^{12}CO spectrum from observations made during 1990-91. A fourth order polynomial has been subtracted to remove the baseline curvature due to frequency switching. The back-end was an AOS with 100 kHz resolution.

listed in Table 3.3 the noise levels, measured antenna temperatures and the LSR velocity found by fitting gaussians to the lines from the heads of the CGs. These observations are interpreted in Chapter 4.

3.6   Detection statistics

To establish the reason for non-detections during the previous run, we have plotted in figure 3.8, a histogram of the number of detections and non-detections in the 1989 observations as a function of the co-ordinate errors (defined as the co-ordinates used in the first run *minus* measured co-ordinates used in the second run). Those CGs having large headsizes (CGs 1,2,4,6,22 and 30) have been excluded from the histogram because the errors will not affect their detection. Those CGs for which co-ordinates were not remeasured have also been excluded. It is seen from figure 3.8 that there are no detections if the error is larger than 1'. The four non-detections with error < 1' are CGs with small head sizes (< 1') for which the effect of even small errors and beam dilution are important.

We therefore conclude that the primary cause for non-detections during the first run was the use of wrong co-ordinates.

3.7   Observations of tails

Typically, four points were observed along the tails for 21 CGs. The observation procedure was the same as for the heads. The points observed were spaced equally along the tails. These observations are summarised in table **3.4.** The velocities, widths and line strengths were obtained by fitting gaussians to the lines. A part of Chapter 4 is devoted to a discussion of these observations.

3.8   Mapping of CG22

The head of the globule CG22, and a part of its tail were mapped in ^{12}CO and ^{13}CO with a grid spacing of 1' both in RA and DEC. Most of the grid points were observed twice and were compared for consistency before averaging. In addition, the center point of the grid was observed every day to ensure uniform calibration. These observations were made with a filter bank back-end of 250 kHz resolution. After

Table 3.3. 1990-91 observations.

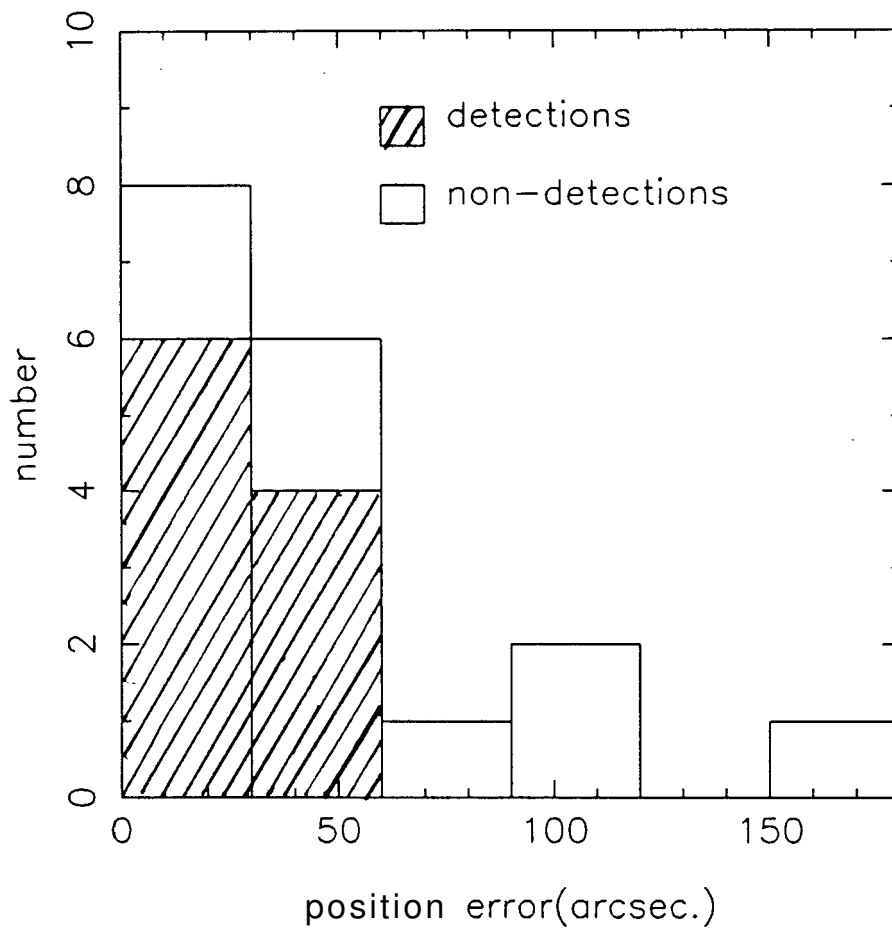| source	T_a^* K	v_{LSR} kms^{-1}	v_{FWHM} kms^{-1}	rms K
CGO1	5.3	3.3	1.4	0.33
CG02	4.2	4.1	0.9	0.22
CG03	3.3	0.1	1	0.32
CGO4	1.2	1.7	1.2	0.25
CG06	2.9	0.9	1.1	0.26
CG07	5.2	−1.1	0.6	0.54
CGOS	1.7	−5.8	1	0.2
CG09	3.9	−4.2	1.3	0.59
CG10	3.9	−5.5	1.0	0.19
CG13	3.7	**3.7**	0.8	0.41
CG14	3.0	−0.9	1	0.28
CG15	3.6	−0.8	0.6	0.57
CG16	2.9	−0.7	0.7	0.22
CG17	0.8	3.7	0.8	0.33
CG18	1.0	2.0	0.4	0.26
CG22B1	6.4	6.5	1.1	0.41
CG22B2	6.8	6.8	1.3	0.28
CG22B3	3.4	6.4	1.4	0.22
CG24	2.9	−12.5	1.2	0.2
CG25	2.2	−1.8	0.8	0.29
CG26	3.5	2.0	1	0.51
CG27	2.8	5.0	0.8	0.44
CG28	2.9	5.2	1.1	0.54
CG29	2.4	5.2	0.7	0.31
CG30	3.8	5.8	2.2	0.25
CG31A	4.5	6.0	1.3	0.44
CG31B	4.2	6.0	1	0.36
CG31C	6.8	6.3	1.6	0.3
CG31D	1.5	6.9	1.6	0.29
CG32A	4.5	4.9	1.2	0.43
CG32B	4.7	4.S	1	0.38
CG33	2.3	1.6	0.6	0.46
CG36	1.4	−8.5	0.7	0.39
CG37	3.0	6.2	0.4	0.48
CG38	1.7	7.0	1.2	0.23
GDC1	5.6	5.3	1.3	0.36
GDC2	5.1	6.0	1.4	0.36
GDC3	1.9	5.9	1.0	0.43
GDC4	3.1	4.9	1.3	0.52

Figure **3.S:** **A** histogram showing the number of detections and non-detections in the observations done in 1989.

Table 3.4. observations of the tails.

source	T_a^*	v_{LSR}	v_{FWHM}	rms	distance from head in arcmin
	K	kms^{-1}	kms^{-1}	K	
CG1H	5.3	3.3	1.4	0.33	0.0
CG1T2	4.0	3.7	1.1	0.55	14.2
CG1T3	4.2	3.7	1.4	0.39	21.2
CG1T4	4.3	3.4	1.4	0.43	7.0
CG2H	4.2	4.1	0.9	0.24	0.0
CG2T1	1.0	5.1	0.6	0.19	25.3
CG2T3	1.5	4.9	0.9	0.28	19.1
CG2T4	3.4	4.5	1.4	0.41	6.5
CG3H	3.3	0.0	0.9	0.33	0.0
CG3T2	2.0	0.1	0.9	0.32	2.1
CG3T3	2.6	0.1	0.8	0.37	3.2
CG3T4	4.3	0.3	1.1	0.36	1.0
CG4H	1.2	1.7	1.2	0.23	0.0
CG4T1	4.9	1.9	1.2	0.49	17.4
CG4T2	5.6	1.3	1.5	0.43	8.7
CG4T3	5.3	1.7	1.3	0.50	13.0
CGGH	2.9	0.9	1.1	0.26	0.0
CG6T1	1.7	1.6	1.5	0.22	10.9
CG6T2	1.5	0.8	0.8	0.20	5.4
CG6T3	1.0	0.9	1.1	0.21	8.1
CG6T4	3.5	0.8	1.0	0.35	2.7
CG7H	5.4	−1.1	0.6	0.54	0.0
CG7T2	4.1	−1.3	0.7	0.51	1.0
CG7T3	2.4	−1.3	0.9	0.43	1.4
CG7T4	5.4	−1.2	0.8	0.25	0.5
CG9H	2.7	−4.1	1.1	0.20	0.0
CG9T2	4.1	−4.1	1.0	0.45	1.6
CG9T3	3.3	−3.8	1.1	0.32	2.5
CG9T4	3.5	−3.9	1.1	0.32	0.9

Table 3.4. continued.

source	T_a^*	v_{LSR}	v_{FWHM}	rms	distance from head in arcmin
	K	kms^{-1}	kms^{-1}	K	
CG10T2	5.8	−4.7	2.0	0.48	1.4
CG10T3	5.9	−4.5	1.9	0.36	2.0
CG10T4	4.4	−4.4	2.0	0.33	0.7
CG14H	3.0	−0.8	1.0	0.28	0.0
CG14T2	1.5	−0.9	1.0	0.44	7.4
CG14T3	4.6	−1.0	0.7	1.37	11.3
CG15H	3.6	−0.8	0.5	0.58	0.0
CG15T2	3.6	−0.8	0.8	0.52	8.1
CG15T4	3.8	−0.7	0.9	0.34	4.0
CG16H	3.1	−0.7	0.8	0.20	0.0
CG16T1	1.3	−0.8	1.0	0.17	6.6
CG16T2	3.9	−0.7	1.1	0.53	3.4
CG16T3	2.7	−0.8	1.0	0.52	5.0
CG24H	2.9	−12.4	1.14	0.19	0.0
CG24T1	0.3	−12.4	2.14	0.15	4.2
CG24T2	0.6	−12.0	2.00	0.21	2.1
CG24T4	2.9	−12.0	1.20	0.44	1.0
CG26H	2.5	2.1	0.9	0.18	0.0
CG26T1	1.7	2.2	1.0	0.24	3.5
CG26T3	2.3	2.2	0.9	0.18	2.6
CG26T4	4.6	2.2	0.9	0.41	0.9
CG27H	2.0	5.2	0.7	0.25	0.0
CG27T2	4.2	5.1	0.7	0.40	1.2
CG27T3	2.5	5.2	0.8	0.37	1.8
CG27T4	2.5	5.1	0.8	0.29	0.6
CG29H	2.4	5.2	0.7	0.30	0.0
CG29T1	2.6	5.3	0.7	0.24	2.5
CG29T3	1.7	5.2	0.8	0.18	1.9

Table 3.4. continued.

source	I'	v_{LSR}	v_{FWHM}	rms	distance from head
	K	kms^{-1}	kms^{-1}	K	in arcmin
CG31A	4.5	6.0	1.3	0.42	0.0
CG31AT1	1.7	6.9	1.9	0.22	25.3
CG31AT2	3.8	6.3	1.9	0.15	12.6
CG31AT3	3.5	6.6	1.8	0.14	19.0
CG32AT2	2.5	5.2	1.2	0.39	7.7
CG32AT3	4.9	5.5	1.4	0.35	10.5
CG32AT4	6.6	5.0	1.0	0.36	3.8
CG32AH	4.5	4.9	1.2	0.43	0.0
CG32BH	4.7	4.8	1.0	0.38	0.0
CG32BT2	3.8	5.4	1.0	0.41	5.5
CG32BT4	3.0	4.8	1.4	0.41	2.7
CG33H	2.4	1.6	0.5	0.45	0.0
CG33T1	1.6	1.9	0.5	0.35	3.0
CG33T2	3.1	1.8	0.7	0.43	1.6
CG33T3	2.0	1.8	0.6	0.24	2.2
CG33T4	2.3	1.8	0.5	0.51	0.7
CG36H	3.1	10.4	0.7	0.35	0.0
CG36T2	2.8	10.7	0.9	0.35	2.4
CG36T4	4.2	10.6	1.1	0.40	1.2
CG37H	3.0	6.7	0.4	0.46	0.0
CG37T3	1.0	6.8	0.6	0.22	2.9
CG37T4	2.0	6.9	0.8	0.20	1.0

Note: CG33H, for expample, refers to the head of the globule CG33. Similarly. T refers to the tail. T4,T2,T3,T1 represent the sequence of points along the tails moving away from the head. The numbers in parenthesis are estimated errors in the velocity gradients(see text).

initial data reduction using POPS, the maps were made on AIPS. These observations are interpreted in Chapter 5.

3.9   Comparison with other observations

From the observations described above, we have radial velocities for all CGs except CG23 and CG34 which were not detected. The radial velocities were obtained as the *center velocity of the best fitting gaussian to the lines*. As CG10 and CG30 show two components, we take the velocity of the stronger component.

The Columbia CO survey of the third galactic quadrant (May *et al.*, 1988) covered a part of the region over which the CGs are distributed. Since this survey was done with $0.5°$ resolution we do not expect to see the small CGs because of beam dilution. But any large scale distribution of CO along lines of sight to the CGs *will* show up. We can use these to check if our detections are contaminated by molecular gas not associated with the CGs. We see from the published survey data that CGs 1-6,8-10,13-16 and 25 are *outside* the region covered in the Columbia survey. This, therefore, leaves one with some uncertainty. But the CGs 1-4,6,13-16 and 25 have $b < -12°$ and so their detections are unlikely to be confused by more widespread gas. CGs 5,8,9 and 10 have $b \sim -9°$ and have nearby dark clouds distributed over larger spatial scales. These dark clouds show signs of being affected by ζ Pup and γ^2 Vel. These four CGs show more or less the same radial velocities. All the other CGs are in a region covered by the survey. The GDC complex of which GDCs 1 and 2 show CG features is extended consisting of 7 clouds and has been detected by the survey. The velocities are consistent. Similarly, the CG 30-31 complex, which is extended with more dark clouds in the same region, and the largest globule CG 22, have been detected by the survey with velocities consistent with our values. All other CGs which are small and isolated have not been detected. The survey detected strong CO emission from what is called the Vela Molecular Ridge (VMR), but it has been shown that this emission arises from GMCs at distances 800-2400 pc (Murphy, 1985).

A comparison of our velocities with those of Z83 shows general agreement, except for CG17 for which we measure a velocity of $+3.7$ kms^{-1} as against the value of -6.5 kms^{-1} due to Z83. The radial velocity we measure for CG18 ($\approx 1°$ away from CG17) is $+2.0$ kms^{-1}. The velocities of the clouds in the GDC1-7 complex which is nearby are again in the range $+5$ to $+6$ kms^{-1}. GDC1 and GDC2 have a windswept appearance with tail-like structures pointing in the same general direction as the other CGs and bright rims facing the center. The rough agreement between the

velocities of CG17, CG18 arid the GDC's suggests that the value reported by 283 for CG17 may be in error. As they have not published their spectra, nor mentioned their S/N, we are not in a position to comment any further.

From the above it seems clear that the radial velocities we have obtained are reliable and do nof suffer from contamination from other line of sight material. In addition, the fact that the 1989 observations using co-ordinates with errors resulted in a lower detection rate supports this conclusion.

REFERENCES

Feitzinger, J.V., Stuwe, J.A. 1984, Asti-on. *Astrophys. Suppl.*, 58, 365.

Hartley, M., Manchester, R.R., Smith, R.M., Tritton, S.B., Goss, W.M. 1986, *Astron. Astrophys. Suppl.*, **63**, 27.

Hawarden, T.G., Brand, P.W.J.L. 1976, *Monthly Notices* Roy. Astron. *Soc.*, 175, 191'.

May, J.,Murphy, D.C., Thaddeus, P. 1988, Astron. *Astrophys. Suppl.*, 73, 51.

Murphy, D.C. 198.5, Ph.D. Thesis, Massachusetts Institute of Technology.

Patel, N.A. 1989, Ph.D. Thesis, Indian Institute of Science, Bangalore.

Reipurth, B. 1983, Astron. *Astrophys.*, 117, 183.

Sandqvist, Aa. 1976,*Monthly Notices* Roy. Astron. *Soc.*, 177, 69P.

SAO Star Catalog, 1966 (Smithsonian Institution, Washington, D.C.).

Zealey, W.J., Ninkov, Z., Rice, E., Hartley, M., Tritton, S.B. 1983, *Ap.* Letters, 23, 119(Z83).

Chapter 4

Kinematics of the Cometary Globules

4.1 Introduction

In this chapter we interpret the radial velocities measured for the heads and along the tails of the cometary globules. We first deduce a morphological center for the distribution of the CGs. Then the distance estimate is discussed. These steps are necessary to remove systematic effects like galactic rotation and for the interpretation of the velocities.

4.2 The center of the distribution of the CGs

For any assumed center, the tail position angle θ_{TH} with respect to the line joining the head and the center can be calculated using spherical geometry, as illustrated in figure 4.1. The center and the head of a CG can be joined by a great circle on the celestial sphere. The tail forms a part of another great circle. The angle between these two great circles is what we want. The equation for a great circle is

$$\tan 6 = \sin(\alpha - \alpha_0) \tan i \qquad (4.1)$$

where α_0 is the point of intersection of the great circle and the celestial equator and i is the inclination between the great circle and the celestial equator. We can find α_0 and i for the the two great circles: one formed by joining the center and the head and the other being the great circle of which the tail forms a part. Let us call them α_{0h}, i_h and α_{0t}, i_t. In the spherical triangle ABC (refer to figure 4.1) we are interested in A, which is θ_{th}. By the four parts formula (Smart 1977),

$$b = \cot^{-1}((\cos a \cos C + \sin c \sin C)/\sin a) \qquad (4.2)$$

Then from the sine formula

$$\theta_{th} = A = \sin^{-1}(\sin B \sin a / \sin b) \qquad (4.3)$$

where

$$a = \alpha_{0t} - \alpha_{0h}$$

$$B = i_h \ ; \ C = \pi - i_t \ \text{if} \ \alpha_{0h} > \alpha_{0t} \quad \text{and}$$

$$B = i_t \ ; \ C = \pi - i_h \ \text{if} \ \alpha_{0h} < \alpha_{0t}.$$

To identify a center for the CG system we associate with every point in the central region a fraction f, defined as the fraction of CGs with θ_{TH} (calculated using that
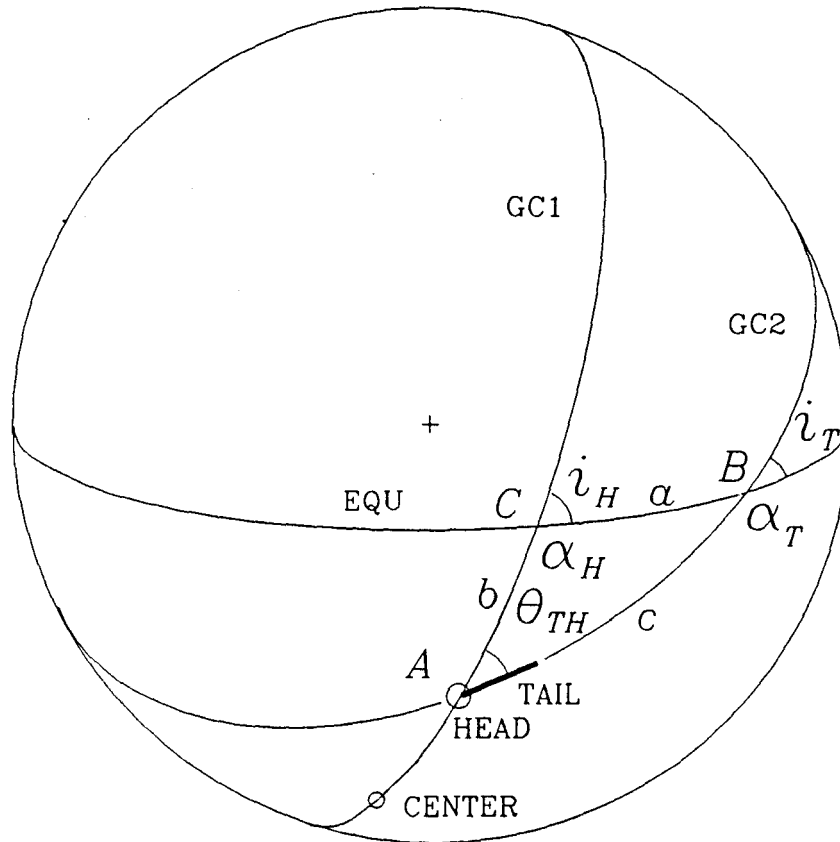
Figure 4.1: Geometric constructions used for deriving the tail position angle θ_{TH} relative to the line joining the head and any assumed center for a CG. GC1 is the great circle on the celestial sphere of which the line joining the center and the head of a CG forms a part. GC2 is the great circle of which the tail forms a part. GC1 and GC2 are characterised by (α_H, i_H) and (α_T, i_T), the RAs at which the great circles intersect the equator and their inclinations to the equator. θ_{TH} is the angle between these two great circles.

point as the center) within ± 10°. We evaluated f over a 15° × 15° area in the central region with grid points separated 0.5° in both a and 6. Figure 4.2 shows a contour plot of j. Only those CGs have been used for which we have measured the co-ordinates. CG24 has riot been included because of its anomalous tail direction. The CGs used in the analysis are shown as filled circles with tails and the CGs not used are shown as open circles with tails. For clarity tlie tail lengths shown have been scaled up 10 times. The contour spacing is 0.05 with every third contour drawn as a solid line. One can see that there is a central maximum with which 60% of the CGs are associated. The locations of the various interesting objects such as ζ Pup, γ^2 Vel, the Vela SNR etc. are also marked in tlie figure. The SNR Puppis A lies very close to the center but we show in the next section that it is very unlikely to be associated with the CGs. There are no strong local maxima associated with any of these objects. This indicates that most CGs are affected by a combination of objects rather than a particular one. The co-ordinates of the central maximum are $\alpha = 8^h\ 17^m$, and $6 = -43°$. We will refer to this point as the *morphological* center or *center* for short, hereafter. The center deduced by us is 1.5° north of *center1* of Z83. Reducing the limiting θ_{TH} from ±10° to ±5° for calculating f merely results in increased noise on the contour plot. The apparently anomalous CG24 tail can be understood by noticing that it is so close to *center* that even small errors in the location of center can make the tail direction look anomalous.

4.3 Is Puppis A associated with the CGs?

In view of the remarkable near coincidence of tlie deduced *center* with the SNR Puppis A, it is worth briefly discussing whether the two may be causally connected. Zarnecki et al.(1978) estimate a distance of 1 kpc for Puppis A from X-ray absorption measurements. The $\Sigma - D$ distance to Puppis A is 2-2.5 kpc (Milne,1979,Casewell & Lerche,1979) although it should be emphasised that this method has been severely criticised in tlie literature (Srinivasan and Dwarakanath 1982; Green 1984). The latest estimate based on the kinematic distance to molecular clouds interacting with Puppis A gives 2.2 kpc (Dubner & Arnal,1988). We will therefore adopt a distance of 2 kpc to Puppis A. At this distance it would be very difficult to detect CGs, especially ones close to the galactic plane. If the CGs are placed at the estimated distance to Puppis A, then they will be $\approx$ 200 pc away from the SNR. From the size of the SNR it is clear that the SN shock has not reached the CGs. So the only way Puppis A may be associated with the formation of the CGs is through the photon pulse at the time of the explosion or alternatively the UV radiation and stellar wind from its *progenitor*. The age of Puppis A has been estimated to be $\sim$ 3700 yrs (Winkler et al.,1988).
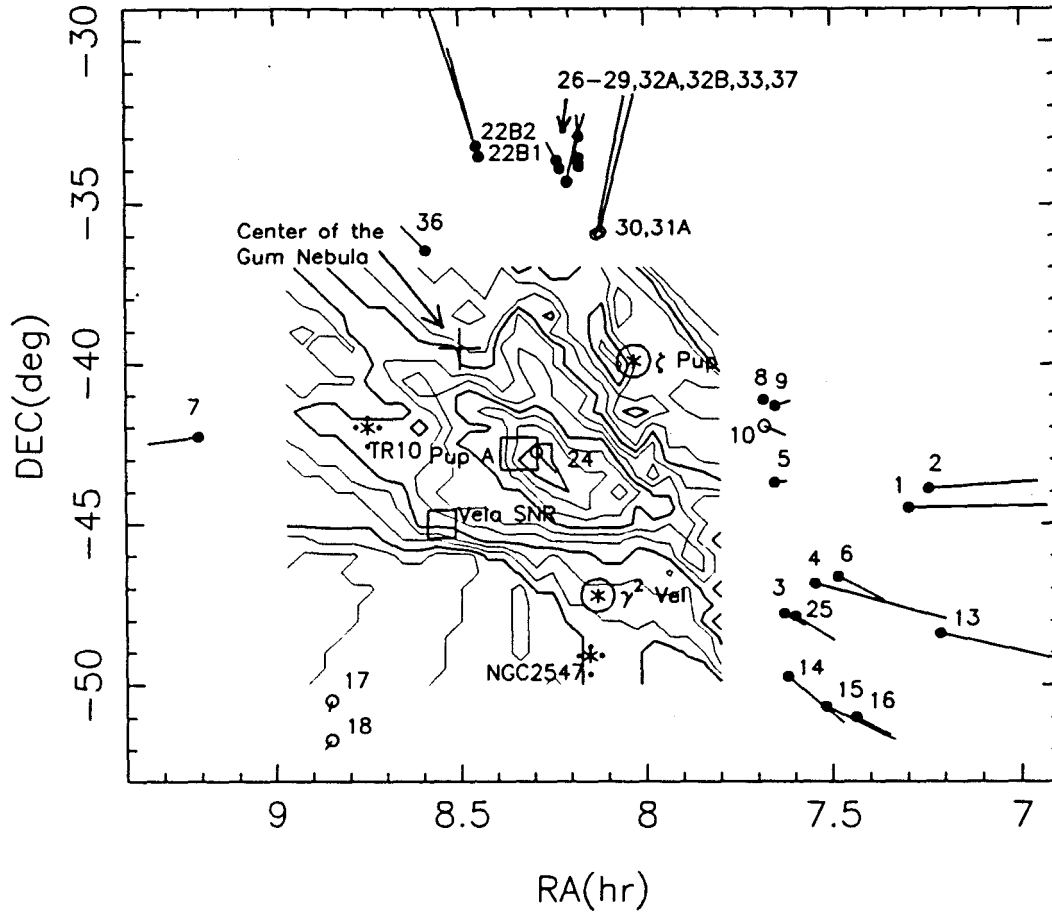
Figure 4.2: The figure shows contours of constant f, where f is the fraction of the cometary globules with position angles of their tails $\leq 10°$. The position angles are measured with respect to the line joining the head of the globule and any particular point in the region. The inner most contour bounds the region where for at least 60% of the globules the position angles of the tails are $\leq 10°$. The contours are drawn in steps of 0.05 in f and were evaluated with a grid spacing of $0.5° \times 0.5"$. Every third contour is shown as a thick line. We designate the central maximum as the morphological center of the system. The globules used for evaluating the contours are shown as filled circles with tails, and those not used as open circles with tails. For clarity, the the tails have been scaled up 10 times. In addition, the figure shows several other interesting objects such as the Pup A SNR, the Vela SNR, ζ Pup, γ^2 Vel and the open clusters TR10 and NGC2547.

From the measured electron density of $\sim$ 100 cm^{-3} for the bright rim of CG30 (Pettersson,1984) we estimate a recombination lifetime $t_{recomb} = (n_e \alpha)^{-1}$ ■ 1200 yrs. So it is difficult to see how the presently observed bright rims can be due to the initial excitation by the supernova flash. Further. both the expansion age of the system of CGs and the age of the tails estimated in later sections are $\sim$ a few million years, thus making a causal association between Puppis **A** and the CGs very unlikely. We therefore conclude that the coincidence of Puppis A and tlie center is a chance superposition. On similar grounds we rule out any role for the Vela SNR in the formation of the CGs.

Figure 4.3 shows the distribution of θ_{TH}. We see that apart from the central peak there is a peak at 35° consisting of four globules, viz. CGs 26,27,29 and 33. The directions of their tails suggest that they may be associated with ζ Pup alone. It is possible that they are closer to ζ Pup in tlie direction perpendicular to the plane of the sky. Even though we cannot associate a single object of any importance with the center, we will use it as the center of the distribution of CGs for further analysis. The other objects in figure 4.2 are discussed in the next section.

4.4   Distance to the CGs

The most important objects in the region of the CGs from the point of view of momentum and energy budgets are ζ Pup, γ^2 Vel, and tlie clusters NGC 2547 and TR10. All these objects are at a distance of $\sim$ 450 pc (Eggen 1980, Claria 1982). As seen in figure 4.4, a histogram of the distances to early type stars towards the Gum Nebula used by Wallerstein, Silk and Jenkins(1980) to study gas in the nebula shows a peak at 450 pc. In an earlier study of the Gum Nebula, Brandt et *al.*(1971) had identified a possible B Association at 450 pc distance which has later been named Vela OB2. So it is clear that at a distance of 450 pc there exists a significant population of early type stars. The location of some of these objects are shown in figure 4.2. The point to note is that these objects, some of which have to be necessarily invoked to explain the CGs, are at about the sarne distance and are centrally located with respect to the distribution of CGs. So we assume that the CGs are at the same distance as these objects, viz. at $\sim$ 450 pc. Further, Pettersson(1987) has estimated a lower limit for the distance to CG30-31 complex to be 420 pc using a foreground star. and the distance to tlie young star in the head of CG1 has been estimated to be $\sim$ 500 pc (Brand et *al.*, 1983). Adopting a distance of 450 pc would imply that the distribution of the CGs extends to about 150 pc perpendicular to tho line of sight.
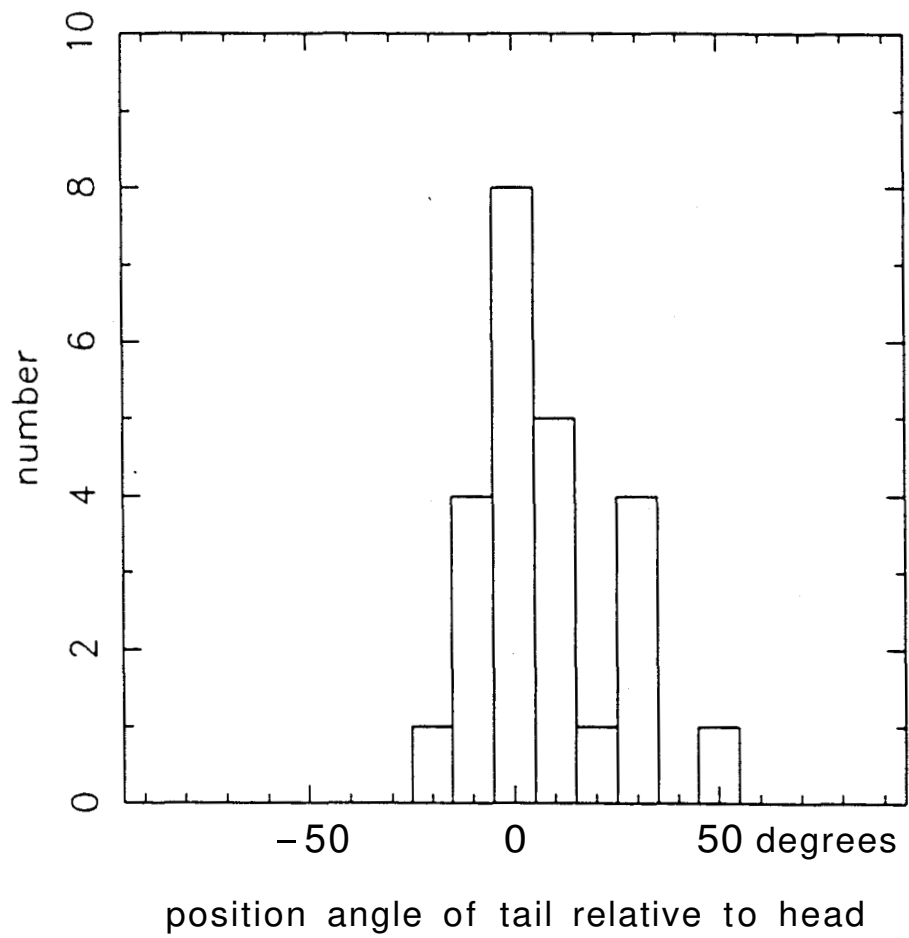
Figure **4.3:** The distribution of the position angles θ_{TH} of the tails relative to the line joining the center and the respective heads for 24 CGs (see figure 4.1).
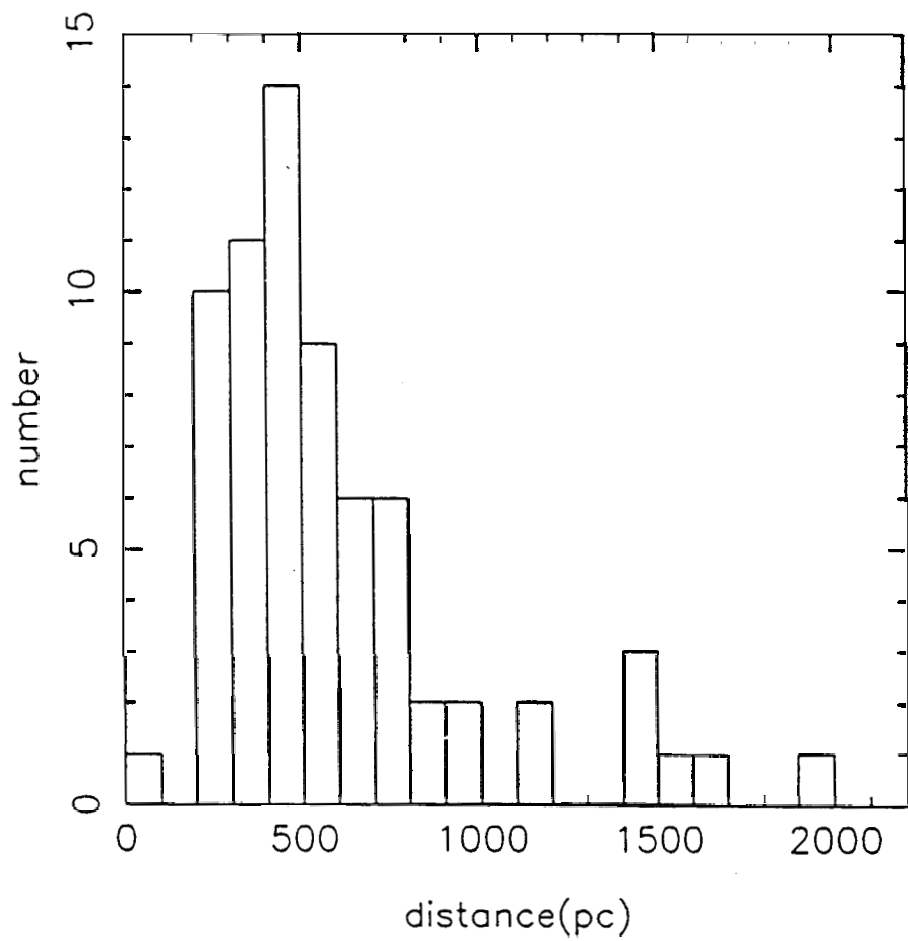
Figure 4.4: The distribution of the distances to the early type stars towards the Gum Nebula. The distances are from Wallerstein, Silk and Jenkins(1980).

4.5 Radial velocities

We now wish to discuss the implications of tlie measured radial velocities listed in Table **3.3.** First, we briefly touch upon the suggestion made by Z83, viz. that the velocity distribution can be understood in terms of the large scale galactic rotation effects. In figure 4.5 we have plotted the radial velocities against the position angles of the CGs measured with respect to the *center* with zero towards north and increasing through east. The sinusoid fitted by Z83 which led them to suggest a rotation of the system of CGs is also shown. Clearly, the fit is very poor. There are two reasons why the sinusoid is a poor fit to tlie new data; (i) the revised value of the radial velocity of CG17, and (ii) velocities of CGs not detected earlier. Our main conclusion from this figure is that the model of tlie CG system rotating about an axis perpendicular to the galactic plane is untenable. In figure 4.6 we have plotted the radial velocities against galactic longtitude. Again, tlie new data does not permit a simple straight line fit as suggested earlier (Z83), and therefore an explanation based on galactic rotation effects is hard to reconcile. Nevertheless, tlie contributiori due to galactic differential rotation will be present and should be removed before attempting to interpret the velocities.

Before one can correct for the galactic differential rotation one must assume a mean distance to the CGs. Based on the discussion given in section 4, we will adopt a distance of 450 pc. The dashed line in figure 4.6 represents the expected radial velocities for different galactic longitudes from the well known formula

$$v_r = Ar\sin(2l)\cos^2 b \tag{4.4}$$

with the heliocentric distance $r = 450$ pc and $b = 0$. We have assumed a value of 14.5 kms^{-1}kpc^{-1} for Oort's constant A (Kerr & Lynden-Bell 1986). The significarit deviations of the observed radial velocities from the expected value given by the dashed line suggests local motions in the CG system. Figure 4.7 shows the residuals after galactic rotation effects have been subtracted out using eq. 4.4. It sliould be remarked that the differences in the line-of-sight distances to the various globules (~ 150 pc) can only account for a scatter ~ 1.4 kms^{-1}.

4.6 Expansion of the globules

In this section we wish to argue that the velocity residuals can be easily understood in terms of an expansion of the system of globules from a common center. If tlie CGs are distributed over a shell expanding with uniform velocity then, as can be
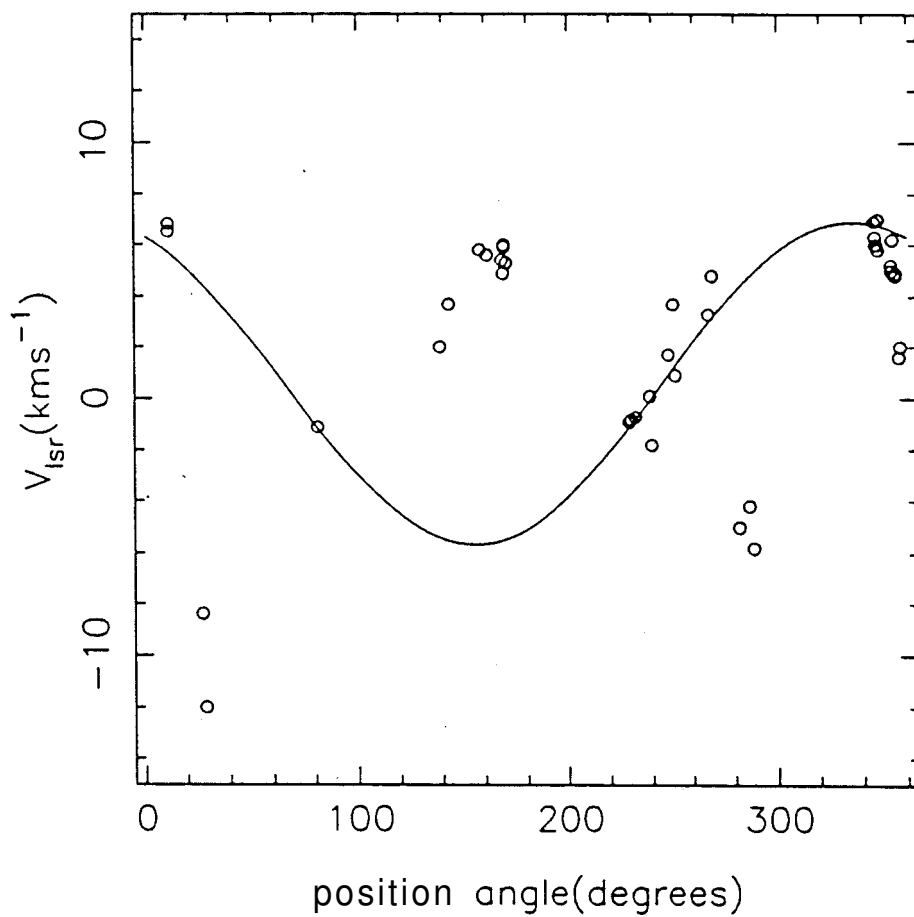
Figure 4.5: The velocities of the globules in the Gum Nebula with respect to the Local Standard of Rest. The horizontal axis is the position angle of the globules; zero is North and the position angle increases through East. The sinusoid shown is the fit made by Zealey et. *al.*(1983) for their data.
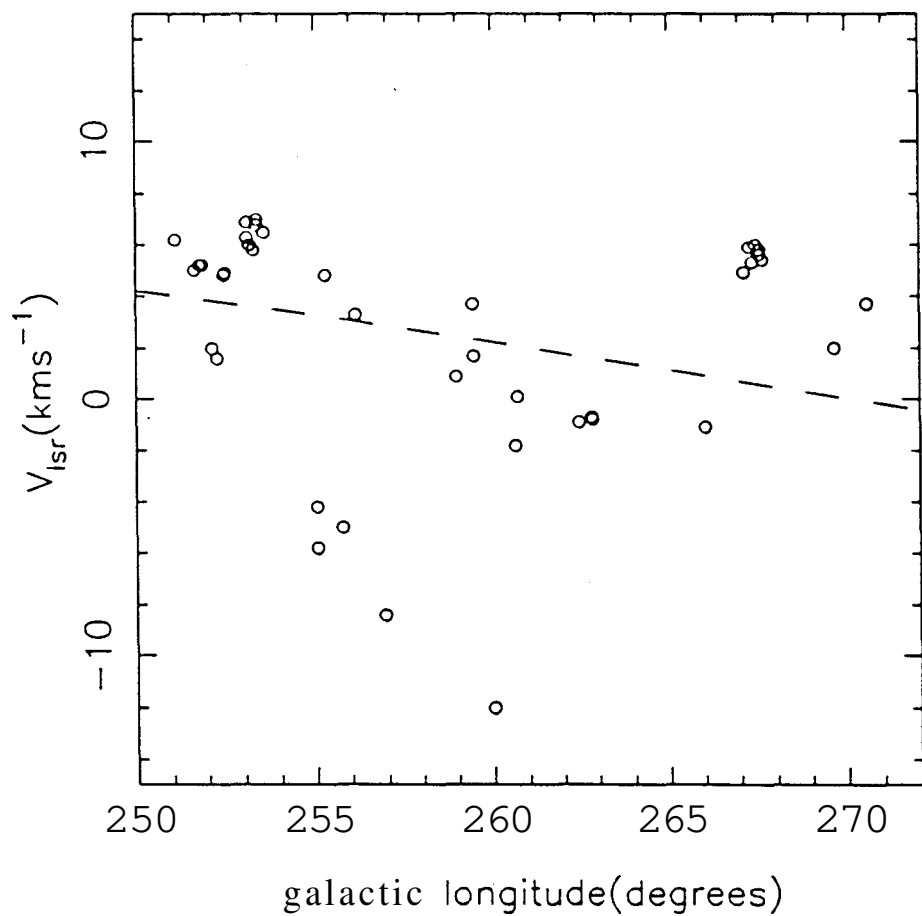
Figure 4.6: The velocities of the globules in the Gum Nebula with respect to the Local Standard of Rest versus the galactic longitude. The broken line shows expected velocities due to galactic differential rotation for an assumed heliocentric distance of 450 pc and b = 0.
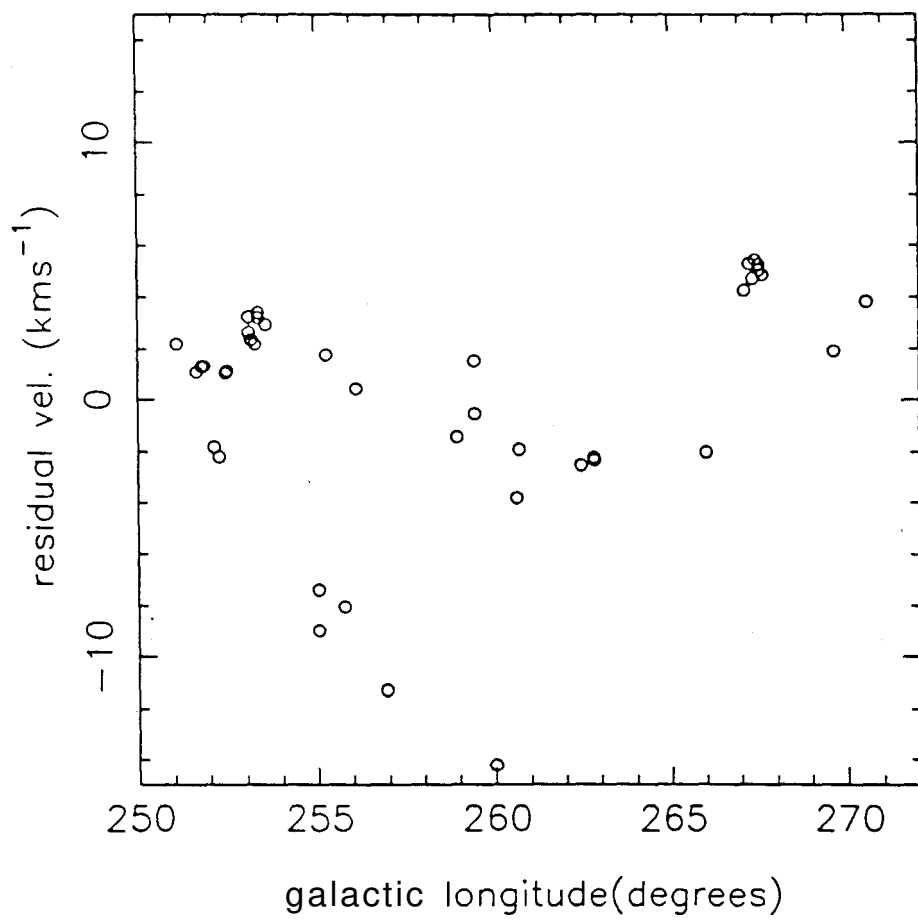
Figure 4.7: The residual velocities of the globules in the Gum Nebula after removing the contribution of the galactic differential rotation. A mean distance of 450 pc to the globules has been assumed.

seen from figure 4.8(a), the expected velocities are given by

$$v_{rad} = \pm v_{exp}(1 - \sin^2\theta / \sin^2\theta_{max})^{1/2} \qquad (4.5)$$

where v_{exp} is the expansion velocity of the shell, v_{rad} is its line of sight component, and θ_{max} is the angular distance of the farthest CG from the *center*. In this case one would expect the residual velocities, when plotted against $(1 - \sin^2\theta / \sin^2\theta_{max})^{1/2}$, to fall on two straight lines as shown in figure 4.8(b). If the CGs are not on a shell but distributed throughout the sphere, then the region between the lines will be filled-up provided the inner CGs move slower than the outer CGs. If the distribution of the CGs within the sphere is not uniform one will find an incomplete filling of this region.

Figure 4.9 shows the absolute value of the residual velocities plotted against $(1 - \sin^2\theta / \sin^2\theta_{max})^{1/2}$ for all the CGs and the GDCs. We have taken θ_{max} to be $12.5°$, corresponding to CG13. It is clear that there is an upper limit to the velocities which increases as one goes closer to the center (abscissa $= 1$) implying an expansion of the system. A contraction of the system will also have the same signature, but is very unlikely. The two straight lines shown correspond to expansion velocities of 15 kms^{-1} and 9 kms^{-1}. We will adopt an expansion velocity of 12 kms^{-1}. The figure further shows that the CGs are distributed over a volume rather than in a shell, and that the distribution is not uniform. Finally, the inferred expansion velocity of 12 kms^{-1} implies an *expansion age* of ~ 6 Myrs.

4.7 Radial velocities along the tails

In addition to measuring the radial velocities of the heads of the cometary globules, we also measured the velocities along the tails (listed in Table 3.4). In this section we discuss the results of these observations.

Out of 21 CGs for which at least three points along the tails were observed, seven show very pronounced and systematic velocity shifts. In figure 4.10 the measured velocities are plotted against the distance from the head for some of these. The velocity gradients Av, in kms^{-1}arcmin^{-1} were obtained by fitting straight lines which are also shown in the figure. These gradients are also listed in Table 4.1. along with the estimated errors in the gradients. In figure 4.11 the velocity difference between the head and the extreme end of the tail is plotted against the velocity of the head for all the 21 CGs. More precisely, the ordinates are calculated as product of the velocity gradient along the tail and the tail length. The velocity differences so calculated are affected less by errors in the individual measurements. As may
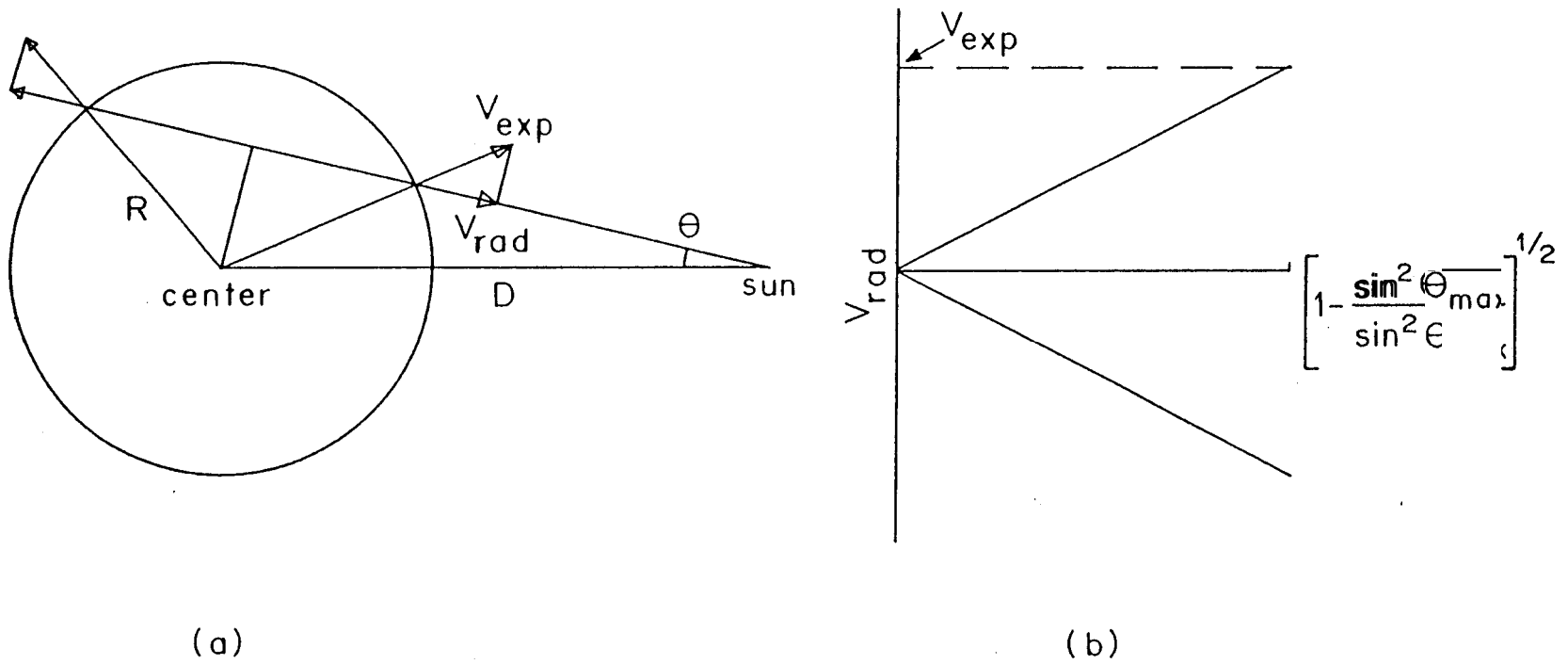
Figure 4.8: (a) A schematic diagram for deriving expected velocities from an expanding shell of objects. $V_{,,}$. is the expansion velocity whose radial component is V_{rad} and θ is the angular distance to any point on the shell from the center of the shell. (b) The expected velocity plotted against $(1 - \sin^2 \theta / \sin^2 \theta_{max})^{1/2}$.
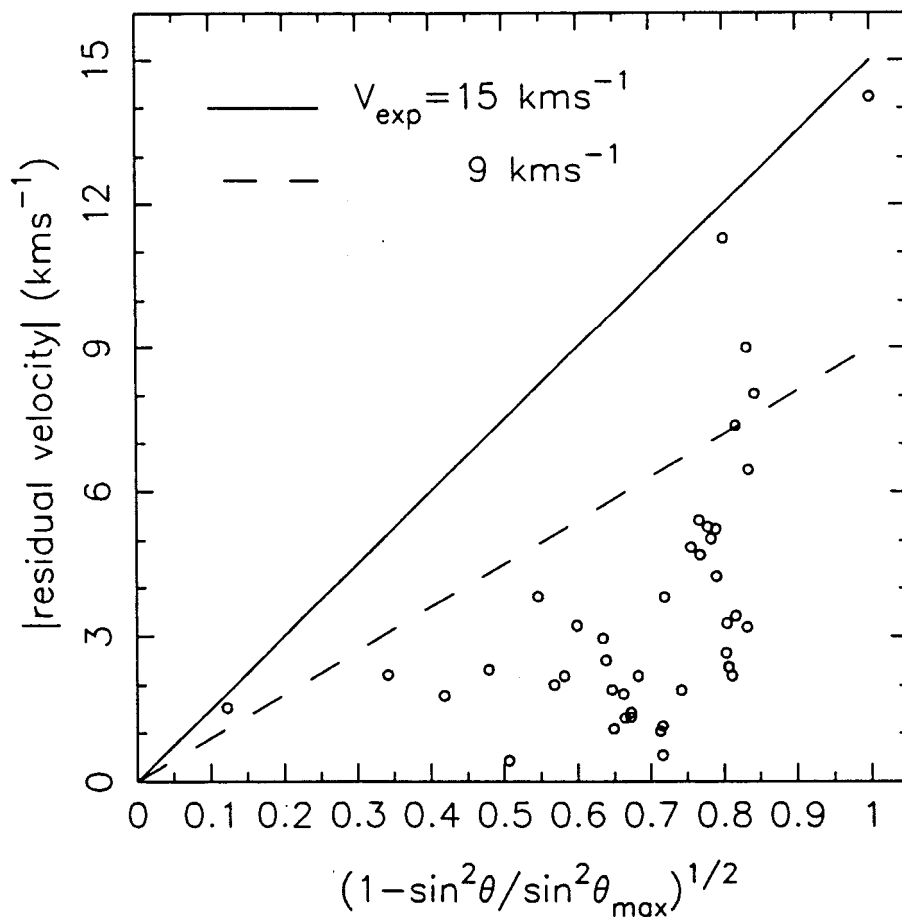
Figure 4.9: The absolute values of the residual velocities of the globules plotted against $(1 - \sin^2\theta/\sin^2\theta_{max})^{1/2}$ where 8 is the angular distance to the globule. The lines shown correspond to uniform expansion at 9 and 12 kms^{-1}
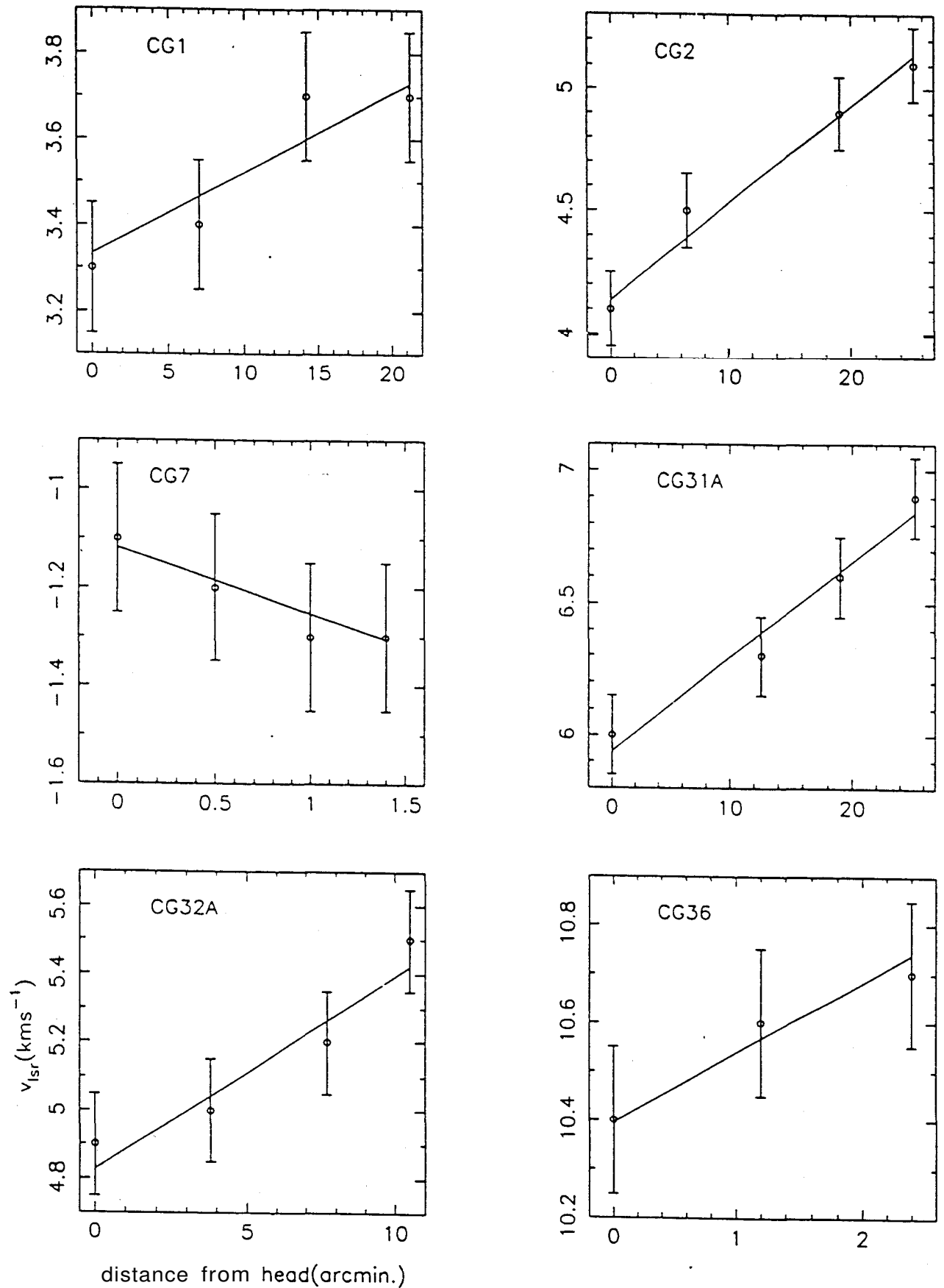
Figure 4.10: The velocity gradients along the tails for 6 out of 7 CGs which show pronounced gradients. The straight lines are least square fits to the **data** points.

Table 4.1. velocity gradients along the tails.

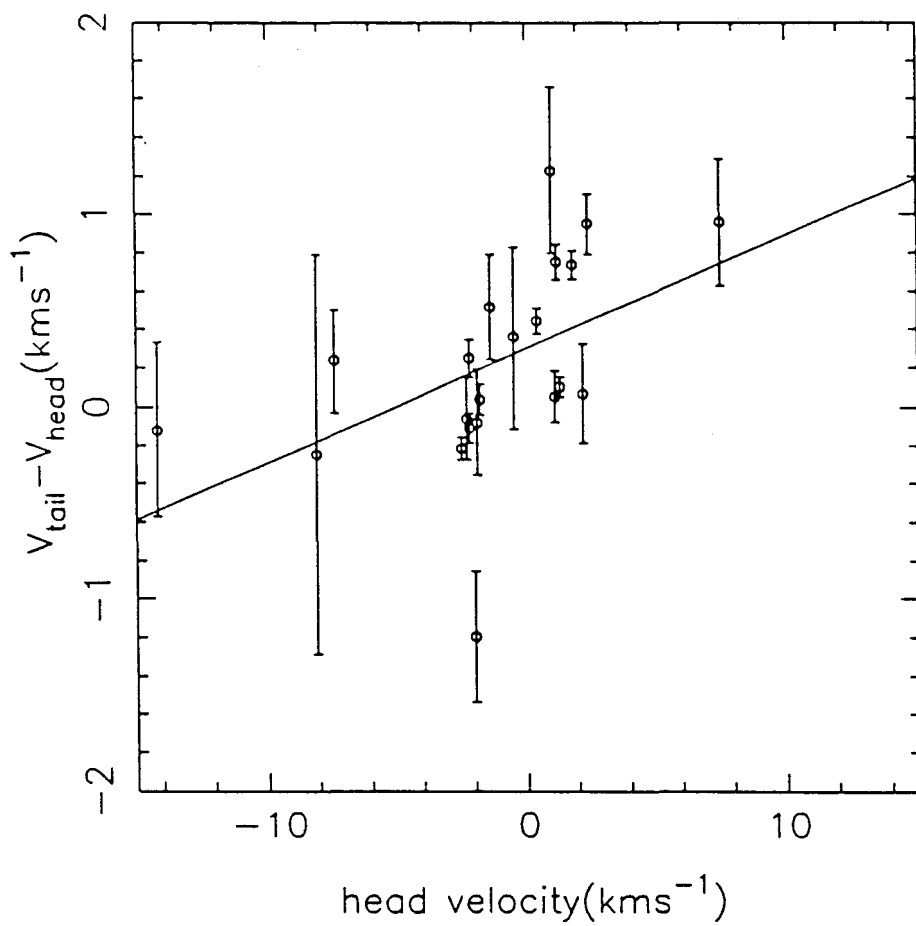| source	velocity gradient $\text{kms}^{-1}\text{arcmin}^{-1}$	error in gradient $\text{kms}^{-1}\text{arcmin}^{-1}$
CG1	0.019	0.003
CG2	0.040	0.004
CG3	−0.014	0.068
CG4	0.016	0.021
CG6	0.061	0.032
CG7	−0.133	0.038
CG9	0.080	0.09
CG10	−0.0.56	0.25
CG14	−0.018	0.005
CG15	−0.005	0.018
CG16	−0.018	0.013
CG24	−0.024	0.089
CG26	0.010	0.02
CG27	0.021	0.052
CG29	0.041	0.02
CG31A	0.036	0.006
CG32A	0.057	0.007
CG32B	0.114	0.043
CG33	0.082	0.032
CG36	0.144	0.05
CG37	0.017	0.064

Figure 4.11: The difference in velocities between the ends of the *tails* and the respective heads plotted against velocities of the heads of the CGs.

be seen, the data points fall approximately on a straight line passing close to the origin. This implies that the gas at the end of the tails is moving faster than the heads and in the same direction as the heads.

If we assume that the tails are formed due to the stretching effect of these velocity differences over the course of time, one can calculate an age for the tails as the time taken for the presently observed velocity difference to result in an elongation equal to the measured tail length. Since we have only the *radial* component for the velocity differences and the *transverse* component of the tail lengths, the calculated ages suffer from projection effects. Figure 4.12 shows the distribution of the estimated apparent ages of the tails in millions of years; a distance of 450 pc has been assumed. The apparent age is related to the real age through the relation

$$t_{apparent} = t_{real} \times \tan \theta \qquad (4.6)$$

where 9 is the angle between the tail and the line of sight. Since most of the CGs are distributed towards the periphery of the system, we believe that most CGs have $\theta > 45^0$. Thereore, the apparent age represents an over estimate of the real age. We feel that ~ 3 Myrs is a reasonable estimate for the ages of the tails.

4.8   Conclusions

From an analysis of the mesured velocities of the cometary globules we come to the following conclusions:

The kinematics of the CGs cannot be interpreted in terms of a model where galactic rotation effects dominate. as was suggested by ZS3 based on their study of a smaller sample of CGs. Our study points to two clear interpretations:

1. The distribution of the radial velocities of the heads of the cometary globules, after galactic differential rotation is subtracted, is best understood in terms of an expansion of the system about a common *center*. The data is better fit by a model in which the globules are non-uniformly distributed throughout the interior of a sphere, rather than in a shell. The expansion velocity of the outermost globules is ~ 12 kms^{-1}. The implied *expansion age* of the system is ~ 6 Myr.

2. Some of the cometary tails show systematic velocity gradients. It is interesting that the estimated age for the formation of the tails inferred from these velocity gradients is about the same (~ 3 Myr) as the expansion age.
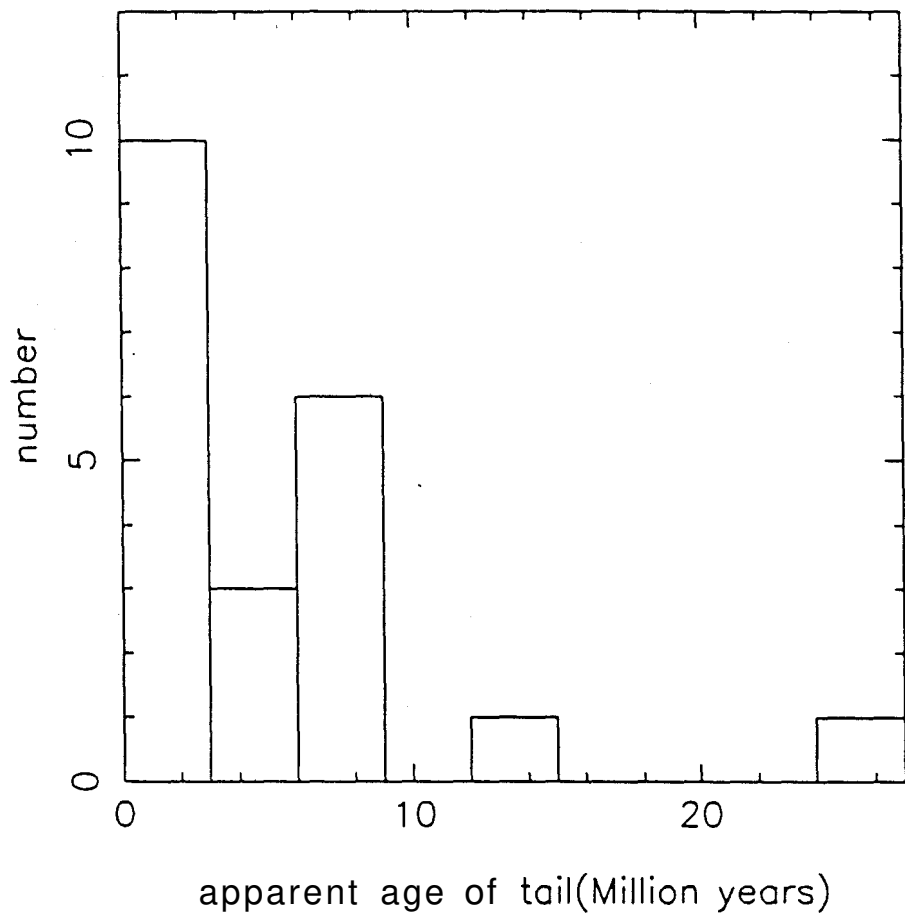
Figure 4.12: A histogram of the apparent *tail stretching ages* defined as the time required for the velocity difference between the heads and the tail-ends of the CGs to stretch the globules to their observed lengths.

REFERENCES

Brand, P.W.J.L., Hawarden, T.G., Longmore, A.J., Williams, P.M., Caldwell, J.A.R. 1983, *Monthly Notices* Roy. *Astron. Soc.*, 203, 215.

Brandt, J.C., Stecher, T.P.,Crawford, D.L.,Maran, S.P. 1971, Ay.*J.(Letters)*, 163, L99.

Caswell, J.L., Lerche, I. 1979, *Monthly Notices* Roy. Astron. *Soc.*, 187, 201.

Dubner, G.M., Arnal, E.M. 1988, *Astron. Astrophys. Suppl.*, 75, 363.

Eggen, O.J. 1980, *Ap.* J., 238, 627.

Green, D.A., 1984, *Monthly Notices* Roy. Astron. *Soc.*, 209, 449.

Kerr, F.J., Lynden-Bell, D. 1986, *Monthly Notices* Roy. *Astron. Soc.*, 221, 1023.

Milne, D.K. 1979, Aust. J. Phys., 32, 83.

Pettersson, B. 1984, *Astron. Astrophys.*, 139, 135.

Pettersson, B. 1987, *Astron.* Astrophys., 171, 101.

Smart, W.M., 1977, *Text Book* on Spherical *Astronomy*, Cambridge University Press: Cambridge.

Srinivasan, G., Dwarakanath, K.S. 1982, J. Astrophys. *Astr.*, 3, 351.

Wallerstein, G., Silk, J., Jenkins, E.B. 1980, Ay. **J.**, 240, 834.

Winkler, P.F., Tuttle, J.H., Kirshner, R.P., Irwin, M.J., 1988, in Suyernova Rentnants and the Interstellar.*Medium*,ed. R.S. Roger & T.L. Landecker(Cambridge: Cambridge University Press), p.65.

Zarnecki, J.C., Culhane, J.L., Toor, A., Seward, F.D., Charles, P.A. 1978 *Ap.* **J.** (Letters), 219, L17.

Zealey, W.J., Ninkov, Z., Rice, I.,. Hartley, M., Tritton, S.B. 1983, *Ap.* Letters, 23, 119 (Z83).

Chapter *5*

Maps of CG 22

5.1   Introduction

In this chapter we derive the mass of Blob 1 of CG22. This globule has three regions of high obscuration along its tail which may, in fact, be seperate CGs. These have been called Blob 1,2 and **3** respectively. From the maps of the Blob 1 arid associated tail of CG 22 made in the J=1 $\rightarrow$ 0 lines of ^{12}CO and ^{13}CO we derive temperature and column density distributions. We estimate the mass of Blob 1 by three different methods. The chapter ends with a discussion of the results.

5.2   Data Reduction

The observations and basic data reduction have been described in chapter **3.** The temperature scale obtained by these reduction steps is what has been called T_A^* in the literature. This quantity is telescope dependent. We have to correct this further for the forward coupling efficiency and the image-band to signal-band gain-ratio to obtain T_R^*, the main beam antenna temperature. This quantity has also been called the radiation temperature. This is the closest one can get to the source brightness temperature in the absence of any knowledge about the source structure, and is less dependent on the telescope. We describe below briefly the basis of these corrections.

5.3   Basics of calibration

An observation consists of a run of ON and OFF measurements, and a run of AMB and OFF measurements for calibration. The ON and OFF measurements may correspond to two different positions in the sky (beam or position switching) or two different frequencies (frequency switching) and the AMB measurement is made with an ambient temperature absorber in front of the receiver. Let the corresponding voltages measured he V_{ON}, V_{OFF} and V_{AMB}. Let the system, including the atmosphere, have gains G_s and G_i in the signal arid image bands. Then for a spectral line observation with a double side-band (DSB) system we have

$$V_{ON} = G_s T_{sys,s} + G_i T_{sys,i} + G_s T_{source} \tag{5.1}$$

$$V_{OFF} = G_s T_{sys,s} + G_i T_{sys,i} \tag{5.2}$$

$$V_{AMB} = G_s T_{sys,s} + G_i T_{sys,i} + (G_s + G_i) T_{amb} \tag{5.3}$$

from which we derive

$$T_{source} = T_{AMB}(1 + \frac{G_i}{G_s})\frac{V_{ON} - V_{OFF}}{V_{AMB} - V_{OFF}} \qquad (5.4)$$

T_{source} is what is normally referred to as T_A^* in literature, the antenna temperature after correction for all telescope losses occuring at ambient temperature (for example, a lossy element at room temperature in the beam path or beam truncation due to or spill-over onto ambient temperature objects). It is not corrected for that part of the telescope response on the sky outside the main beam due to spill over past the secondary, the error pattern etc. This correction is done by dividing T_A^* by η_{fss}, the forward spill over and scattering efficiency.

5.4   Calibration at the 10.4m telescope

For the DSB receivers used at the 10.4m telescope, tlie ratio of tlie side-band gains have been measured to be same within 0.5dB. We assume that the gains are same because the signal and image frequencies are only 3 GHz apart. So G_s ane G; can be different only because of tlie frequency dependence of atmospheric absorption. The measured atmospheric absorption in the 3 mm window reproduced in figure 5.1 from Ulich and Haas(1976) shows that the frequency dependence is appreciable at 115 GIIz arid needs to be taken into account. We estimate the ratio G_i/G_s from this figure to be $e^{0.17}$ for ^{12}CO observations with LO at 113.8 GHz. The measurements do not necessarily correspond to conditions at Bangalore but we assume that the effect on tlie gain ratio will only he of second order. So all our ^{12}CO line strengths liave to be multiplied by a factor $(1 + e^{0.17})/2 = 1.09$. As can be seen from the figure, the atmospheric absorption flattens off at 110 GHz and therefore ^{13}CO line strengths do not need such a correction. To make tlie more important correction for forward spill over and scattering, we can use the measured value of 0.61 for η_{fss} at 113.8 GHz (Patel, 1990). We assume that η_{fss} is 0.61 at both 110 GHz and 115 GHz and multiply both ^{12}CO and ^{13}CO data by $1/\eta_{fss} = 1.64$. By doing this we get what is referred to as T_R^*, the source *brightness temperature convolved* with the antenna *diffraction* pattern, tlie closest one can get to the source brightness temperature in the absence of any knowledge about the source structure. This is the quantity that is reported nowadays in tlie literature. So *the correction factors* to be applied *for* ^{12}CO and ^{13}CO *data* are 1.79 and *1.64, respectively.* On applying these corrections the line strengths on Orion **A** obtained at tlie 10.4m telescope are 73.4 K for ^{12}CO and 13.9 K for ^{13}CO in agreement with values reported in tlie literature. Table 5.1 lists the values obtained by various telescopes.
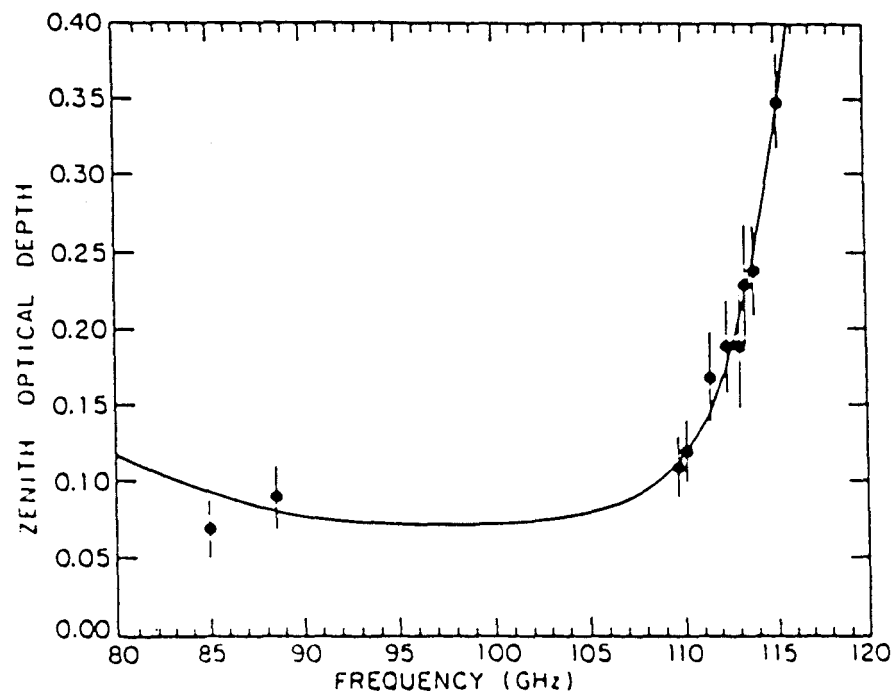
Figure 5.1: The atmospheric attenuation curve over the 3-mm window (after Ulich and Haas 1976).

Table 5.1: CO line strengths on ORI A				
Telescope	^{12}CO K	^{13}CO K	beam "	ref.
FCRAO 14m	70	17	50	Snell et. *al.* 1984.
AT&T Bell Labs 71n	76	14.9	100	Bally et. al. 1987.
RRI 10.4m	73.4	13.9	G0	

The forward spill over and scattering efficiency, η_{fss}, is a function of elevation but since all the data for the maps were taken over a small elevation range of 25°-40°, we do not make any elevation dependent corrections. The T_R^* for Orion **A** values quoted above were made at $\sim$45° elevation. We assume that the correction applied is not much in error for the elevation range of our observations.

The final spectra were written on tape in FITS format and further data reduction to obtain temperatures, optical depths arid column densities were carried out on AIPS. We give a brief summary of the methods used to derive these quantities and the results.

5.5   Temperature

The most common method used to determine the kinetic temperature in a molecular cloud is to use a line that is optically thick and thermalised. These conditions are met by the $J=1 \rightarrow 0$ transition of ^{12}CO. Due to its small dipole moment, CO reaches thermal equilibrium for relatively low density of H_2 (300 cm^{-3}). In addition, this line is almost always optically thick. The disadvantage of this method is that tlie temperature obtained corresponds to the outer regions of the cloud where the line becomes optically thick. However, unless detailed modelling is done a constant temperature for the cloud is assumed even though this is unrealistic. Keeping in mind that for typical molecular cloud temperatures $h\nu \ll kT$ is not valid and taking into account the 2.7 K background. the kinetic temperature is given by

$$T_{kin} = \frac{5.532}{\ln(1 + \frac{5.532}{(T_{Lp}+0.8182)})} \tag{5.5}$$

as derived in the Appendix. Figures 5.2(a) arid (b) show a contour plot and a , psuedo-color image, respectively, of the distribution of T_{kin} in CG22-Blob 1.

5.6 Optical Depth

The spectral line from ^{12}CO being optically thick, it is ^{13}CO whose optical depth is determined directly from the observations. One first assumes that the excitation temperatures for both ^{12}CO and ^{13}CO are the same. Then one obtains the ^{13}CO optical depth from the observed ^{13}CO line using simple radiative transfer. We reproduce below the expression for optical depth derived in the Appendix:

$$\tau_{13} = -\ln\left[1 - \frac{T_{13}}{5.289}\left\{\left[e^{\frac{5.289}{T_{ex}}} - 1\right]^{-1} - 0.1642\right\}^{-1}\right] \tag{5.6}$$

Figures 5.3(a) and (b) show, respectively, a contour plot and a pseudo-color image of $\int \tau dv$, the integrated optical depth distribution in CG 22-Blob 1.

5.7 Column Density

To derive the column density $\mathcal{N}_{H_2}$ of molecular hydrogen, we first obtain the $\mathcal{N}_{^{13}CO}$, the column density of ^{13}CO from $\int \tau dv$ using the following relation derived in the Appendix:

$$\mathcal{N}_{^{13}CO} = 2.42 \times 10^{14} \frac{T_{ex} \int \tau_{13} dv}{(1 - e^{-5.289/T_{ex}})} \tag{5.7}$$

From $\mathcal{N}_{^{13}CO}$ we get $\mathcal{N}_{H_2}$ using the proportionality factor given by Dickman(1978) viz.,

$$\mathcal{N}_{H_2} = (5.0 \pm 2.5) \times 10^5 \mathcal{N}_{^{13}CO} \tag{5.8}$$

This conversion has been derived from observations of 38 'dark clouds in ^{12}CO and ^{13}CO and extinction measurements. A universal value for the ratio $\mathcal{N}_{H_2}/\mathcal{N}_{^{13}CO}$ has been questioned by Frerking, Langer and Wilson(1982) who found that this number can vary by as much as a factor of 10. We use Dickman's number as more information is not available. Figures 5.4(a) and (b) show a contour plot, and a pseudo-color image of the distribution of $\mathcal{N}_{^{13}CO}$ in CG 22-Blob 1.

5.8 Mass estimates

Masses for molecular clouds can be estimated by three different methods. The first method uses an optically thin line such as ^{13}CO to get $\mathcal{N}_{H_2}$ as done above. If the distance to the cloud is known, $\mathcal{N}_{H_2}$ can be integrated over the projected area of the

Psak flux = 1.5706E+01 K
Levs = 1.0000E+00 * (2.000, 4.000, 6.000,
8.000, 10.00, 11.00, 12.00, 13.00, 14.00,
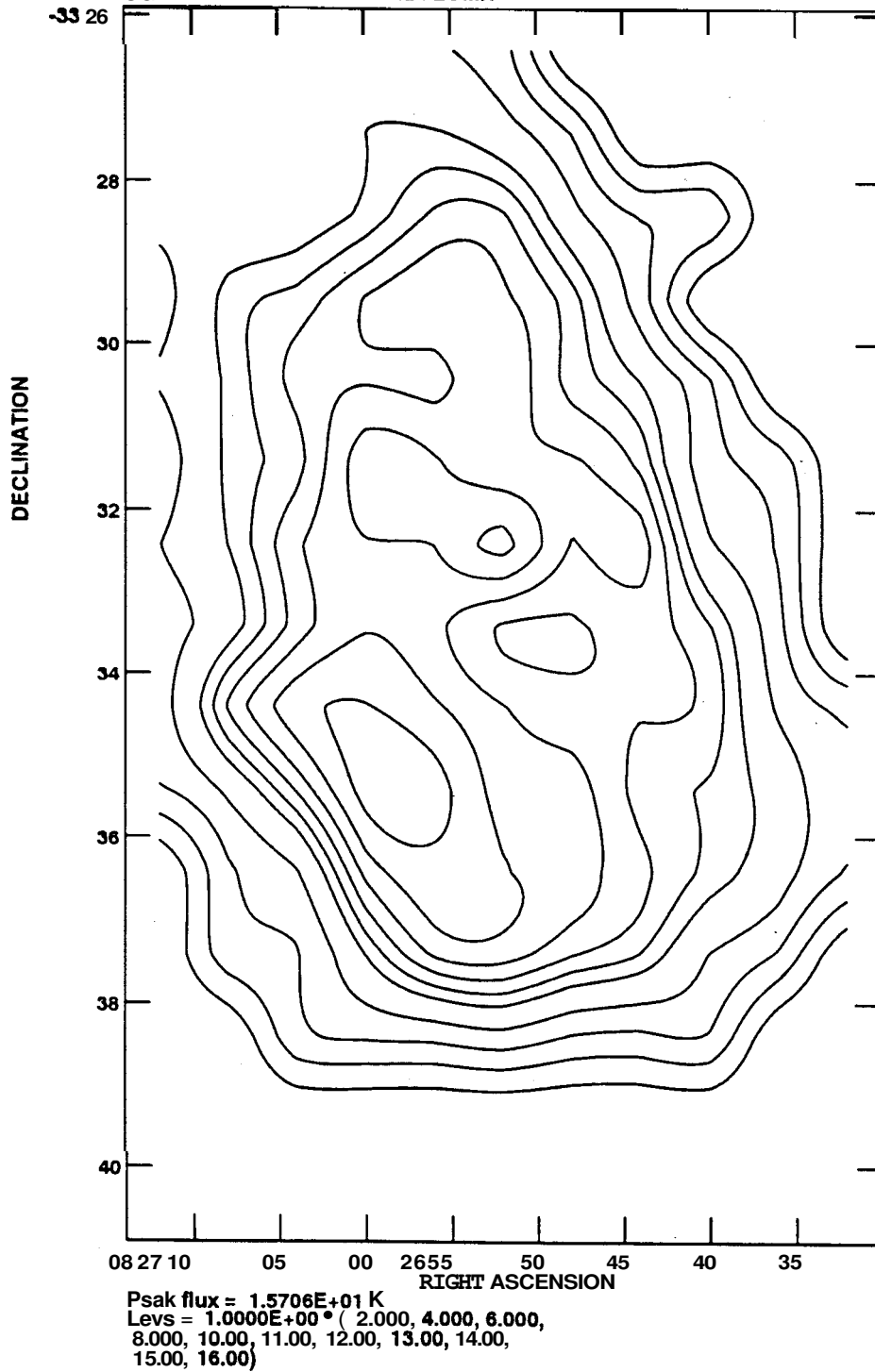15.00, 16.00)

Figure 5.2 (a) **A** contour plot of the kinetic temperature distribution over CG22-Blob-1. The levels are in Kelvins. (*From* ^{12}CO *observations*)
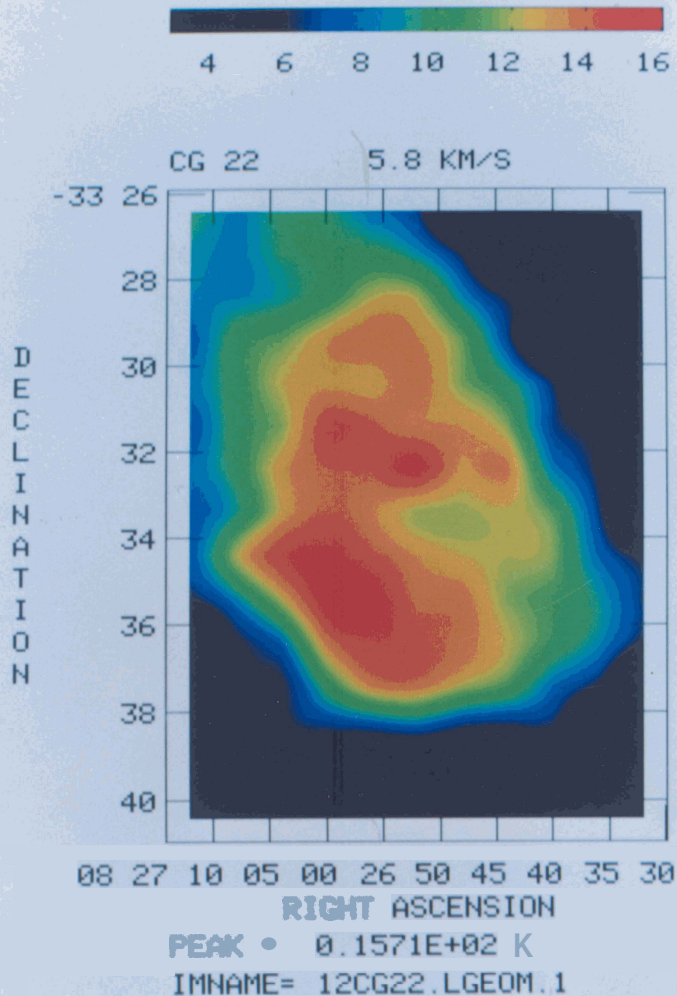
Figure 5.2 (b) **A pseudo color image of the kinetic temperature distribution** over **CG22-Blob-1. The scale is in units of Kelvin.**
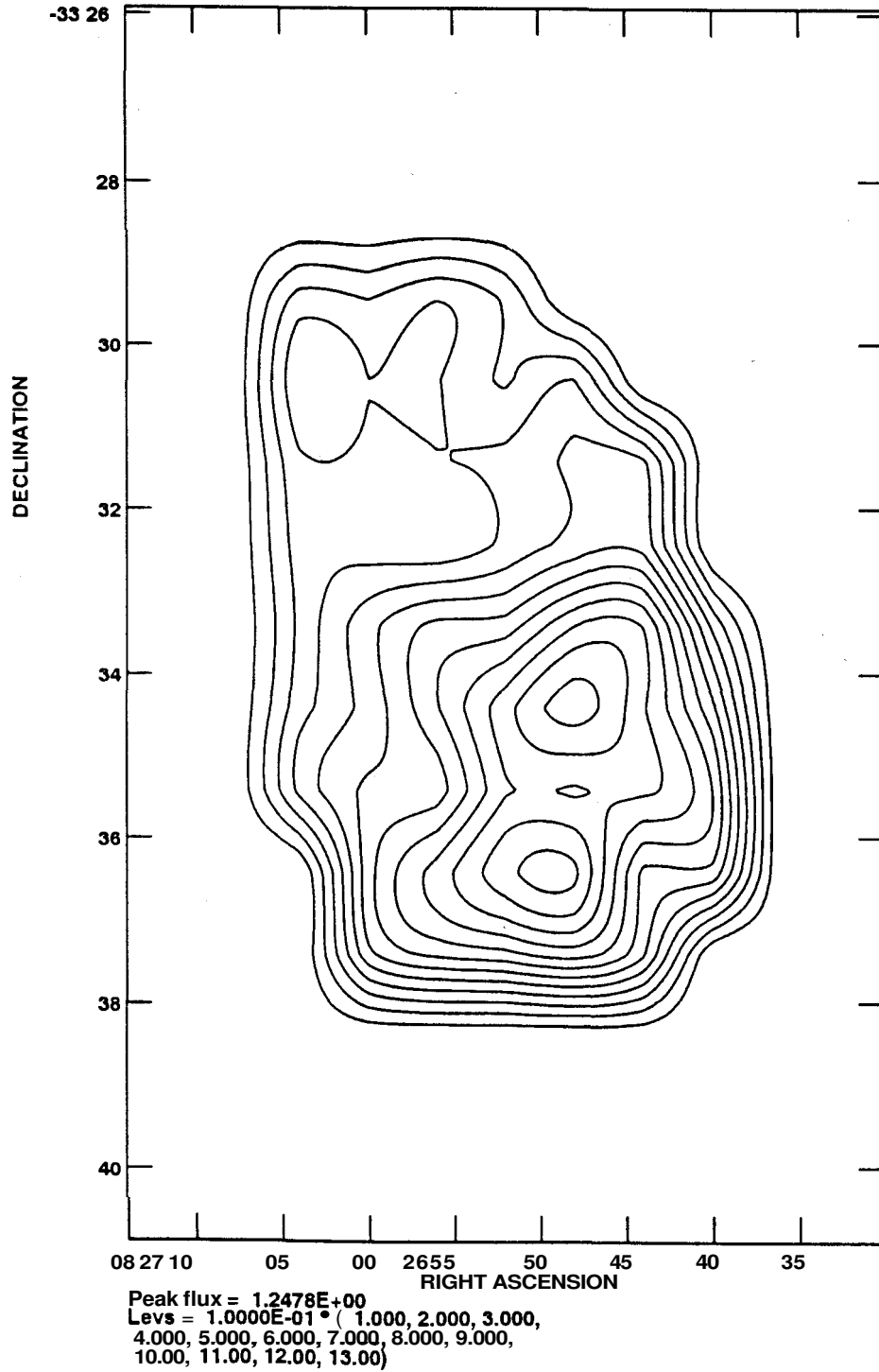
Figure 5.3 (a) **A** contour plot of the integrated ^{13}CO optical depth distribution over CG22-Blob-1.
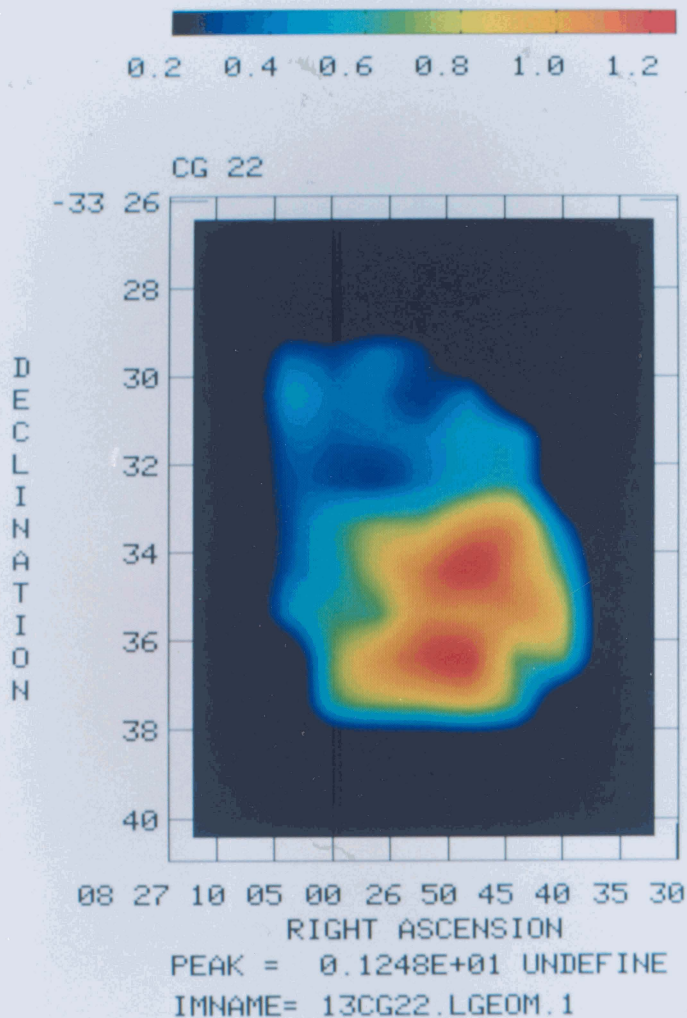
Figure **5.3** (b) A pseudo color image of the integrated ^{13}CO optical depth distribution over CG22-Blob-1.

Peak flux = 8.8217E+15 PRODUCT
Levs = 2.0000E+14 * (4.000, 8.000, 12.00,
16.00, 20.00, 24.00, 28.00, 32.00, 36.00,
40.00, 44.00, 48.00, 52.00, 56.00, 60.00,
64.00, 68.00, 72.00, 76.00, 80.00, 84.00,
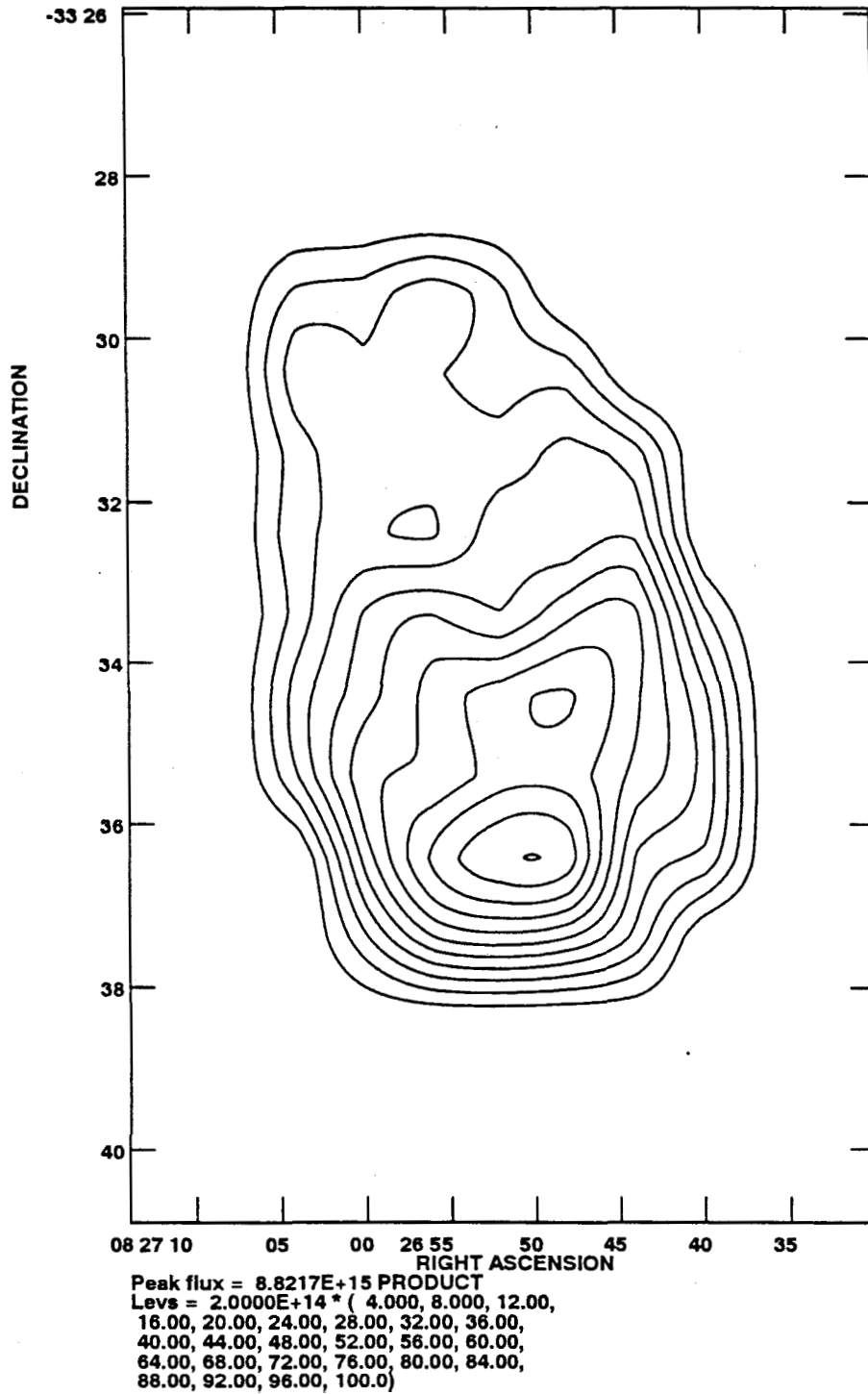88.00, 92.00, 96.00, 100.0)

Figure 5.4 (a) **A** contour plot of the ^{13}CO column density distribution over CG22-Blob-1. The levels listed are in units of cm^{-2}.
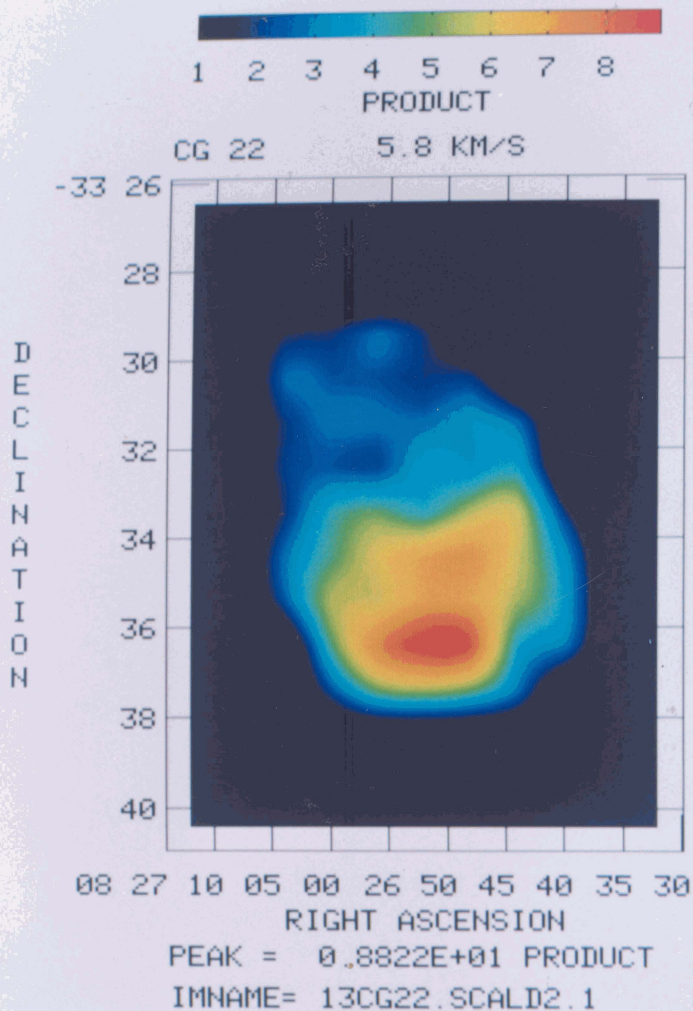
Figure 5.4 (b) A pseudo color image of the ^{13}CO column density distribution over CG22-Blob-1. The scale is in units of $10^{15} cm^{-2}$.

cloud to obtain the gas mass. Based on this method **we derive a mass of 27 M$_\odot$ for CG 22-Blob 1.**

The second method uses the empirically determined proportionality between I_{12CO} and $\mathcal{N}_{H_2}$ (Dickman 1978; Young and Scoville 1982). The basis for this proportionality has remained unclear although explanations based on the clumpy nature of molecular clouds and virial equilibrium have been proposed (Solomon *et. al.* 1987). We have used a value of 2.3×10^{20} cm^{-2}/Kkms^{-1} for the ratio $I_{12CO}/\mathcal{N}_{H_2}$. **Based on this method we obtain a mass of 71M$_\odot$ for CG 22-Blob 1.**

The third method assumes that the cloud is in *virial equilibrium,* and estimates the mass from the observed velocity dispersion. Approximating CG 22-Blob 1 by a sphere with radius 5', using the observed v_{FWHM} of 1.2 kms^{-1} **we obtain a virial mass of 250 M$_\odot$.**

5.9   Discussion

Figure 5.5 shows the ^{13}CO column density distribution superimposed on an optical picture of CG 22 from the ESO plates. Clearly, there is excellent agreement between the two. The individual streaks seen on the optical tail are well traced in CO. In addition, the CO emission is restricted to the regions delineated in the optical picture. The gradient in $\mathcal{N}_{13CO}$ is quite sharp on the side which faces the center of the system of CGs (roughly south) whereas on the northern side the cloud is diffuse. These evidences point directly to the profound effect of the environment on the globule.

There is evidence for an embedded young star which shows up in the IRAS maps of Sahu *et.al.*(1989) as a point source. This star has been seen in 2.2μ scans and is the same as the Hα emission star Wra220 (also PHα92). This is believed to be a pre-main sequence star in the mass range 0.5-2 M$_\odot$ forming in CG 22- Blob 1. This makes the star formation efficiency of the globule $\sim$ *a few* percent. This point source has an IR luminosity of $\sim$4L$_\odot$ with a large error (1L$_\odot$-8L$_\odot$). The ratio L$_{IR}$/M is only 0.15. Sugitani *et.al.*(1989) have established an empirical criterion for externally triggered star formation based on this ratio. According to them a ratio > 0.3 implies external mechanisms. It would appear that this star in CG 22 is not being formed by external mechanisms but it is not possible to say this conclusively because the error in L$_{IR}$ is too large.

The mass derived here from CO observations (27-70M$_\odot$) is in reasonable agreement with the estimate ($\sim$40M$_\odot$) obtained by Sahu *et.al.*(1989) from the IRAS
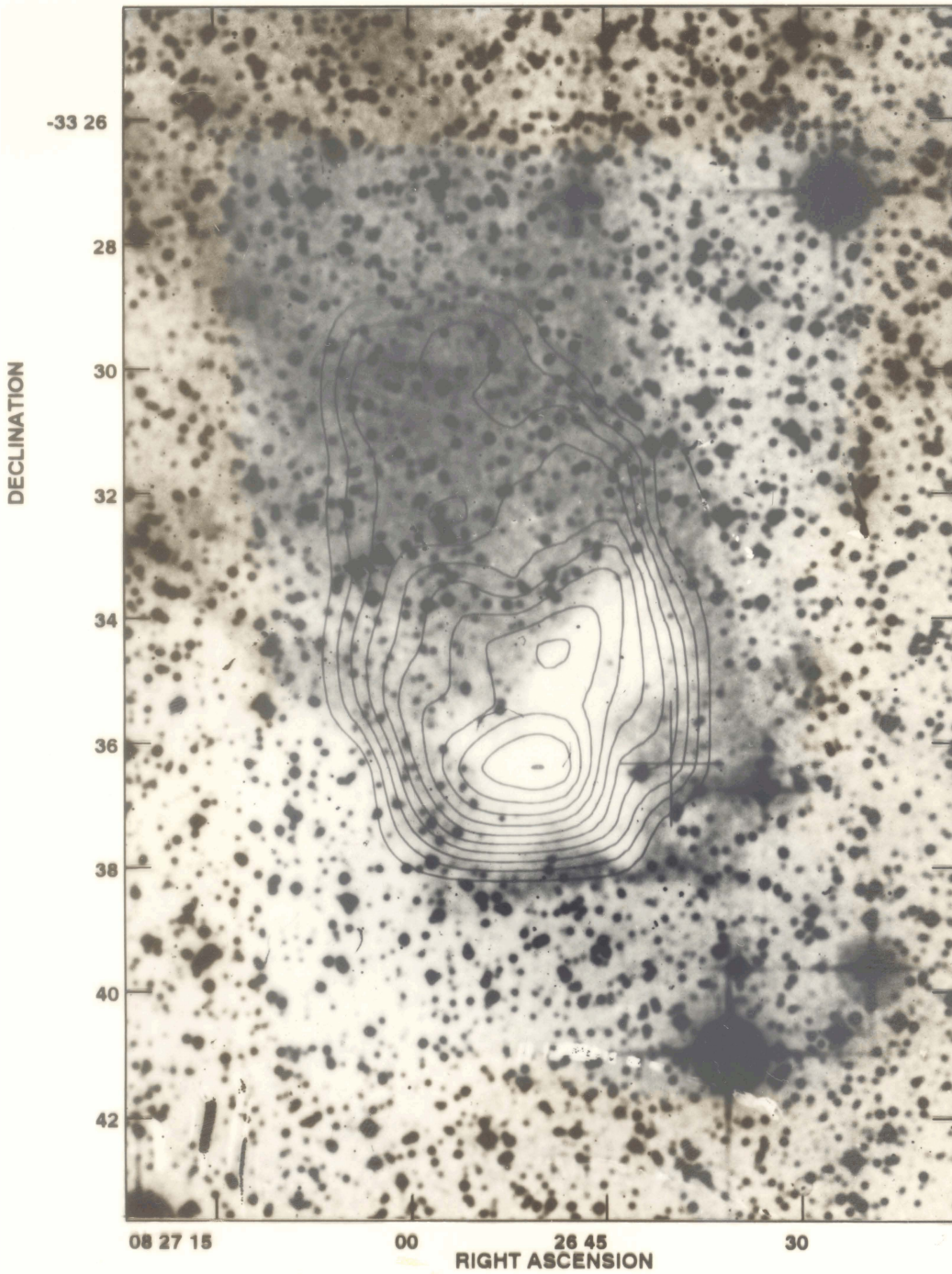
Figure 5.5: Contours of the ^{13}CO column density superposed on an optical negative image of CG 22-Blob 1. The lowest contour is at $8 \times 10^{14} cm^{-2}$ and the step size is 8 x $10^{14} cm^{-2}$.

maps. The virial mass is too large compared to the mass derived from CO observations. This may imply that the cloud is disintegrating due to the effects of its environment.

REFERENCES

Bally, J., Langer, W.D., Stark, A.A., Wilson, R.W. 1987, Ap. J., 312, L45.

Dickman, R.L., 1978, *Ap. J. Suppl.*, 37, 407.

Sahu, M., Pottasch, S.R., Sahu, K.C., Wesselius, P.R., Desai, J.N. 1988, Astron. Astrophys., 195, 269.

Sugitani, K., Fukui, Y., Mizuno, A. and Ohashi, N. 1989, Ap. *J.(Letters)*, 342, L87.

Frerking, M.A., Langer, W.D., Wilson, R.W. 1982, *Ap. J.*, 262, 590.

Snell, R.L., Scoville, N.Z., Sanders, D.B., Erickson, N.R. 1984, Ap. **J.**, 284, 176.

Solomon, P.M., Rivolo, A.R., Barret, J.W., Yahil, A. 1987, Ap. **J.**, 319, 730.

Ulich, B.L., Haas, R.W. 1976, *Ap. J. Suppl.*, 30, 247.

Young, J.S., Scoville, N.Z. 1982 *Ap. J.*, 258, 467.

Chapter 6

IRAS sources in the dark clouds in the Gum Nebula

6.1 Introduction

In this chapter we discuss the young stars embedded in dark clouds in the Gum Nebula as revealed by tlie Infra-Red Astronomy Satellite(IRAS) survey data. The aim is to study the locations of Young Stellar Objects(YSOs) inside the dark clouds with respect to the center of the distribution of the CGs in the Gum Nebula. If tlie star formation in the dark clouds in the Gum Nebula has been triggered by *external events*, the locations of the YSOs should reveal this as a tendency for the YSOs to lie towards (1) the periphery of tlic clouds, and (2) towards tlie side facing tlie center. There have been two such studies of IRAS sources in dark clouds in the past, between them, covering tlie whole of the sky (Emerson 1985; Parker 1988). They looked for enhancement in the density of IRAS sources towards edges of the clouds. In such whole-sky studies, since there is no obvious center for the processes possibly triggering star formation. the second effect mentioned cannot be stutlied. Both these studies conclude that there is no evidence for externally triggered star formation in dark cloutls. The first of these studies done by Emerson(1985) for the southern sky uses the Southern Dark Cloud(SDC) catalog compiled by Hartley *et. al.*(1986) from the ESO/SERC J Survey plates. This catalog gives in addition to the co-ordinates the major and minor axes of the ellipse which best approximates tlie cloud. Unfortunately it does not list the orientation of the ellipse making the interpretation of the IRAS source locations difficult. In other words, based on this information it is not possible to say reliably if an IRAS source lies towards the periphery of a cloud or not. This is a major drawback for any study which seeks to draw conclusions based on the distances of the IRAS sources from their respective cloud-centers as in Emerson's study. The second study done by Parker(1988) for the northern sky is based on the accurate shapes of Lynds dark cloutls and so can give reliable information about external triggering of star formation. The results of these studies indicate only that external triggering of star formation is not wide spread.

In tlie case of tlie dark cloutls in the Gum Nebula, there is already substantial evidence for external processes affecting them and also an apparent *center-of-influence*. We can take advantage of these circumstances and modify the method of analysis of the location of the IRAS sources. If the processes originating in tlie central region are important for triggering star forniation. then apart from expecting tlie IHAS sources to lie towards the edges of the clouds, one also expects that they be on the sides of the clouds facing the center as mentioned before. We use this second property of tlic exepectetl distribution of IRAS sources. The advantage of this method is that it is not affected by the exact shape of the cloud and its orientation.

In the next section we will describe the criterion we have used for selecting YSOs. In the third and fourth sections we describe tlie search and analysis procedures. Then the statistical method used to obtain tlie confidence level is described. The last section discusses tlie results.

6.2 Selection Criteria of the YSOs

The criteria used for selecting a YSO are the same as the ones used by Parker, along with those proposed by Emerson These are listed below:

1. Detection at 25μ and 60μ with [60-25] > 0

2. [25-12] > 0, if also detected at 12μ

3. Detection only at 60μ.

4. Detection at 60μ and 100μ only with [100-60] > OG

5. [100-25] > 0

Here [25-12] means the *25 to 12 micron color.* $\equiv \log[S_{25}/S_{12}]$, S_{25} being the IRAS catalog flux density in Jansky at 25μ wavelength. The fifth criterion, used by Parker is simple and picks up sources whose temperatures are less than ~ 70 K, thus rejecting the more evolved stars. The first four criteria from Emerson are more detailed and were arrived at based on the regions occupied by known classes of objects in the IRAS *color-color plots.* Parker has shown that objects meeting criterion 5 fall in regions in the color-color diagram recognisecl by Emerson to be populated by T-Tauri stars, embedded cores and galaxies. If any one of these conditions is satisfied, the source is considered a candidate. *We take an IRAS source to be an embedded YSO if it meets one of the above criteria and falls within a specified distance from the center. of a dark cloud.* Emerson has shown that the number of IRAS sources so selected falls off as one goes towards the edge of the clouds implying that they are physically associated with tlie clouds. In other words, it is unlikely that there are many *galaxies* in the selected sample. Also, galaxies will be far outnumbered by galactic objects at tlie low latitudes of the dark clouds. The association with dark clouds makes it unlikely that the sources are galaxies.

6.3 The Search

The dark clouds are from the SDC catalog of Hartley *et. al.*(1986) We have chosen the distance limit from the center of the cloud to be the mean of the minor and major axes of the cloud. Since the analysis does not depend on the distance of the source from the center of tlic cloud, this larger area of search than what was used by both Emerson and Parker is not a handicap. On tlie other hand it takes care of errors in the co-ordinates of the cloud centers and tlie IRAS sources. The search was carried out over the RA range 7 hr to 9.5 hr and dec range −53° to −30°. The total number of clouds involved is **1.500.** A total of 294 IRAS sources met at least one of the above criteria. Most of the sources (257) met the fifth criterion. A database of the search results was created with the following information:

1. IRAS source co-ordinates

2. associatetl dark cloud co-ordinates

3. major and minor axes of the cloud.

4. the IRAS fluxes at four wavelengths

5. the four flux qualities

This data base is used for carrying out the statistical analysis described in tlie next section.

6.4 Analysis

For each IRAS source meeting one of the criteria we calculate using plane geometry the angle θ shown in figure 6.1 from

$$\cos \theta = \left(a^2 - b^2 - c^2 \right) / 2bc \tag{6.1}$$

where

$$a^2 = [(\alpha_{IR} - \mathbf{a},) \cos (\delta_{IR} + \delta_0)/2]^2 + (\delta_{IR} - \delta_0)^2 \tag{6.2}$$
$$b^2 = [(\mathbf{a},- \alpha_0) \cos (\mathbf{6}, + \delta_0)/2]^2 + (\delta_c - \delta_0)^2 \quad and \tag{6.3}$$
$$c^2 = [(\alpha_c - \alpha_{IR}) \cos (\delta_c + \delta_{IR})/2]^2 + (\delta_c - \delta_{IR})^2 \tag{6.4}$$
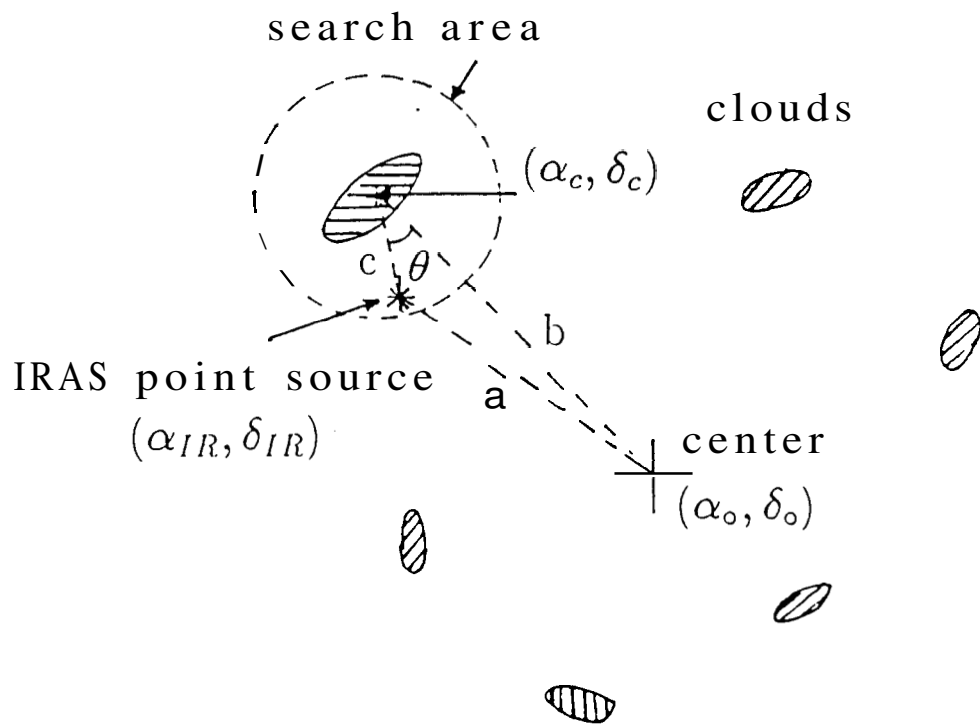
Figure 6.1: A schematic diagram showing the scheme for IRAS sources search. The search area is circular with radius equal to the mean of the major and minor axes of the cloud.

The angle θ simply represents the location of the source in the cloud with respect to the center of the distribution of the CGs regardless of the location of the cloud itself. If the YSOs are located randomly throughout the dark clouds (with or without systematic radial dependence), one expects no dependence of their distribution on the polar angle in the cloud co-ordinate system with respect to any reference direction. On the other hand if the central processes are important, one expects a dependence on the angle 0. We simply study the distribution of the YSOs as a function of the absolute value of θ with a coarse binning of 45°. We have plotted in figure 6.2 histograms of this distributions for clouds of different sizes taking in each case sources falling within different fractional areas in the clouds. We have restricted this analysis upto a cloud size of $20'$. We see that in all these ranges the distribution peaks towards the side facing the center of the distribution of the CGs. In other words there seems to be a real tendency for the YSOs to fall on the side facing the center. To get a quantitative estimate for the confidence level of this conclusion we adopt a simple statical method as explained in the following section.

6.5 Confidence Level

We first divide each cloud into two semi-circles, one facing the center and the other facing away from it. These partitions correspond to the ranges 0°-90° and 90°-180° in the absolute value of θ defined previously. We will call these ranges *the front arzd the back sides*. In the case where the locations of the YSOs are unaffected by the central processes, on an average we expect equal number of YSOs in these two ranges. The distribution is binomial with $p = q = 0.5$ and $n = $ total number of YSOs. Here p and q are the probalilities that an IRAS YSO falls on the front or the back side. As mentioned in section 6.4 the histograms in figure G.2 peak on the front side (0" $-$ 90°), i.e., there is an asymmetry in the distribution of YSOs. We now ask if the asymmetry seen is sufficient to indicate a deviation from $p = q = 0.5$ and hence a central origin. If X is the number of YSOs in the first range (0°-90°) then the confidence level for the hypothesis that the distribution is biased towards front side is equal to the $P(X > x)$, the area under the distribution curve upto $x = X$, where x is the binomially distributed random variable. To get this area we approximate the binomial distribution by a *normal distribution*. This is a good approximation when $p = 0.5$ as in our case with n around a few tens (theorem of De Moivre and Laplace: Kreyscig 1970). The mean and variance of the normal distribution are $\mu = np = n/2$ and $\sigma^2 = npq = n/4$. Then the confidence level is

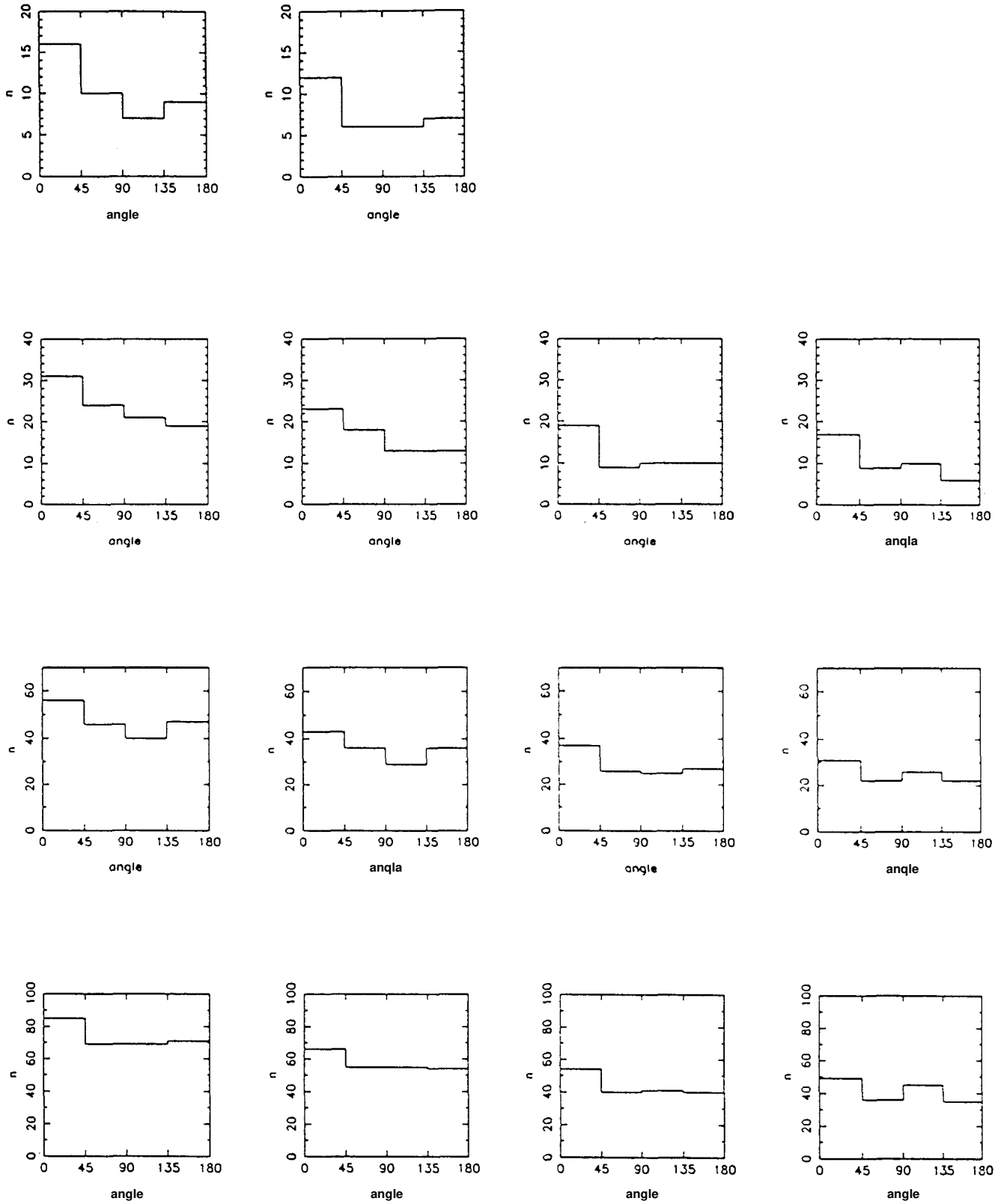$$P(x > X) = 1 - P(x < X) \approx 1 - \Phi((X - \mu)/\sigma) \tag{6.5}$$

Figure 6.2: Histograms of distribution of IRXS sources in θ, the angle with respect to the center (see figure 6.1). Horizontally, the plots are for the effetctive area ranges 0-1,0.1-1,0.2-1 and 0.3-1. Vertically the plots are for the mean cloud ranges 0-5,0-10,0-15 and 0-20 arcminutes.

Table 6.1 Confidence Levels

size	fractional area			
arcmin.	0.0-1.0	0.1-1.0	0.2-1.0	0.3-1.0
0- 5	94	82		
0-10	94	97	87	94
0-15	86	87	85	69
0-20	79	79	84	65

where Φ is the area under the normal distribution curve. We have listed the confidence values in Table 1 for the different ranges of sizes and fractional area mentioned earlier.

6.6 Conclusion

From the above analysis it appears that there is a real tendency for the YSOs to fall on the front side rather than the back side. The confidence level for this conclusion is highest for clouds of sizes 0'-10'. This may be because in larger clouds the effects of external mechanisms get shadowed by normal star formation. Even among the smaller clouds it seems that external triggering is not the only method of star formation. It is to be remarked that not all the IRAS sources identified as YSOs are necessarily YSOs. Because of the larger search area the inclusion of sources not physically associated with the clouds at all is possible. But for this confusion the confidence level would have been even higher.

References

Emerson, J.P. 1987, in *Star Forming Regions*, ed. M.Piembert & J.Jugaku, D.Riedel Publishing Company

Hartley, M., Manchester, R.N., Smith, R.M., Tritton, S.B., Goss, W.M. 1986 *Astron. Astrophys. Suppl.*, **63,** 27.

Kreysig, E. 1970, *Introductory Mathematical Statistics*, John Wiely & Sons.

Parker, N.D. 1988, *Monthly Notices Roy. Astron. Soc.*, 235, 139.

Chapter 7

Discussion

7.1 Introduction

The main results obtained from the study presented in the previous chapters are
the following:

(i) The system of cometary globules in the Gum Nebula appears to be
expanding from a common center. The *expansion age* is $\lesssim$ 6 Myr.
(ii) The observed velocity gradients along the tails of the globules suggest
a *stretching age* for the tails of $\sim$ 3 Myr.
(iii) The mass of a typical globule is $\sim$ 20 $M_\odot$
(iv) Star formation triggered by external mechanisms appears to be going
on in this region

In this chapter we discuss several scenarios that may have a bearing on the above
results.

The rough agreement between the expansion age and the ages of the tails sug-
gests that both the formation of the tails and the expansion of the globules may
be due to a common cause. The presence of young stars in this region with esti-
mated ages ranging from 10^5 to a few 10^6 years may be an important clue. Some
of these are embedded in the heads of the CGs, while others are isolated. CG1 has
an embedded star with age $\sim$ 10' yrs (Brand *et al*.1983, Reipurth 1983), and the
embedded IR source CG30IRS4 in CG30 has an age $\sim$ 10^6 yrs (Pettersson, 1984).
The bipolar molecular outflows associated with HH46-47, HH120 and HH56-57 have
dynamical ages of $\sim$ 10^5 yrs (Olberg *et al*.1988). As already mentioned the study of
the distribution of IHAS sources indicates that star formation triggered by external
means is indeed going on in this region. All these strongly point to the possibility
that the processes responsible for the expansion of the globules, as well as their
cometary appearance, have also triggered star formation in some of them. The var-
ious possible mechanisms are (i) supernova explosion(s), (ii) radiation from massive
stars found in the central region, and (iii) stellar wind from these massive stars.
Before discussing each of these scenarios it would be useful to have an estimate of
the kinetic energy of a typical globule and its momentum. Assuming a typical CG
mass $\sim$ $20 M_\odot$ (see chapter 5 and Harju *et al.* 1990) and an expansion velocity of
12 kms^{-1}, the kinetic energy is $\sim$ 3 x 10''' ergs per globule, and its momentum
$\sim$ 5 x 10^{40} gm cm s^{-1}. We now proceed to make simple estimates for energy and
momentum that can be imparted to a globule from each of the processes mentioned
above.

7.2.1 Supernova explosions

According to prevalent opinion, the Gum Nebula is an old supernova remnant with an age $\sim 10^6$ yrs (Reynolds, 1976; Leahy, Nousek and Garmire **1992**). Therefore it is natural to ask if the original explosion that created tlie Gum Nebula could itself be responsible for the observed properties of the system of CGs. The energy and momentum intercepted by a globule are given by

$$E = 3.1 \times 10^{48} \left(\frac{E_{SNE}}{5 \times 10^{51} ergs} \right) \left(\frac{r}{0.25pc} \right)^2 \left(\frac{d}{5pc} \right)^{-2} \tag{7.1}$$

$$P = 8 \times 10^{39} \left(\frac{E_{SNE}}{5 \times 10^{51} ergs} \right)^{0.5} \left(\frac{M_{ej}}{8M_\odot} \right)^{0.5} \left(\frac{r}{0.25pc} \right)^2 \left(\frac{d}{5pc} \right)^{-2} \tag{7.2}$$

where E_{SNE} is the energy of explosion of the SNE, M_{ej} is tlie ejected mass and r and d are the radius of a globule and its distance from the explosion center at the time of explosion. Assuming an ejected mass of $8M_\odot$, an energy of explosion equal to 5 x 10^{51} ergs, and a typical size of **0.5** pc for the CGs, we estimate that a typical CG has to be not more than a few parsec from the explosion center in order to. intercept sufficient momentum.

This is a plausible scenario but it should be pointed out that the center of the Gurn Nebula shell is 4.5° north of the *morphological center* derived from tlie tail directions of the CGs. However, we would not like to over-stress this point because of the inherent difficulties in determining the center of explosion of such an old SNR. A more serious difficulty is the following: Although the original explosion could have caused the expansion of the system of CGs and the observed tail structures, the presently observed ionised bright rims cannot be attributed to it, as arguecl before in chapter 4 in a similar context, viz., that the bright rims have a recombination time scale ~ 1000 years and so cannot survive for 10^6 years.

7.2.2 Radiation pressure

The most massive star in the region is ζ Pup (Olf)and therefore is the most significant source of photons for exerting radiation pressure. Its luminosity is **9** $\times$ 10^5 $L_\odot$ (Bohannan *et al.* 1986). Models suggest that this star may have just finislied or is in the final stages of core hydrogen burning. Its ZAMS mass is believed to be ~ 60 $M_\odot$. This implies that ζ Pup is a few million years old. It is reasonable to assume that its average luminosity over the past few million years was the same as its present luminosity. The CG closest to ζ Pup is at a distance of **40** pc from it.

a globule and its distance from the star respectively. The stellar wind from ζ Pup has a terminal velocity of 2600 kms^{-1} and the mass loss rate is 5×10^{-6} M$_\odot$yr^{-1} (Bohannan *et al.* 1986). We estimate the energy and momentum intercepted by a typical globule from the wind from ζ Pup to be $\sim 6 \times 10^{**}$ ergs and $\sim 10^{38}$ gm cms^{-1}, respectively, over 6 million years. Stellar wind from γ^2 Vel and the companion of ζ Pup will increase these numbers by a factor of four, and the momentum available will still be less by an order of magnitude (even given the assumed 100% efficiency of conversion of the stellar wind momentum to cloud momentum).

7.2.4 Rocket effect

Finally, we consider the rocket effect which results from the anisotropic expansion of the hot ionised gas from the bright rims. When a neutral cloud is exposed to ionising radiation from a star, an ionisation front is driven into the cloud. The ionised hydrogen produced on the side of the cloud facing the star is at a much higher pressure than the gas outside because of its high density. This gas then expands towards the star forming a dense cloud of ionised gas between star and the cloud. Making the simplifying assumption that this gas expands into vacuum, the expansion velocity will be close to the velocity of sound in the ionised region. It is this expanding layer of gas that is seen as the bright rim. The effect of this streaming of gas in the bright rim produces a recoil on the cloud accelerating it away from the star. It also leads to evaporation of the cloud. This process has been called the *rocket* effect and was first proposed by Oort and Spitzer(1955) for accelerating interstellar clouds.

We estimate below the velocity that the CGs can acquire as a result of such a rocket effect. The temperature and density at the bright rim of CG30 has been measured by Pettersson(1984) to be $\sim 10^4$K and ~100cm^{-3}. Reipurth(1983) has estimated that ζ Pup alone can easily account for the observed ionisation level ($n_e \sim 100$ cm^{-3}) at the bright rims. Using mass loss rates of $\sim 9\times 10^{-5}$ M$_\odot$yr^{-1} as derived by Reipurth(1983), and an expansion velocity of the hot gas -10 kms^{-1} (velocity of sound in the bright rim), we estimate the total momentum acquired by a typical globule due to the rocket effect operating for 6 million years to be $\sim 10^{42}$ gm cms^{-1}. This should be compared with the required momentum $\sim 5 \times 10^{40}$ gm cms^{-1}. If we include the former companion of ζ Pup, γ^2 Vel and the other B stars, the clouds can be easily accelerated to the observed velocities even with larger initial masses. From the above discussion it appears that the only plausible mechanism which can explain *both* the bright rims and the expansion velocities is the heating caused by radiation (and possibly stellar wind) from the stars in the central region,

and the consequent rocket effect. We have not yet attempted to explain the tail structures. It is conceivable that a part of the expanding ionised gas will be swept back by the radiation and stellar wind from the central stars forming the tail. This flow should also entrain some neutral material to account for the CO emission from the tails. The ionisation front may also dislodge neutral material from the periphery of the globule (as compared to the center of the globule, where a large column of gas is present) which can then flow along the tail. In larger globules shadowing by the head may be important. We hope to investigate this in detail in the near future. We wish to mention in passing that Bertoldi and McKee(1990) have shown that UV radiation and stellar wind can result in molecular clouds developing tail-like structures.

7.3   The proper motion of ζ Pup

The star ζ Pup is very remarkable from several view points. First of all, it is a very massive star. It is tlie most luminous star in the southern sky. It has a large proper motion of .033" (-0.031" in α and 0.012" in δ)(SAO star catalog 1966), translating to a transverse velocity of 74.3 kms^{-1} at the assumed 450 pc distance. It was proposed very early that ζ Pup must, be a *runaway star* resulting from tlie explosion of its binary companion (Reynoltls 1976). It was also suggested that the Gum Nebula is the remnant of this explosion. If, indeed, ζ Pup is a runaway star. its companion which exploded must have been more massive to have evolved faster to explode first. Also, if the explosion is spherically symmetric then the binary will disrupt only if the mass ejected is greater than half the total mass. This means that tlie companion of ζ Pup must have been the more massive star *even at the time of explosion.* This suggests that the region where we now find the CGs there were atleast five massive stars a million years back (including the progenitor of the Vela pulsar and γ^2 Vel).

We have shown in figure 7.1, the proper motion of ζ Pup and its past trajectory. The path passes very close to the morphological *center* of the system of CGs. As can be seen it was closest to the *center* half a million years back. We suggest that this is the original site of the binary whose disruption resulted in the present large proper motion of ζ Pup. It is possible that the Vela progenitor, the proposed ζ Pup binary and γ^2 Vel are all part of the Vela OB3 association found by Brandt *et. al.*(1971). Such *a* scheme naturally accounts for the lack of any object of significance near the *center* at present. The ζ Pup binary would have been the dominant object in the region causing most of the tails which have grown over a few million years to point away from it.
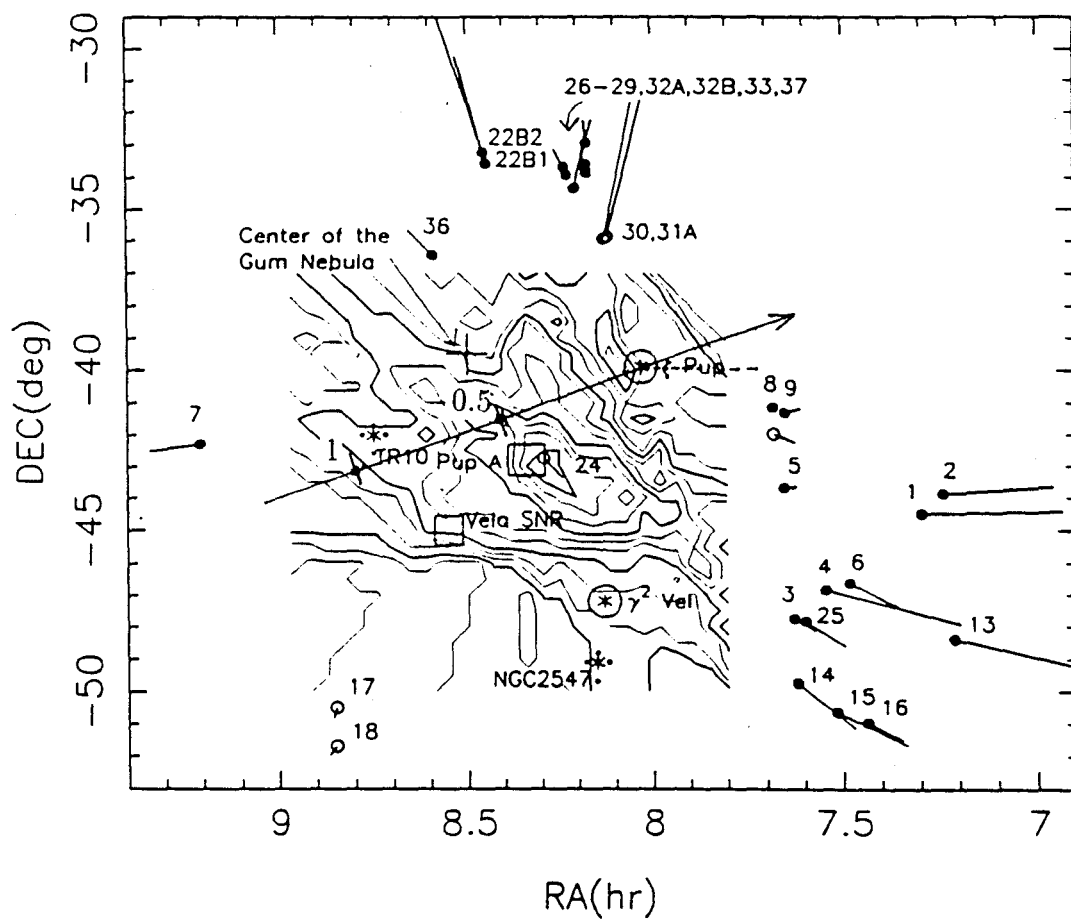
Figure 7.1: Diagram showing the proper motion of ζ Pup extrapolated back in time. The past trajectory is graduated in millions of years. The star would have been close to the *morpohological center* half a million years back.

As we have already mentioned the bright rims of the of the CGs are short lived and therefore should reflect the effects of the changing position of ζ Pup. An examination of the orientation of the bright rim of CG 31A the CG closest to ζ Pup (in projection) shows that this indeed is the case. This is shown in figure 7.2 where the CG 30-31 complex is shown with the directions to ζ Pup and the *center* marked. The bright rim is normal to the vector pointing to ζ Pup whereas the tail is along the direction to the *center.*

7.4   The Gum Nebula

Based on the above discussion we propose the following qualitative model for the Gum Nebula. We have shown in figure 7.3 tlie region including the H a emission regions collectively called tlie Gum Nebula. The region to the south is more intense in H a and tlie CGs are distributed over this region. The location of the original ζ Pup binary is in the southern part of tlie Gum Nebula. We propose that this region of enhanced Hα emission is tlie remnant of the explosion of tlie companion of ζ Pup (the two northern filaments may be also connected with this explosion; but this would require a highly asymmetric expansion of tlie SNR). This picture can be tested by the analysis of the radial velocities of the Hα filaments with respect to the *center.* One might also look for soft X-ray emission from the interior of the remnant which should be restricted to the southern part. There is already an indication that this may be the case from the HEAO X-ray data (Leahy, Nousek and Garmire 1992). This study is incomplete as the coverage of the nebula is poor. Data from ROSAT should definitely throw much light on this picture.

We propose the following picture for the Gum-Vela region: The stars ζ Pup, its past companion, the progenitor of the Vela pulsar/SNR, the binary γ^2 Vel, all formed around the same time, a few million years ago, from the same molecular cloud, and were part of the Vela OBR association. The parent molecular cloud from which these stars formed was-slowly evaporated away by the UV radiation and stellar winds from these stars. The denser regions in this molecular cloud were not destroyed completely, although they lost a significant part of their original mass due to the harsh environment. These surviving pieces of the original molecular cloud may be what are now seen as the cometary globules. About half a million years ago the companion of ζ Pup exploded whose ejecta and swept up material is probably what is seen in H a in the Gum Nebula. The ionisation in the nebula is now maintained by the other stars in the region. This explosion resulted in the disruption of the binary giving ζ Pup its large proper motion.The expansion of the

system of cometary globules is largely caused by the rocket effect and the tails are partly the ablated material flowing down-stream. The effect of the UV radiation, stellar winds and the SN shock compressed the clouds leading to star formation as evidenced by the IRAS sources.
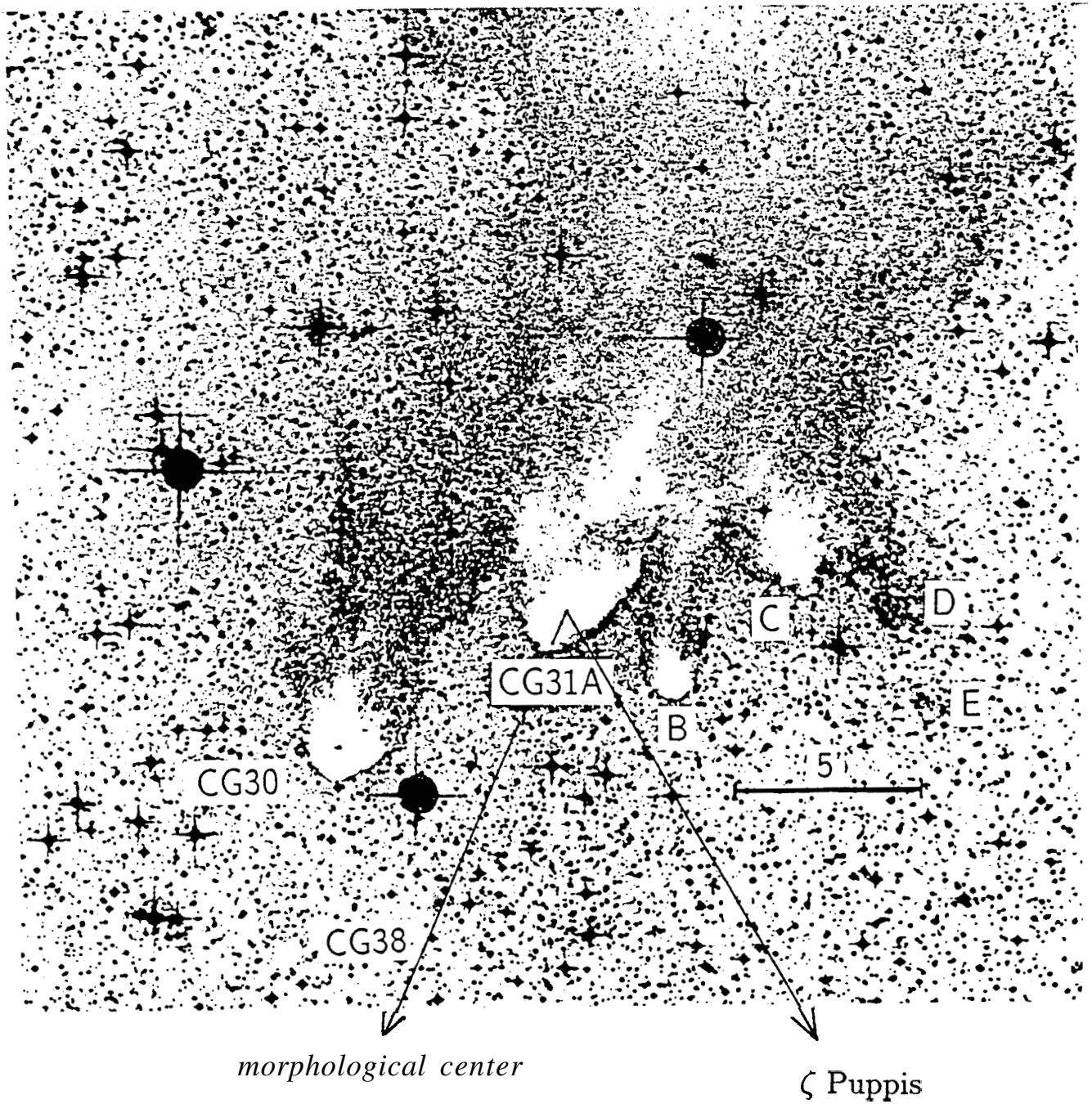
Figure 7.2: The orientation of the bright rim of CG31A with respect to the tail directions in this region. The directions to ζ Puppis and the morphological center are marked. The tails point away from the morphological center whereas the bright rim is perpendicular to the direction to ζ Puppis.
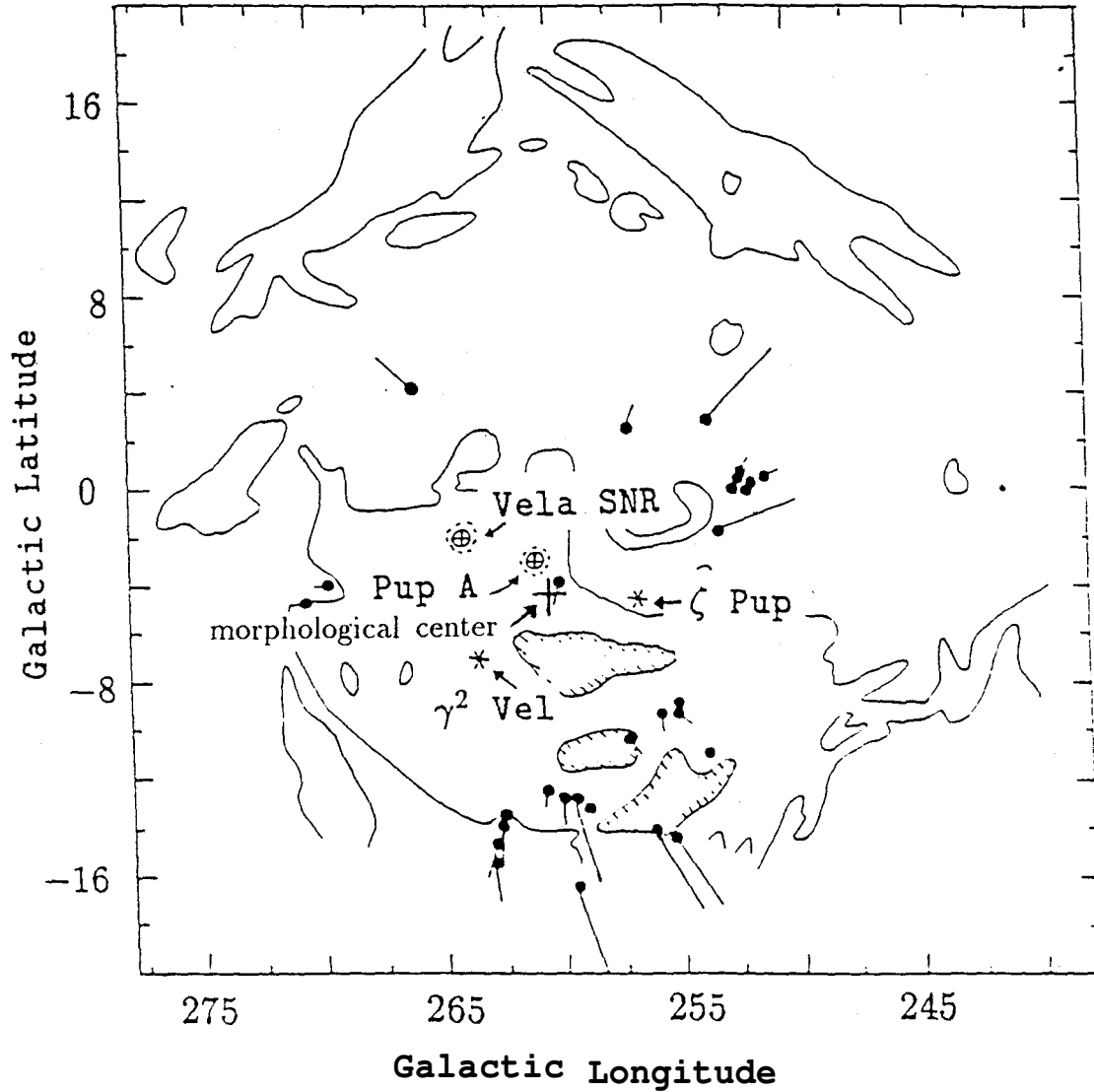
Figure **7.3:** Overall picture of the Gum-Vela region showing the H_α emission as solid lines, the CGs as filled circles with tails (scaled up 10 times for clarity), the *morphological center* derived from the tails and other important objects in the region. The locations of objects shown are approximate (adapted from Pettersson 1991).

REFERENCES

Bertoldi, F., McKee, C.F. 1990,*Ap. J.*,354, 529.

Bohannan, B., Abbot, D.C., Voels, S.A., Hummer, D.G. 1986, Ap. **J.**,308. 728.

Brand, P.W.J.L., Hawarden, T.G., Longmore, A.J., Williams, P.M., Caldwell, J.A.R. 1983, *Monthly* Notices Roy. Astron. *Soc.*, 203, 215.

Brandt, J.C., Stecher, T.P.,Crawford, D.L.,Maran, S.P. 1971, *Ap.J.(Letters)*, 163, L99.

Harju, J., Sahu, M., Henkel, C., Wilson, T.L.. Sahu, K.C., Pottasch, S.R. 1990, Astron. *Astrophys.*, 233. 197.

Leahy, D.A., Nousek, J., Garmire, G. 1992,*Ap. **J.**,385, 561.

Olberg, M., Reipurth, B., Booth, R.S. 1988, in *Symposium on* Physics *and Chemistry* of *Interstellar Molecular Clouds: mm and Sub-mm Observations in Astrophysics*, ed. Winnewisser, G. & Armstrong, J.T., (Hiedelberg:Springer Verlag), p. 120.

Oort, J.H., Spitzer,L. 1955, *Ap. J.*, 121, 6.

Pettersson. B. 1984, *Astron. Astrophys.*, 139, 135

Reipurth, B. 1983, *Astron. Astrophys.*, 117, 183.

Reynolds, R.J. 1976,*Ap. **J.**,**206,** 679.

SAO Star Catalog, 1966 (Smithsonian Institution, Washington, D.C.).

Appendix A

In this appendix we derive formulae for obtaining the physical parameters of a molecular cloud from the observed J=1→0 transition lines of ^{12}CO and ^{13}CO. We basically follow the procedure outlined by Dickman(1978).

The assumptioris made in tlie derivation are: (1) Tlie excitation temperature of the J=1→0 transition is constant along tlie line of siglit. (2) Both ^{12}CO and ^{13}CO have the same excitation temperatures for tlic J=1→0 transition and this temperature is equal to the kinetic temperature of the gas. (:]) Tlic J=1→0 transition of ^{12}CO is optically thick.

Tlie specific intensity obtained after background subtraction and calibration is given by

$$I_\nu = [B_\nu(T_{ex}) - B_\nu(T_{bg})]\left(1 - e^{-\tau_\nu}\right) \tag{A.1}$$

The measured line temperature after all corrections is related, bydefinition, to I, as

$$I_\nu = 2kT_R^*\nu^2/c^2 \tag{A.2}$$

Keeping in mind that at 11.5 GHz $h\nu \ll kT$ is not valid and using T_{bg}=2.7K, the cosmic microwave background radiation temperature, one gets from equations A.1 and A.2,

$$T_R^* = [J_\nu(T_{ex}) - J_\nu(2.7)]\left(1 - e^{-\tau_\nu}\right) \tag{A.3}$$

where $J_\nu(T) = T_\nu/(e^{T_\nu/T} - 1)$ and $T_\nu = h\nu/k$. We derive below, the formulae for various physical parameters.

A.1 Temperature

For the optically thick line center of the ^{12}CO line, A.3 reduces to

$$T_R^* = T_{Lp} = J_\nu(T_{ex}) - J_\nu(2.7) \tag{A.4}$$

where T_{Lp} is the peak line temperature. Putting in numbers, we get, with the assumption that $T_{ex} = T_{kin}$,

$$T_{kin} = T_{ex} = \frac{5.532}{\ln(1 + \frac{5.532}{T_{Lp} + 0.8182})} \tag{A.5}$$

A.2 Optical Depth

Assuming the excitation temperature for ^{13}CO to be same as that for ^{12}CO we derive from A.3 and A.5

$$\tau_{13} = -\ln\left[1 - \frac{T_{13}}{5.289}\left\{\left[e^{\frac{5.289}{T_{ex}}} - 1\right]^{-1} - 0.1642\right\}^{-1}\right] \tag{A.6}$$

where T_{13} is the T_R^* measured for ^{13}CO.

A.3 Column Density

We can relate the optical depth to the column densities of molecules $\mathcal{N}_0$ and $\mathcal{N}_1$ in the J=0 and J=1 rotational states respectively as

$$\tau_\nu = (h\nu/c)(B_{01}\mathcal{N}_0 - B_{10}\mathcal{N}_1)\phi_\nu \tag{A.7}$$

where B_{01} and B_{10} are the Einstein's co-efficients and ϕ_ν is the line profile function satisfying the condition $\int \phi_\nu d\nu = 1$. Using

$$\frac{\mathcal{N}_1}{\mathcal{N}_0} = \frac{g_1}{g_0}e^{-h\nu/kT_{ex}} \tag{A.8}$$

and

$$B_{01} = \frac{g_1}{g_0}A_{10}\frac{c^3}{8\pi h\nu^3} \tag{A.9}$$

and integrating over the line, we obtain

$$\int \tau_\nu d\nu = \mathcal{N}_0\frac{c^2}{8\pi\nu^2}\frac{g_1}{g_0}A_{10}\left(1 - e^{-h\nu/kT_{ex}}\right) \tag{A.10}$$

The total column density $\mathcal{N}_{13}$ of ^{13}CO including all levels is obtained using the partition function Q for linear molecules (Dickman 1978),

$$\frac{\mathcal{N}_{tot}}{\mathcal{N}_0} = Q = 2T_{ex}/T_0 \tag{A.11}$$

58

With $A_{10} = 7.4$ x 10^{-8} s^{-1} one gets

$$\mathcal{N}_{^{13}CO} = 2.42 \times 10^{14} \frac{T_{ex} \int \tau_{13} dv}{\left(1 - e^{-5.289/T_{ex}}\right)} \tag{A.12}$$

where we have used $\int \tau_{\nu} d\nu = (\nu/c) \int \tau_{\nu} dv$.

REFERENCES

Dickman, R.L., 1978, *Ap. J. Suppl.*, **37,** 407.